# Chapter 3   Average properties of Southern California ground motion envelopes over ranges of magnitudes, distances, and site conditions

In this chapter, I use the envelope attenuation relationships derived in Chapter 2 to study average properties of ground motion. I use the P- and S-wave amplitude attenuation relationships to compare general behavior of different channels of ground motion over ranges of magnitudes ($2 \leq M \leq 7.3$), distances ($< 200$ km), frequency bands, and site conditions. There are a total of 48 ($= 4$ directions $\times$ 3 frequency bands $\times$ 2 site classes $\times$ 2 body wave groups) distinct prediction equations (or channels) for amplitude parameters: the 4 directions are vertical, East-West, North-South, and the root mean square of the horizontal amplitudes, the 3 frequency bands are acceleration, velocity, and filtered displacement, the 2 site classes are rock and soil, and the 2 body wave groups are the P- and S-waves. With all 48 different amplitude attenuation relationships, there are a total of $\binom{48}{2} = 1,128$ unique comparison pairs that could potentially be analyzed. The intent is not to present an exhaustive analysis of such comparisons, but rather, to use these envelope attenuation relationships to point out some general characteristics of, and differences between:

- high and low frequency ground motion

- rock versus soil sites

- horizontal versus vertical ground motion amplitudes

- P- versus S-waves

The primary motivation for this approach to ground motion characterization is to develop predictive relationships for envelopes of ground motion for use in seismic early warning. Examples of various channels of predicted ground motion envelopes are presented at the end of this chapter.

## 3.1 High- versus low-frequency ground motions

I use the attenuation relationships for the root mean square of the horizontal S-wave envelope amplitudes to compare acceleration, velocity, and displacement scaling with magnitude and distance. Acceleration, velocity, and displacement are often used as proxies for high-, mid-, and low-frequency ground motions. The S-wave envelope amplitude is comparable to the peak amplitude when examining horizontal ground motions records. The envelope attenuation relationships developed in this study can be compared with traditional strong motion attenuation relationships described in the literature, which typically examine peak ground motions as functions of magnitude, distance, and site.

Eqn. 2.3 represents the magnitude, distance, and site dependence postulated for both P- and S-wave envelope amplitudes. For each of the 48 envelope amplitude sets, we find the regression unknowns $(a_i, b_i, c_{1i}, c_{2i}, d_i, e_i, i = 1 \ldots 48)$ that minimize the least squares error between the "observed" amplitudes and the fitted values given by Eqn. 2.3. The "observed" amplitudes are not directly observed quantities, but are inversion results; they are the envelope amplitudes obtained from fitting the nonlinear 11-parameter characterization to the observed ground motion envelopes described in the previous chapter. These are henceforth referred to as "observed envelope amplitudes" or "observed amplitudes" for short.

In addition to the errors explicitly accounted for by the $\epsilon$ term in Eqn. 2.3, there are, in principle, additional errors $\eta$ that result from fitting the 11-parameter characterization to the observed envelopes. It is assumed that these errors are small, $\eta \ll \epsilon$.

Figures 3.2, 3.4, and 3.6 show observed S-wave envelope amplitudes for root mean

square (rms) horizontal acceleration, velocity, and displacement, and amplitude curves predicted by Eqn. 2.3 as a function of distance for various prescribed magnitudes. A quick visual examination of these plots shows that saturation effects become important at close distances to large events; these saturation effects are strongest for acceleration, and decrease with decreasing frequency. The constant slope of the predicted amplitude curves with respect to distance is due to the geometric attenuation (coefficient $d$ in Eqn. 2.3) and possibly dispersion; the curvature at larger distances is the effect of the exponential dependence with distance (coefficient $b$ in Eqn. 2.3). Figures 3.3, 3.5, and 3.7 show histograms of the residuals for the various components of ground motion, on rock and soil sites, with and without station corrections. Examination of such residual plots gives a qualitative idea of the scatter about the predicted amplitude levels for rock and soil sites, scatter for the various components of ground motion, and the effect of station corrections; such plots are also useful to verify that the assumptions regarding the residuals in Eqn. 2.3 are valid. Table 3.1 summarizes the regression coefficients for rock (NEHRP site class BC and above) and soil (NEHRP site class C and below) sites for rms horizontal S-wave envelope amplitudes for acceleration, velocity, and filtered displacement.

rms horizontal S-wave acceleration attenuation coefficients

| Site type | a | b | d | $c_1$ | $c_2$ | e | $\sigma_{uncorr}$ | $\sigma_{corr}$ |
|-----------|------|------|------|-------|-------|------|-------------------|-----------------|
| rock | 0.779 | $2.555 \times 10^{-3}$ | 1.352 | 1.478 | 1.105 | -0.645 | 0.308 | 0.243 |
| soil | 0.836 | $2.324 \times 10^{-3}$ | 1.562 | 2.423 | 1.054 | -0.338 | 0.312 | 0.248 |

rms horizontal S-wave velocity attenuation coefficients

| Site type | a | b | d | $c_1$ | $c_2$ | e | $\sigma_{uncorr}$ | $\sigma_{corr}$ |
|-----------|------|------|------|-------|-------|------|-------------------|-----------------|
| rock | 0.894 | $4.286 \times 10^{-4}$ | 1.440 | 1.114 | 1.110 | -2.602 | 0.279 | 0.230 |
| soil | 0.960 | $8.328 \times 10^{-4}$ | 1.589 | 1.982 | 1.067 | -2.351 | 0.296 | 0.230 |

rms horizontal S-wave (filtered) displacement attenuation coefficients

| Site type | a | b | d | $c_1$ | $c_2$ | e | $\sigma_{uncorr}$ | $\sigma_{corr}$ |
|-----------|------|------|------|-------|-------|------|-------------------|-----------------|
| rock | 1.031 | $1.015 \times 10^{-7}$ | 1.438 | 1.098 | 1.133 | -4.342 | 0.277 | 0.233 |
| soil | 1.081 | $1.204 \times 10^{-6}$ | 1.556 | 1.946 | 1.091 | -4.101 | 0.326 | 0.236 |

Table 3.1: Regression coefficients for Eqn. 2.3 for S-wave envelope amplitude parameters for acceleration, velocity, and filtered displacement on rock and soil sites.

Recall that the ground motion model represented by Eqn. 2.3 is valid in the magnitude range $2 \leq M \leq 7.3$. Saturation effects (via $C(M)$) have been prescribed to start at $M \sim 5$. For $M < 5$, $C(M) \approx 0$. Thus, the coefficients $a, b$ and $d$ can be directly interpreted as the "small magnitude" ($M < 5$) scaling factors for magnitude dependence, anelastic attenuation (and scattering effects), and geometric attenuation of ground motion amplitudes. The onset of saturation effects decreases the degree of magnitude-dependence of the ground motion amplitudes. While larger values of regression coefficient $c_1$ mean stronger saturation effects, it is difficult to appreciate this decrease in magnitude-dependence from just examination of Eqn. 2.3 and the corresponding regression coefficients. The concept of "effective magnitude scaling" will be introduced to quantify the decrease in magnitude-dependence due to the onset of saturation effects, which are expected to be important at close distances to large earthquakes.

For small magnitudes ($M < 5$), horizontal ground motion amplitudes scale as (averaging coefficients $a, b$, and $d$ of rock and soil for acceleration, velocity, and displacement)

$$
\begin{aligned}
\text{horizontal acceleration, } \ddot{U} &\sim 10^{0.8M} 10^{-2.4 \times 10^{-3}R} \frac{1}{R^{1.4}} \\
\text{horizontal velocity, } \dot{U} &\sim 10^{0.9M} 10^{-6.3 \times 10^{-4}R} \frac{1}{R^{1.5}} \\
\text{horizontal displacement, } U &\sim 10^{1.1M} 10^{-6.5 \times 10^{-7}R} \frac{1}{R^{1.5}}
\end{aligned}
\tag{3.1}
$$

Note that the scaling in Eqn. 3.1 is valid for $M < 5$, when saturation effects are not expected to be important (and hence $C(M)$ is close to 0).

## Magnitude scaling

Eqn. 3.1 shows that for small magnitudes ($M < 5$), lower frequency ground motions have a stronger magnitude dependence than higher frequency ground motions ($a$ coefficient in Eqn. 2.3). This is consistent with Brune spectral scaling, where high frequency spectra scale as $M_o^{1/3}$ or $\sim 10^{0.5M}$, and low frequency spectra scale with

$M_o$ or $\sim 10^{1.5M}$ (where $M_o$ is seismic moment, which scales with magnitude as $M_o \sim 10^{1.5M}$).

Despite being high-pass filtered, the scaling of displacement amplitudes with magnitude is somewhat consistent with theoretical scaling relationships. Except for the moment magnitude scale of Hanks and Kanamori, present-day magnitude scales define magnitude in terms of $log(D)$, where $D$ is ground displacement. The reasoning is as follows:

Consider a far field displacement pulse $D$ with duration $T$ originating from a rupture with area $L^2$. The seismic moment is defined as $M_o = \mu L^2 D$, where $\mu$ is the shear modulus. It is also the integral of the far field displacement time history ($M_o \sim DT$). The stress drop, $\Delta\sigma$, is equal to $C\mu\frac{D}{L}$. This implies that $D \sim \Delta\sigma L$. Thus,

$$
\begin{aligned}
M_o &\sim L^2 D \sim L^3 \Delta\sigma \\
L &\sim \left(\frac{M_o}{\Delta\sigma}\right) \\
T &\sim \frac{L}{V_R} \sim \frac{M_o^{1/3}}{V_R \Delta\sigma^{1/3}} \\
D &\sim \frac{M_o}{T} \sim M_o^{2/3} \Delta\sigma^{1/3} \\
\log D &\sim \frac{2}{3} M_o + \frac{1}{3}\Delta\sigma \\
\text{since} \quad M &\sim \frac{2}{3} M_o \\
\log D &\sim M + \frac{1}{3}\Delta\sigma \\
\text{hence} \quad M &\sim \log D
\end{aligned}
$$

Based on this reasoning (which is consistent with Richter's definition of magnitude as log of ground motion amplitude), the magnitude-dependence coefficient for displacement should be $a = 1$, if $\Delta\sigma$ is constant.

From theory, we have that

$$\log_{10} D \sim M \qquad \text{far field distances, } M < 6 \qquad (3.2)$$

$$D \sim M_o^{1/3} \qquad \text{at close distances, } M > 6 \qquad (3.3)$$

$$\text{but } \log_{10} M_o \sim 1.5M$$

$$\text{so } M_o \sim 10^{1.5M}$$

$$D \sim (10^{1.5M})^{1/3}$$

$$\text{so } \log_{10} D \sim 0.5M \qquad \text{at close distances, } M > 6 \qquad (3.4)$$

From Table 3.1 and Eqn. 3.1, the magnitude-dependence for $M < 5$ of displacement S-wave envelope ($a \approx 1.1$) is consistent with the definition of magnitude.

The displacement attenuation relationships are also consistent with theoretical displacement scaling at close distances to large events, though this is not immediately obvious from Table 3.1. From Eqn. 3.4, we expect $\log_{10} D$ to have $\sim 0.5$ slope with respect to magnitude in the near-field. At close distances to large events, the saturation term $C(M)$ in our ground motion model (Eqn. 2.3) is non-zero, and the resulting magnitude-dependence will be less that that given by regression coefficient $a$. The concept of "effective magnitude scaling" will be used. It is defined (in this study) as the magnitude-dependence of ground motion amplitudes, taking saturation effects into account. From this definition, effective magnitude scaling is given by the partial derivative of our ground motion model Eqn. 2.3 with respect to magnitude; it is a function of both magnitude and distance. Effective magnitude scaling has its maximum in the absence of saturation effects, or $C(M) = 0$. Thus, the values of $a$ listed in Table 3.1 represent maximum effective magnitude scaling. The partial derivative of Eqn. 2.3 with respect to magnitude, $\frac{\partial \log_{10} A}{\partial M}$, is

$$a - b\left(\frac{c_1 e^{c_2(M-5)}}{1 + (M-5)^2} + c_1 c_2 e^{c2(M-5)}(1.4 + \arctan(M-5))\right) -$$
$$\frac{d\left(\frac{c_1 e^{c_2(M-5)}}{1 + (5-M)^2} + c_1 c_2 e^{c_2(M-5)}(1.4 + \arctan(M-5))\right)}{\sqrt{R^2 + 9} + c_1 e^{c_2(M-5)} \ln(10)} \qquad (3.5)$$

$M = 6, R = 0$ is used to represent the condition "at close distances to large earthquakes". The effective magnitude scaling in this region of magnitude distance space varies with frequency band, as shown by its dependence of the regression coefficients $(a, b, c_1, c_2, d, e)$

$$a - b\left(\frac{c_1 e^{c_2}}{2} + 2.19 c_1 c_2 e^{c_2}\right) - \frac{d\left(\frac{c_1 e^{c_2}}{2} + 2.19 c_1 c_2 e^{c_2}\right)}{3 + 2.19 c_1 e^{c_2} \ln(10)} \tag{3.6}$$

Using the appropriate $(a, b, c_1, c_2, d, e)$ for displacement (on rock sites) from Table 3.1, the effective magnitude scaling of S-wave displacement amplitudes at close distances to large events is approximately

$$\log_{10} D \sim 0.42 M \tag{3.7}$$

which is quite close to the theoretically expected value of $\sim 0.5$. Thus, while the displacement amplitudes predicted by Eqn. 2.3 are smaller than true displacements (due to the high pass filtering to remove microseism effects), the effective magnitude scaling at close distances to large events is consistent with theoretical scaling relations. It would be possible to modify Eqn. 2.3 to achieve better agreement between the predicted amplitudes and true peak displacements observed at close distances to large earthquakes. For now, the form of Eqn. 2.3 is preserved, for the convenience of having a single functional form for ground motion amplitudes from all channels being considered.

The linear magnitude dependence coefficient $a$ of Eqn. 2.3 can be directly interpreted as the scaling term for small magnitudes. For $M > 5$, Eqn. 2.3 allows saturation effects to come into play. The effective magnitude scaling is defined as the magnitude-dependence of ground motion amplitudes, explicitly accounting for the effects of saturation. From this definition, it must be the partial derivative of Eqn. 2.3 with respect to magnitude, and is thus a function of magnitude and distance. Table 3.2 shows effective magnitude scaling at $M = 6, R = 0$ for acceleration, velocity, and displacement on rock and soil sites.

## Distance scaling

In theory, geometric spreading for body waves in a linearly elastic whole space results in amplitudes attenuating as $\frac{1}{R}$, where $R$ is source to station distance. This corresponds to $d = 1$ in Eqn. 2.3. However, a linearly elastic whole space makes for an overly simplistic earth model. From Table 3.1, $d > 1$ for acceleration, velocity, and displacement on both rock and soil sites. Thus, observed ground motion amplitudes attenuate at a faster rate than theoretically predicted for a linearly elastic earth. In a more realistic earth model, body wave velocities increase with depth, basin structures give rise to surface waves (which decay as $\frac{1}{\sqrt{R}}$), heterogeneities in the crust give rise to scattering effects, and the crust is an attenuating medium. These factors cause deviations from results predicted by a linearly elastic whole space. While Eqn. 2.3 has a term for exponential decay ($\log_{10}(A) \sim -bR$), which is usually attributed to anelastic attenuation and scattering effects, in practice, it is difficult to distinguish between geometric spreading, anelastic attenuation, and other effects caused by a heterogeneous, imperfectly elastic, layered earth. One alternative is to view the coefficients in Table 3.1 simply as the coefficients that best fit the data, given the ground motion model in Eqn. 2.3.

The regression results summarized in Table 3.1 and Eqn. 3.1 show that the $\log R$ dependence is relatively constant at $d \sim 1.5$ as we go from acceleration, to velocity, to displacement, but that the coefficient $b$ of the exponential distance dependence increases with frequency. (The relative sizes of these distance decay terms for the different frequency bands is shown in Figure 3.1.) This is consistent with the ideas that:

- high frequencies are more sensitive to small scale heterogeneities in the crust, and thus exhibit stronger scattering effects (Lay and Wallace, 1995)

- higher frequencies (acceleration) attenuate faster than lower frequencies (velocity and displacement) (Hanks and McGuire, 1981)
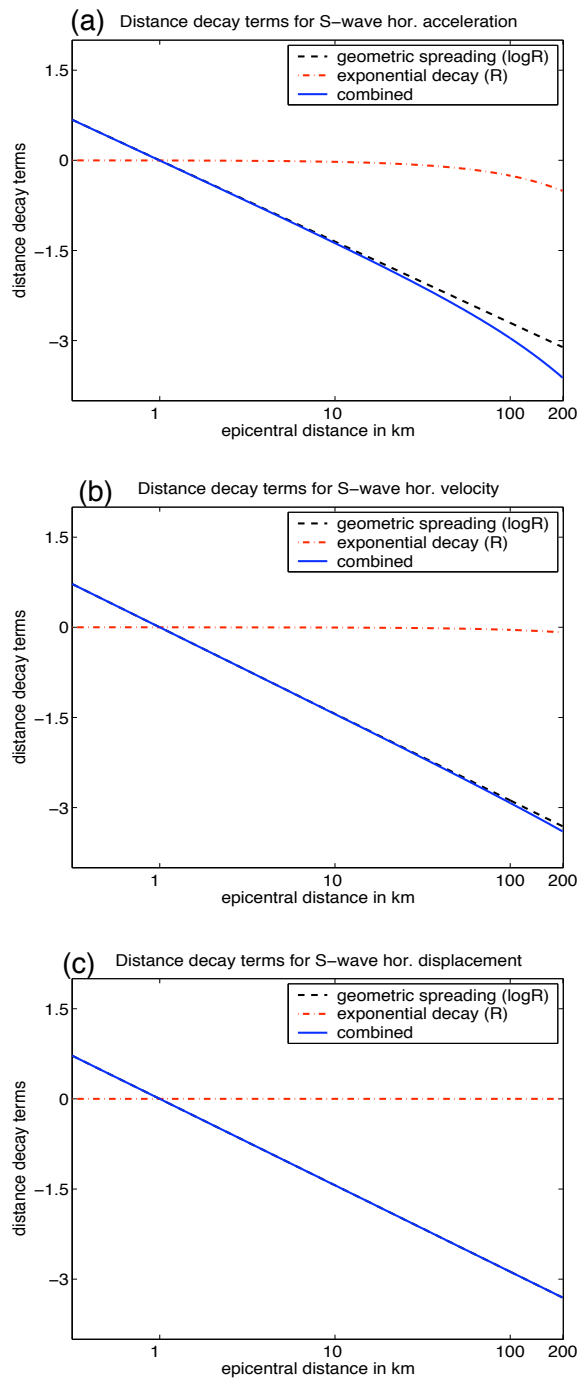
Figure 3.1: The relative sizes of the geometric spreading and exponential decay terms for the horizontal S-wave envelope amplitude attenuation relationships for (a) acceleration, (b) velocity, and (c) filtered displacement. The distance decay is generally dominated by the geometric spreading (power law) decay. The exponential decay term is largest for acceleration, but has practically no contribution to the distance decay of displacement amplitudes.

## Frequency dependence of scattering effects?

The last two columns in Table 3.1 are the standard errors of regression without and with station corrections. When station corrections are not accounted for on rock sites, it appears that the standard error (or scatter) decreases with frequency. This is in contrast to findings of Hanks and McGuire (1981); they observed that peak accelerations decay with "no more and seemingly less scatter than do the velocities and displacements". They attribute the additional scatter in lower frequencies to peak velocities and displacements being a mix of body and surface wave amplitudes (as opposed to peak accelerations consistently being from body waves). Table 3.1 exhibits no such trend. In fact, it shows the opposite trend (high frequencies with largest scatter) when station corrections are not accounted for. For soil sites, it appears that velocities have the smallest scatter, regardless of having corrected for stations or not. There is no such trend in soil sites when station corrections are not accounted for; no such trend is evident for either rock or soil sites after accounting for station corrections. Without formal statistical significance tests, the possibility that the frequency dependence of the scatter (or standard error of regression) is best described by a constant cannot be ruled out.The composition of databases is a possible source of these contrasting observations. Hanks and McGuire examined moderate-to-large earthquakes ($M > 4$); the database for this study has a large percentage of small events ($M < 4$).

In general, there appears a remarkable similarity in the standard errors of regression of the envelope amplitude attenuation relationships for acceleration, velocity, and displacement on both rock and soil sites after accounting for station corrections. Regardless of frequency band or site class, it appears that the standard error of regression is constant, at $\sigma_{corr} \approx 0.23$.

There are a number of factors that give rise to different behavior between low and high frequency ground motions. Hanks (1975) and Hanks and McGuire (1981) performed complementary studies on characteristics of low and high frequency ground motions from large earthquakes. From Hanks (1975), some factors with first order sig-

nificance in determining low frequency ground motion displacements from large events are: seismic moment, source dimension, radiation pattern, source propagation, the development and dispersion of surface waves, and local basin structure. Hanks (1975) found strong coherence in displacement amplitude and phase for small variations in source-station distance and azimuth for a given event (San Fernando mainshock); his primary conclusion was that the "gross structure of long-period strong ground motion recorded at local distances can at least be explained by well understood seismological phenomena". In contrast, high frequency ground motions are generally not as well understood. High frequency ground motions do not have much energy from surface waves, and radiation pattern and directivity effects are not as strong as in the lower frequencies. Hanks and McGuire (1981) found that the phase coherence present in low frequency ground motions for small variations in distance and azimuth was absent at higher frequencies. They observed that high frequencies are only weakly dependent on magnitude at closer distances, and felt it impossible to deterministically synthesize high frequency ground motions in the time domain, except under unusual circumstances of small station spacing, small and simple earthquakes ($M < 5$), close distances ($< 10$ km), and uncomplicated geology (Hanks and McGuire, 1981). They describe high frequency ground motions as "chaotic, but stochastically well-behaved", and attribute high frequency radiation to the source rather than the path.

## 3.2 Rock versus soil sites

The envelope attenuation relationships developed allow comparisons of attenuation characteristics of rock and soil sites as a function of magnitude, distance, and frequency. Again acceleration, velocity, and displacement are used as proxies for high-, mid-, and low-frequency ground motions. Table 3.1 shows that the magnitude- (coefficient $a$) and $\log R$ (coefficient $d$) dependence are slightly stronger for soil throughout the different frequency bands. As shown in Table 3.1, the standard errors of regression without station corrections are consistently higher for soil sites for all frequencies. However, after accounting for station corrections, the standard errors for rock and
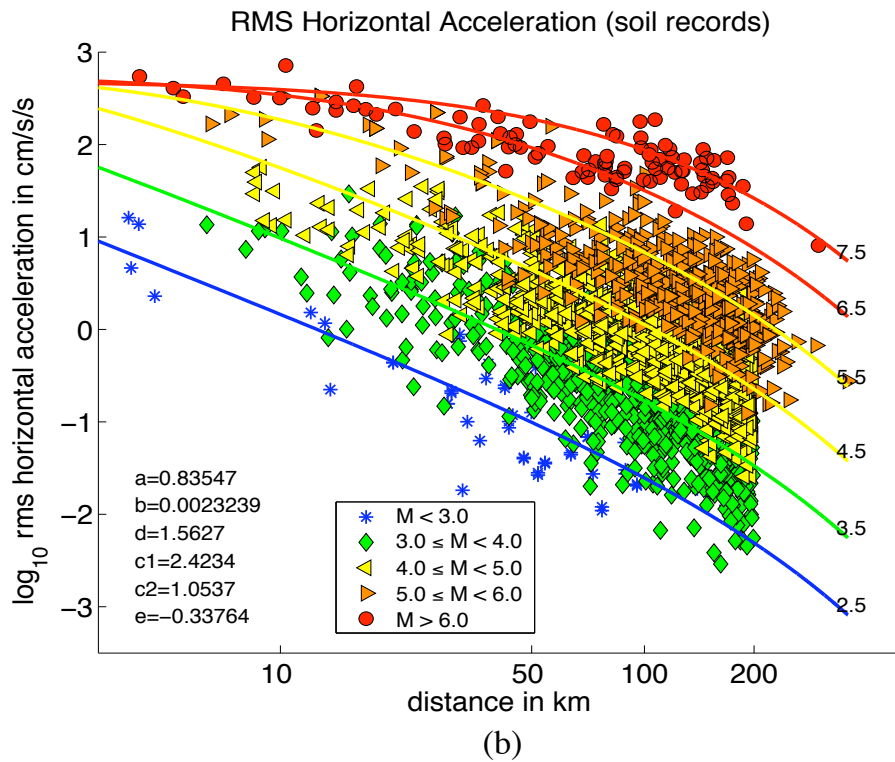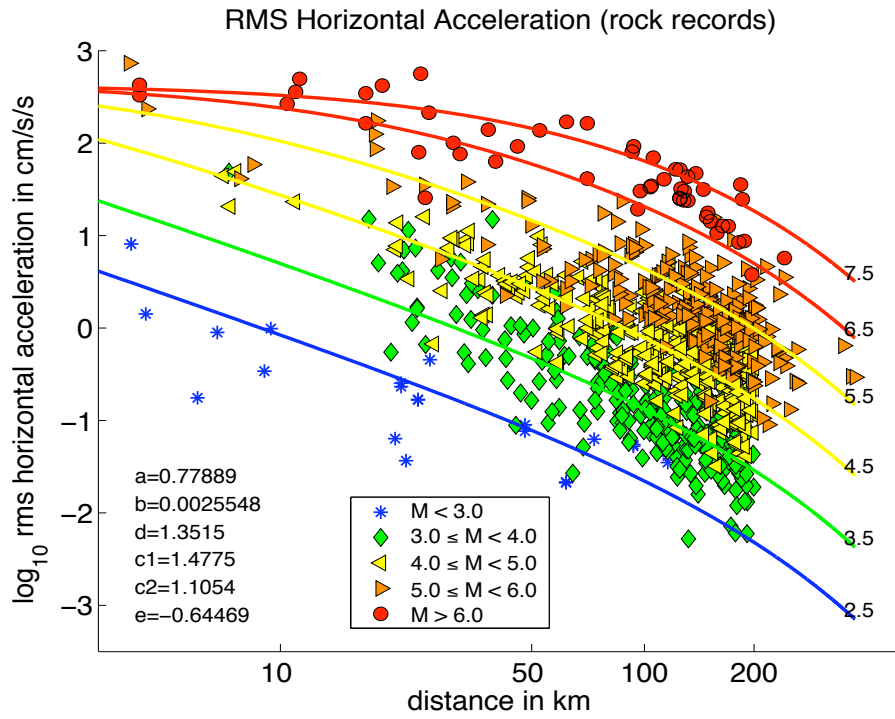
Figure 3.2: Observed S-wave envelope acceleration amplitudes (rms of horizontal, without station corrections) and curves of predicted amplitudes against distance at various prescribed magnitudes for (a) rock sites and (b) soil sites.
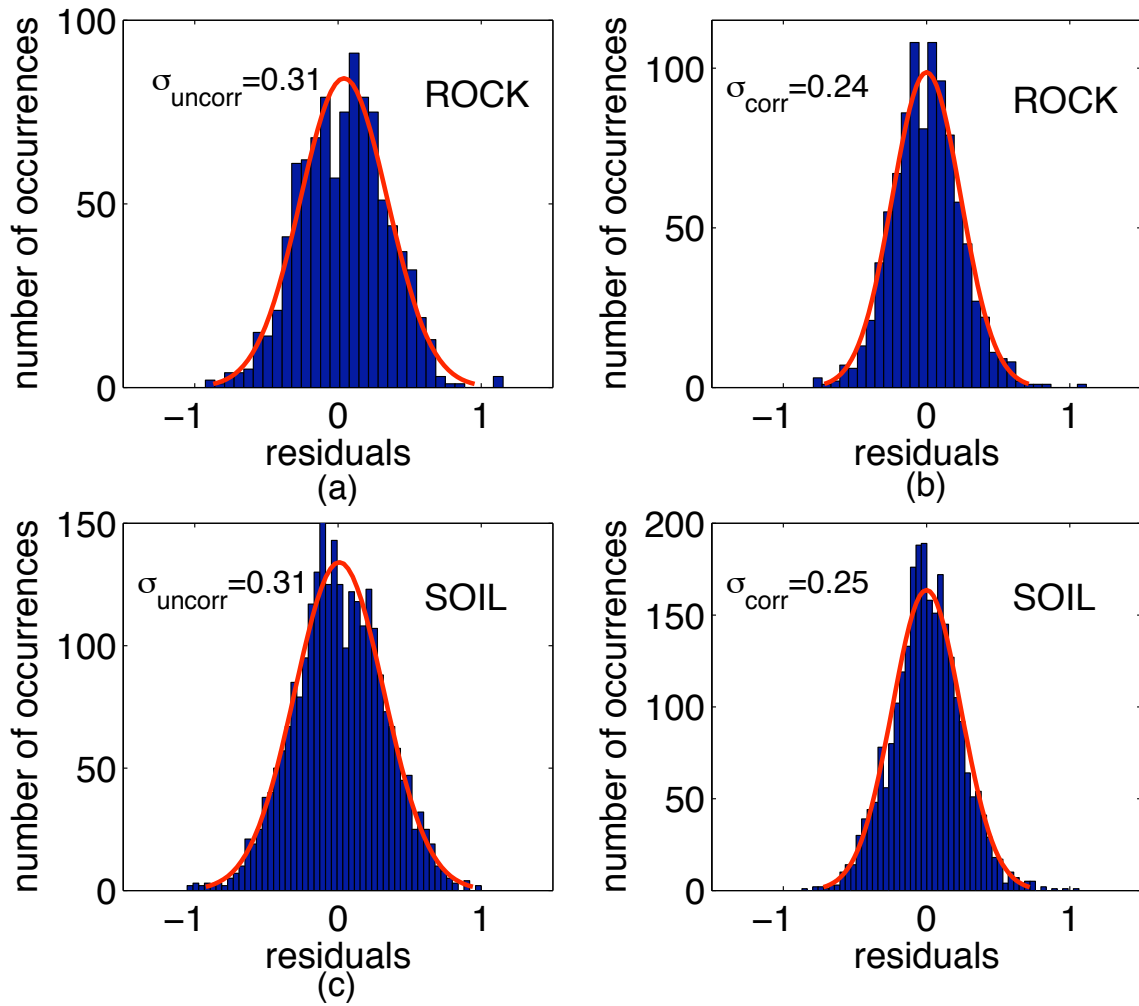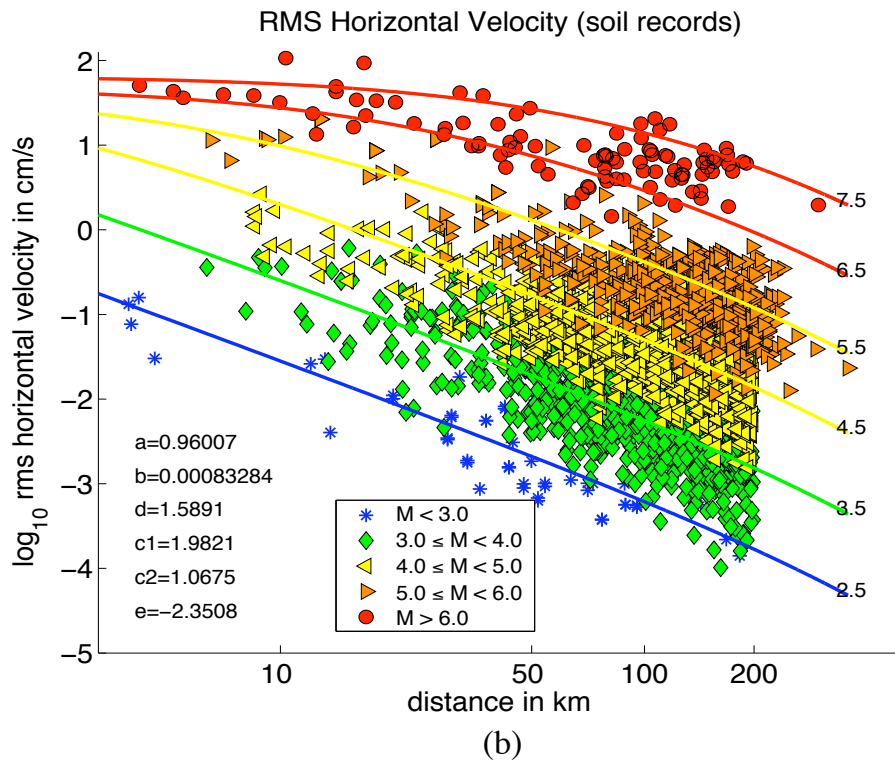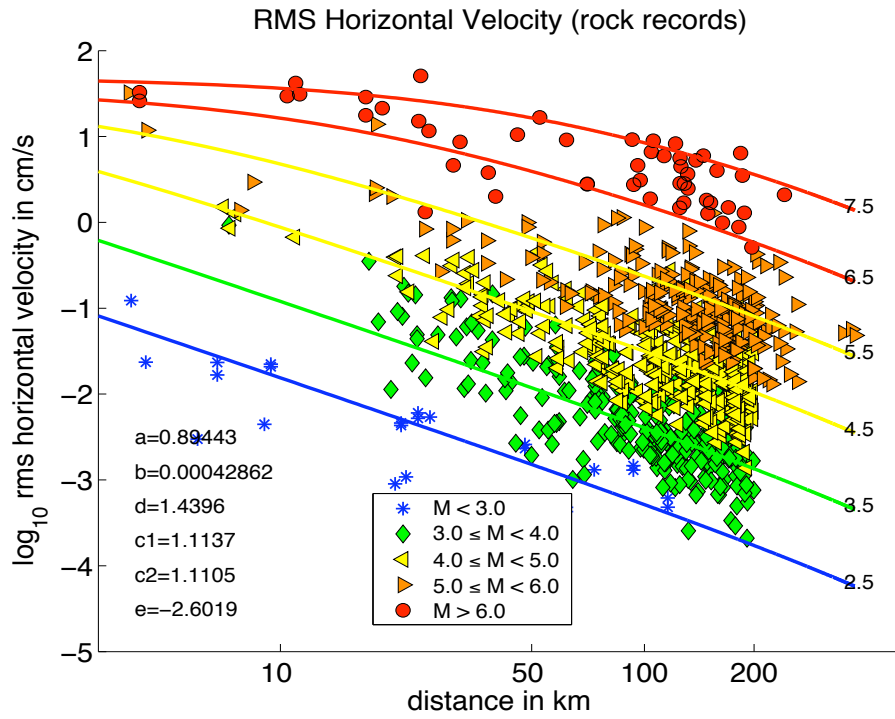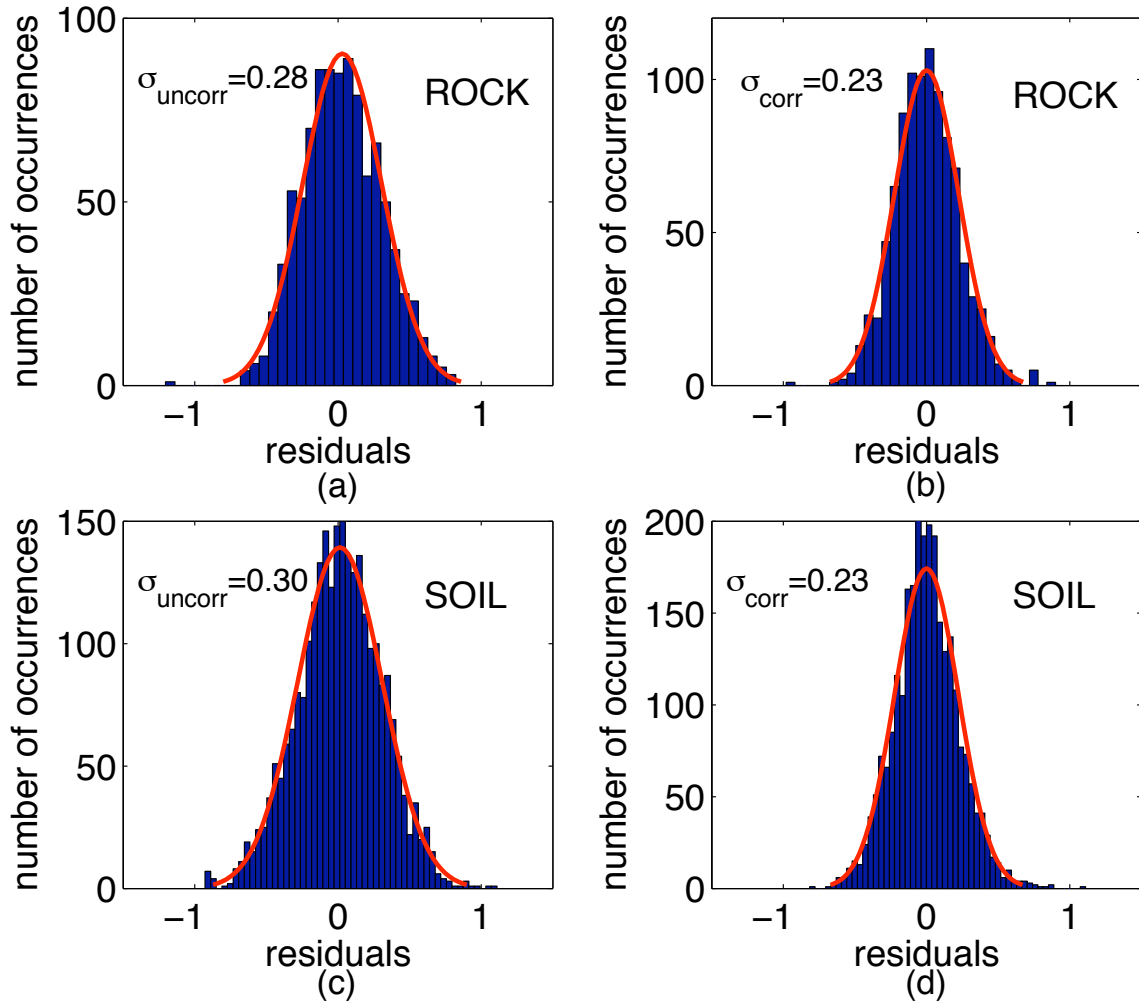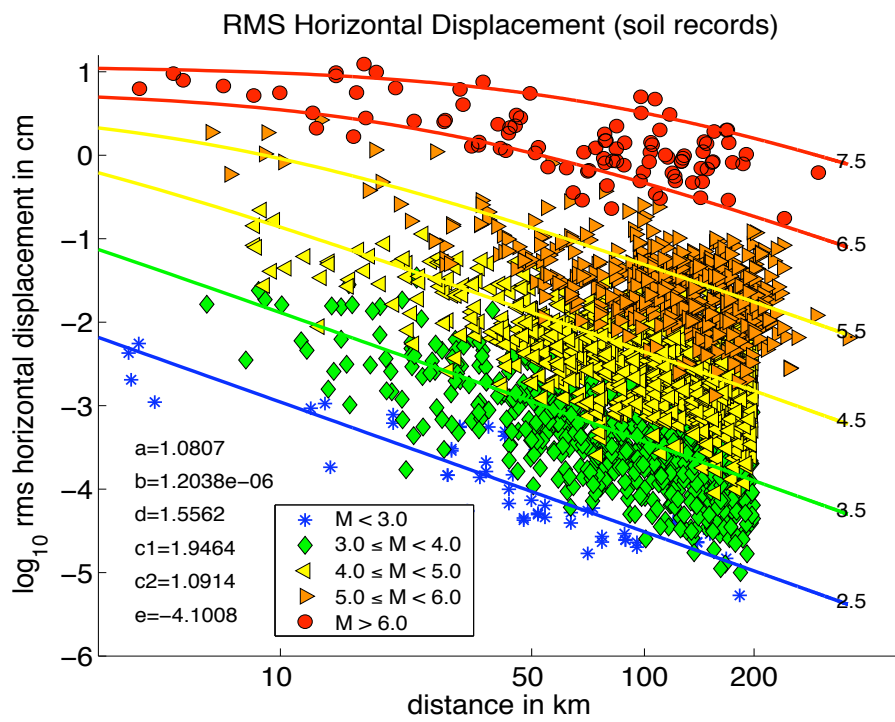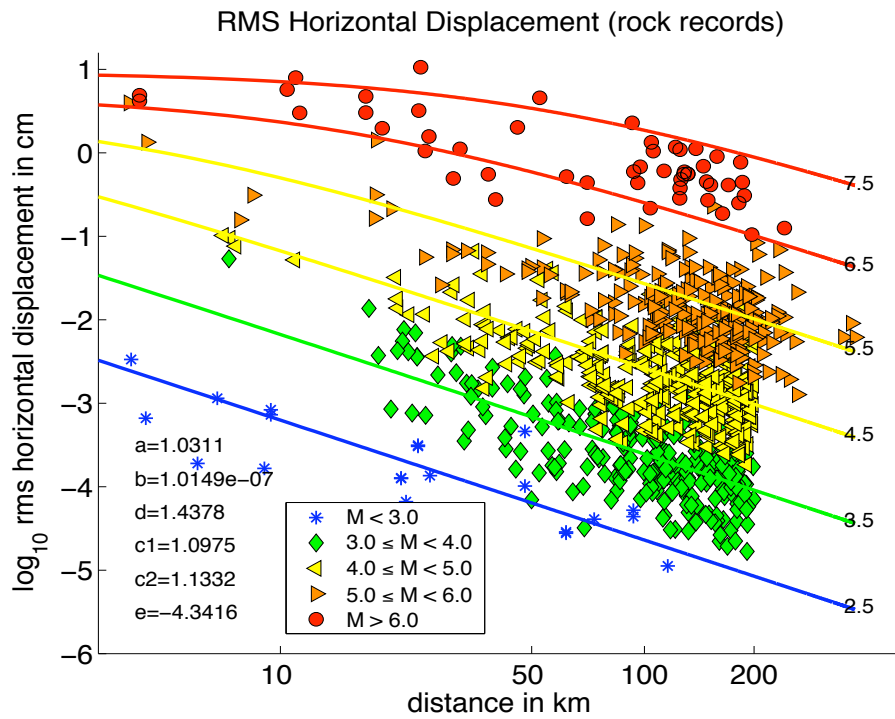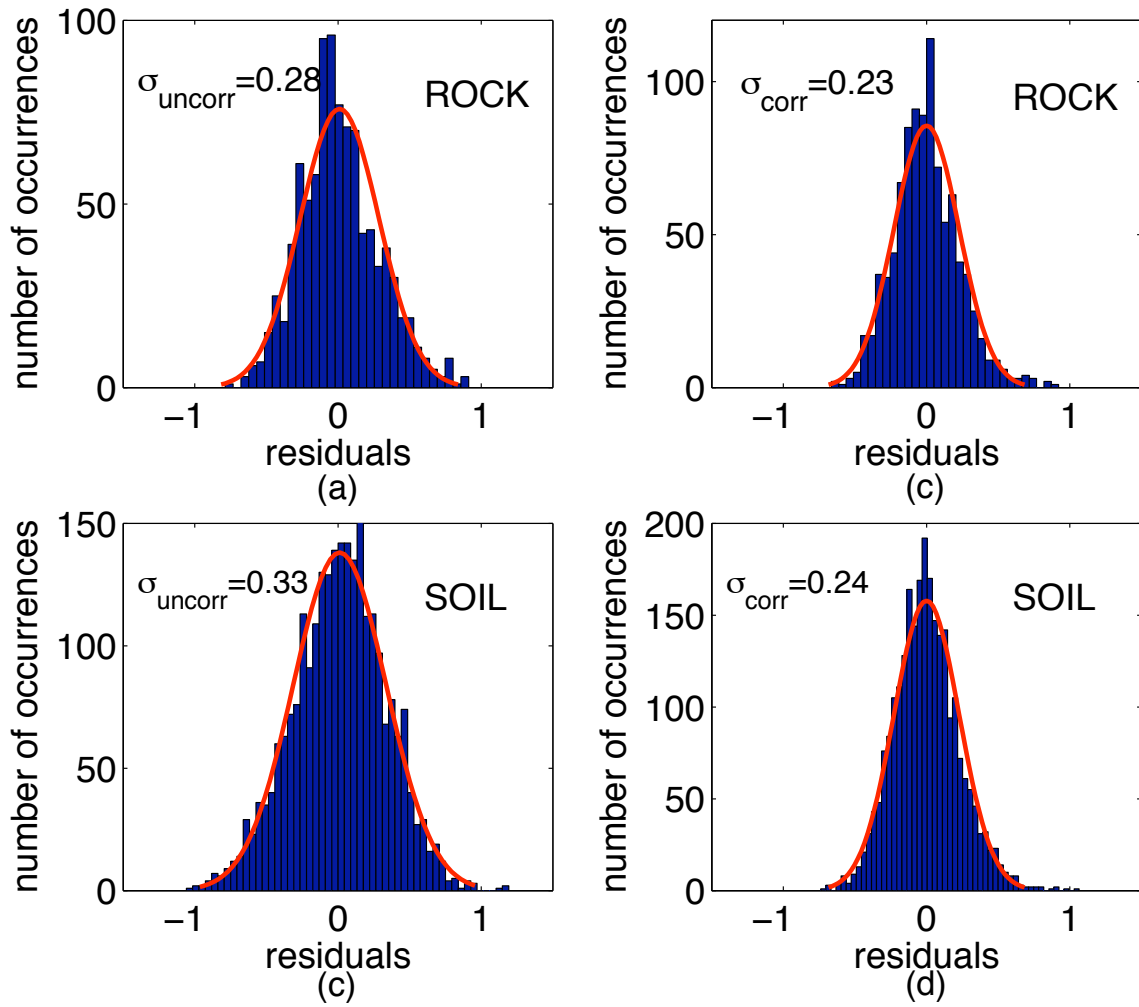
Figure 3.3: Histogram of residuals relative to Eqn. 2.3 for rms horizontal S-wave acceleration for: (a) rock sites without station corrections, (b) rock sites with station corrections, (c) soil sites without station corrections, and (d) soil sites with station corrections. Station corrections introduce a reduction in standard error of about 20%. There appears little difference in standard errors of regression between rock and soil sites.

Figure 3.4: Observed S-wave envelope velocity amplitudes (rms of horizontal, without station corrections) and curves of predicted amplitudes against distance at various prescribed magnitudes for (a) rock and (b) soil sites.

Figure 3.5: Histogram of residuals relative to Eqn. 2.3 for rms horizontal S-wave velocity for: (a) rock sites without station corrections, (b) rock sites with station corrections, (c) soil sites without station corrections, and (d) soil sites with station corrections. Station corrections reduce the standard error of regression by 18% and 23% for rock and soil, respectively. The standard error of regression after accounting for station corrections is identical for rock and soil sites.

Figure 3.6: Observed S-wave envelope displacement amplitudes (rms of horizontal, without station corrections) and curves of predicted amplitudes against distance at various prescribed magnitudes for (a) rock and (b) soil sites.

Figure 3.7: Histogram of residuals relative to Eqn. 2.3 for rms horizontal S-wave displacement for: (a) rock sites without station corrections, (b) rock sites with station corrections, (c) soil sites without station corrections, and (d) soil sites with station corrections. Station corrections reduce the standard error of regression $\sigma$ by 18% and 27% for rock and soil, respectively.

soil sites are remarkably similar. Histograms of residuals with and without station corrections for rock and soil sites are shown in Figures 3.3, 3.5, and 3.7. The average reduction in standard error due to station corrections is about 20% (log units). Thus, station corrections are effective in accounting for localized site effects. (While stations corrections help, the improvements in the standard error due to introducing station corrections are small relative to the improvement from distinguishing between rock and soil.) From Table 3.1, the coefficients having the largest difference between rock and soil sites are the saturation term ($c_1$) and the constant term $e$. The constant term $e$ is consistently $\sim 0.3$ log units ($\sim$ factor 2 on a linear scale) larger for soil sites relative to rock. This does not mean that ground motion amplitudes on soil sites are on average twice as large as those on rock, since there are possible trade-offs between this constant and the magnitude and distance dependencies. Closer examination of saturation effects shows that the difference between rock and soil amplitudes are not constant, but rather, magnitude and distance dependent.

## Comparisons of magnitude and distance scaling for rock and soil sites

Figures 3.8, 3.9, and 3.10 show predicted amplitude curves of ground motion models such as Eqn. 2.3 for rock and soil sites as functions of (a) distance and (b) magnitude for acceleration, velocity, and displacement. Such plots are useful in visualizing the effects of saturation as functions of magnitude and distance for rock and soil sites.

From Figure 3.8, peak acceleration saturates at close distances to large earthquakes. This is evident from the decrease in slope at close distances to large earthquakes of the predicted amplitude curves as functions of distance and magnitude. From Figures 3.9 and 3.10, velocity and displacement also exhibit saturation effects, though of a lesser degree than acceleration. The degree of saturation can be quantified by the effective magnitude scaling discussed earlier in this chapter. Table 3.2 lists effective magnitude scaling (the partial derivative of Eqn. 2.3 with respect to magnitude) evaluated at $M = 6, R = 0$ for S-wave envelope amplitudes on rock and

soil sites for acceleration, velocity, and filtered displacement. The smaller the effective magnitude scaling, the stronger the effects of saturation. Table 3.2 shows that effective magnitude scaling increases with period. Thus, the degree of saturation increases with frequency. Of the three frequency bands, acceleration exhibits the strongest saturation effects. Soil sites consistently show stronger saturation effects relative to rock sites for a given frequency band. This is consistent with the idea that nonlinear soil response contributes to saturation effects.

The difference between rock and soil amplitudes decreases with increasing ground motion amplitude. That is, soil sites exhibit a stronger degree of saturation than rock sites. This is evident from Figures 3.8 through 3.10, as well as from Table 3.1 ($c_1$ is consistently larger for soil than rock). This effect is strongest in peak acceleration, but also present in a lesser degree in velocity and displacement. This is consistent with Campbell (1981), who observed a similarity in level of acceleration recorded on rock and soil sites when subject to strong ground motion. From Figures 3.8 through 3.10, the difference between rock and soil sites for horizontal ground motions is a function of both magnitude and distance. Thus, the difference between their constant regression coefficients $e_{soil} - e_{rock}$ is not a good estimate of the average amplification on soil sites relative to rock. This will be discussed shortly.

$\frac{\partial \log_{10} A}{\partial M}$ evaluated at $M = 6, R = 0$
for rms horizontal S-wave envelope amplitudes

| site | acceleration | velocity | displacement |
|------|-------------|----------|--------------|
| rock | 0.15 | 0.29 | 0.42 |
| soil | 0.064 | 0.22 | 0.36 |

Table 3.2: Effective magnitude scaling of acceleration, velocity, and displacement on rock and soil sites at close distances to large events. These values are the partial derivatives of $\log_{10}(A)$, where $A$ is rms acceleration, velocity, and displacement S-wave envelope amplitude for rock and soil sites, evaluated at $M = 6$ and $R = 0$.

The smaller the "effective" magnitude scaling, the stronger the effects of saturation. Table 3.2 shows that the degree of saturation increases with frequency, with acceleration having the strongest saturation effects. Soil sites also consistently exhibit

stronger saturation effects than rock sites throughout the different frequencies. This is consistent with the idea that nonlinear soil response contributes to saturation-type effects.

## Site amplification

This study examined ground motions recorded at stations of what is currently known as CISN (formerly TriNet and TERRAscope) over an extended period of time. As mentioned in Chapter 1, this allows us to define station corrections that account for the systematic deviations of ground motions at particular stations relative to the average values given by the attenuation relationships for a given ground motion channel. Thus far, station corrections for rock sites were defined relative to the rock attenuation relationships, and corrections for soil sites relative to the soil attenuation relationships. An alternative definition for station corrections is to define corrections for both rock and soil sites relative to the average rock ground motions. Station corrections can then be interpreted as amplification factors relative to average rock ground motions predicted by the envelope attenuation relationships.

Figures 3.11, 3.12, and 3.13 show histograms of rock and soil station corrections (in $\log_{10}$ units) for rms S-wave acceleration, velocity, and displacement. Overlaid are normal density curves that best fit the histograms. The mean $\mu$ and standard deviation $\sigma$ of the best-fit normal density curves are indicated on the plots. The bottom subplot in each of these Figures directs attention to the shift of the mean soil station correction relative to average rock ground motions predicted by the envelope attenuation relationships. These Figures show that the mean soil amplification (location of peak of histogram of soil station corrections, dashed vertical line) relative to the average rock ground motions (corresponding to a station correction of 0, solid vertical line) increases with increasing period. The station corrections in $\log_{10}$ units can be converted to amplification factors on a linear scale by taking $10^{stationcorr}$. From Figures 3.11, 3.12, and 3.13, the average soil site amplifies the acceleration predicted by the rock attenuation relationships by a factor of 1.3; this amplification factor is 1.5
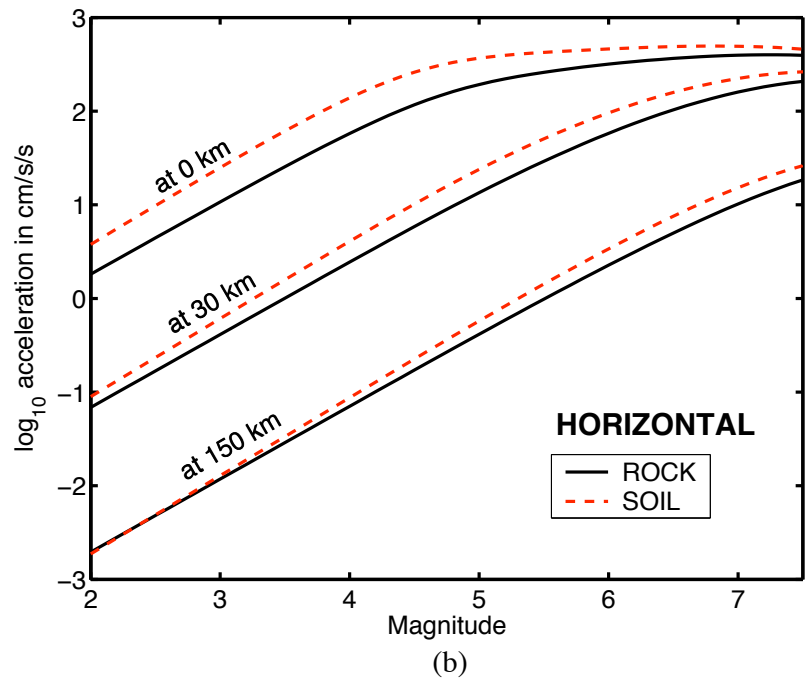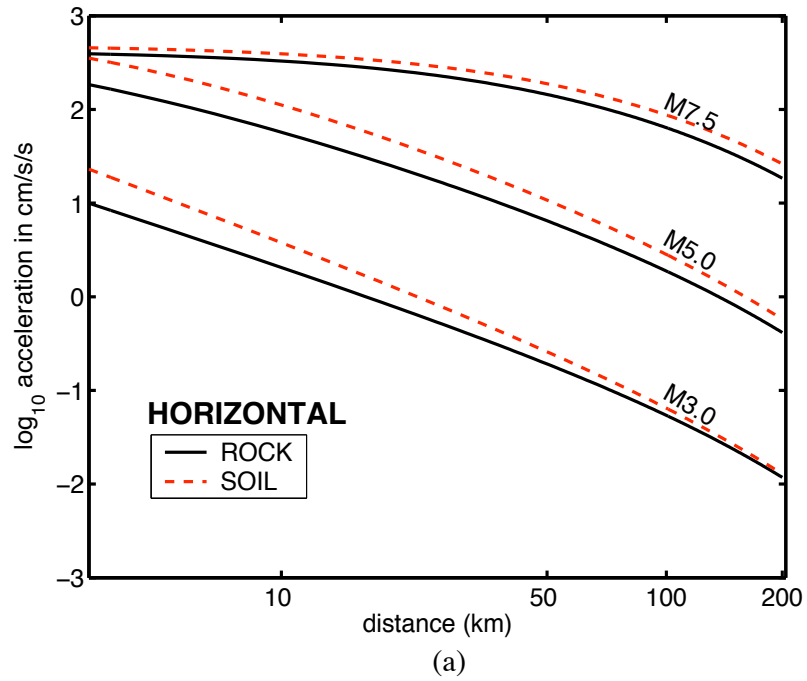
Figure 3.8: $\log_{10}$ of the root mean square of horizontal acceleration as a function of (a) distance and (b) magnitude. From both (a) and (b), the difference between rock and soil for acceleration amplitudes decreases with increasing ground motion amplitude.
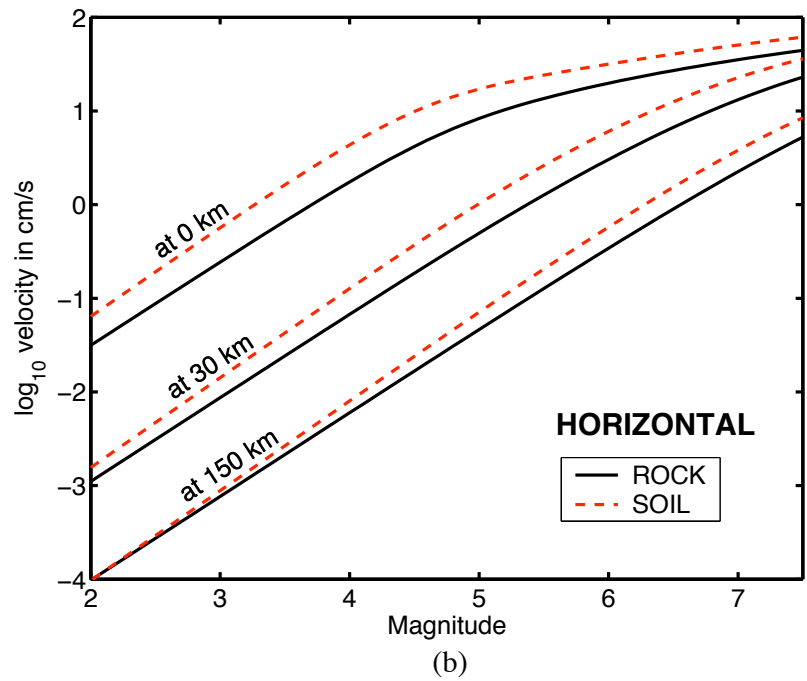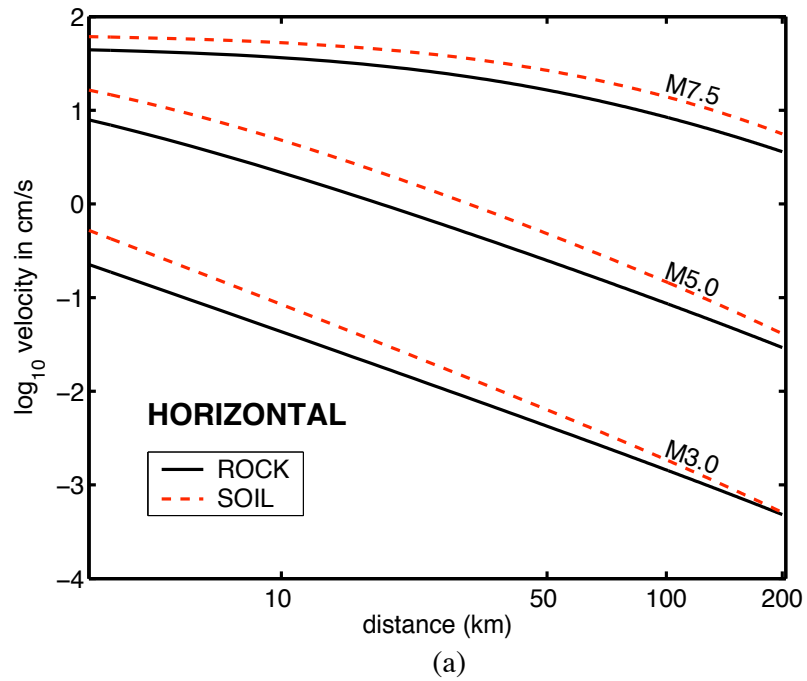
Figure 3.9: $\log_{10}$ of rms horizontal velocity as a function of (a) distance and (b) magnitude. From both (a) and (b), the difference between velocity amplitudes on rock and soil sites decreases with increasing amplitude, though to a lesser degree than for acceleration.
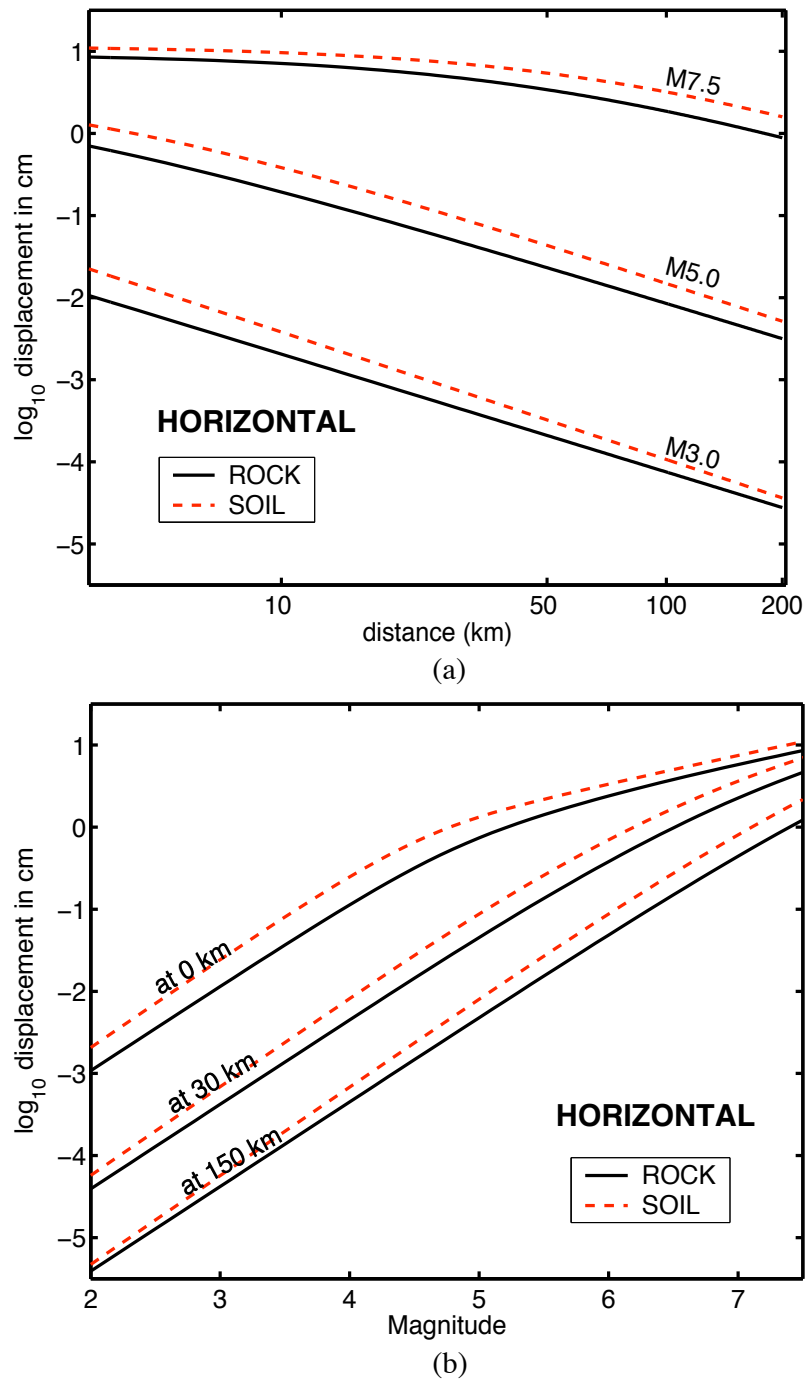
Figure 3.10: $\log_{10}$ of rms horizontal filtered displacement as a function of (a) distance and (b) magnitude. From (b), the slope of the amplitude curves relative to magnitude for $M > 5$ is approximately 1/2, which is consistent with theoretical displacement scaling in the near-field region of large events.

and 1.7 for velocity and filtered displacement, respectively. Thus, the average amplification of soil sites relative to predicted rock ground motions increases with period. Note that the average amplification factors obtained in this manner take into account saturation effects, and are smaller than those obtained by simply taking $e_{soil} - e_{rock}$.

Figures 3.14, 3.15, and 3.16 show amplification maps for peak horizontal acceleration, velocity, and displacement derived from rms horizontal S-wave station corrections relative to average rock ground motions. The letters mark station locations and denote NEHRP site classification; U denotes unknown NEHRP site classification. In these maps, the station corrections in $\log_{10}$ units are converted to linear amplification factors. Delaunay triangulation is used to interpolate amplification factors between station locations over Southern California. A total of 155 stations are used for each of the amplification maps. A common color scale, ranging from 0.1 (deamplification) to 6 (amplification), is used for the different frequency bands. A "brightening" of the amplification maps as the average soil amplification increases with period can be observed. For acceleration (Figure 3.14), the range of amplification factors is approximately $0.18 - 4$; for velocity and displacement, the ranges are approximately $0.3 - 6$ and $0.4 - 6$. Thus, there is about a factor of 10 difference between the smallest and largest amplification factors. Note that there is deamplification at some stations in all frequency bands. This means that ground motions at the "average" rock sites experience some amplification relative to hard rock sites.

Separate station corrections were also derived for P-wave amplitudes in the horizontal and vertical directions. Figures 3.17 and 3.18 show amplification maps for vertical P-wave acceleration and velocity relative to the average rock stations.

These amplification maps are derived entirely from observed ground motion amplitudes. No information on site geology is included. The NEHRP site classes at the various CISN station locations are shown only for comparison. There is general agreement between the NEHRP site classes and the amplification factors from the station corrections - B sites are darker, C sites and below are lighter. This agreement is reassuring, since they are derived from independent data.
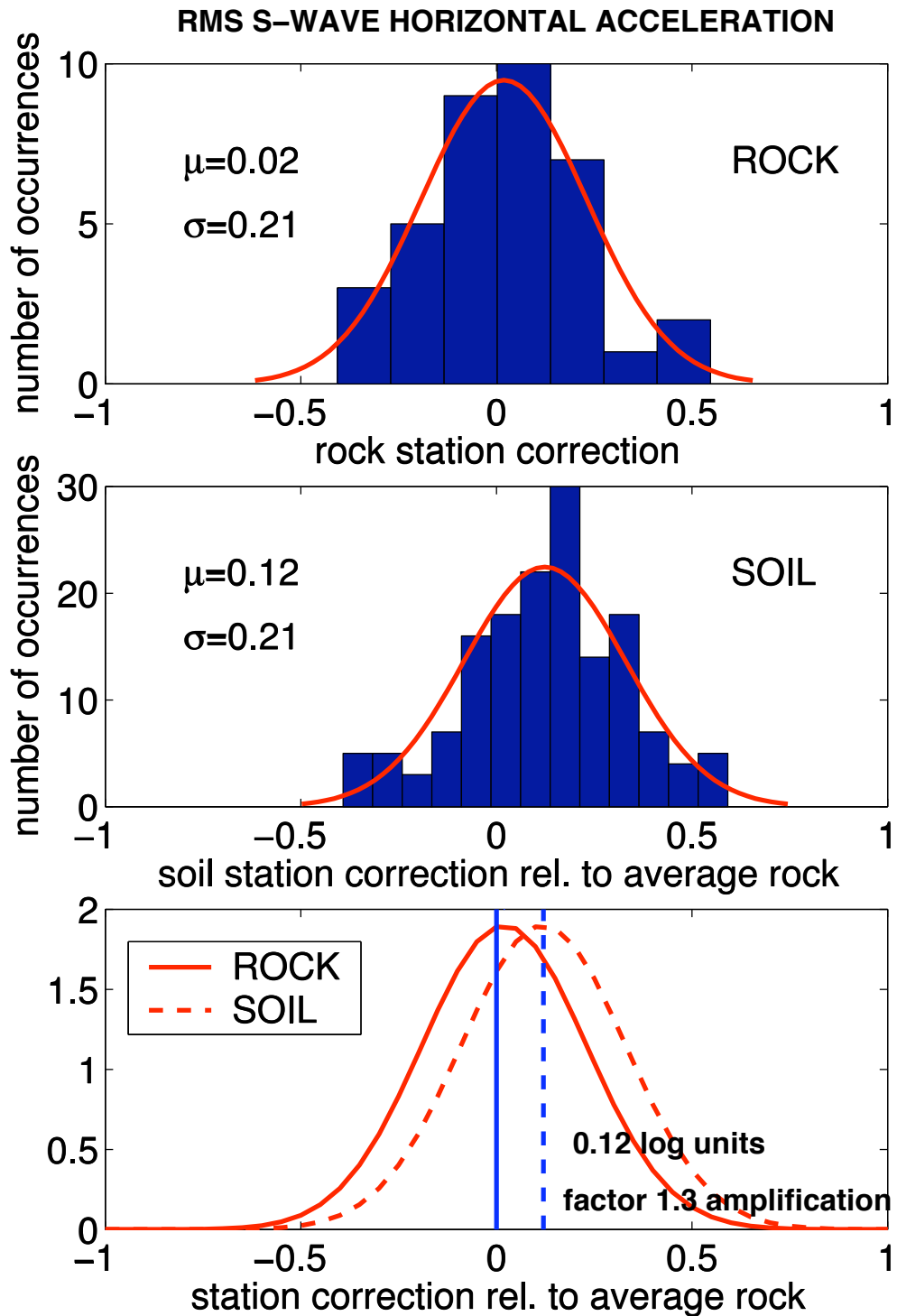
Figure 3.11: Histograms of rms acceleration station corrections for rock and soil sites. Curves are normal densities that best fit the histograms. The mean amplification of soil sites relative to average rock acceleration is a factor of 1.3.
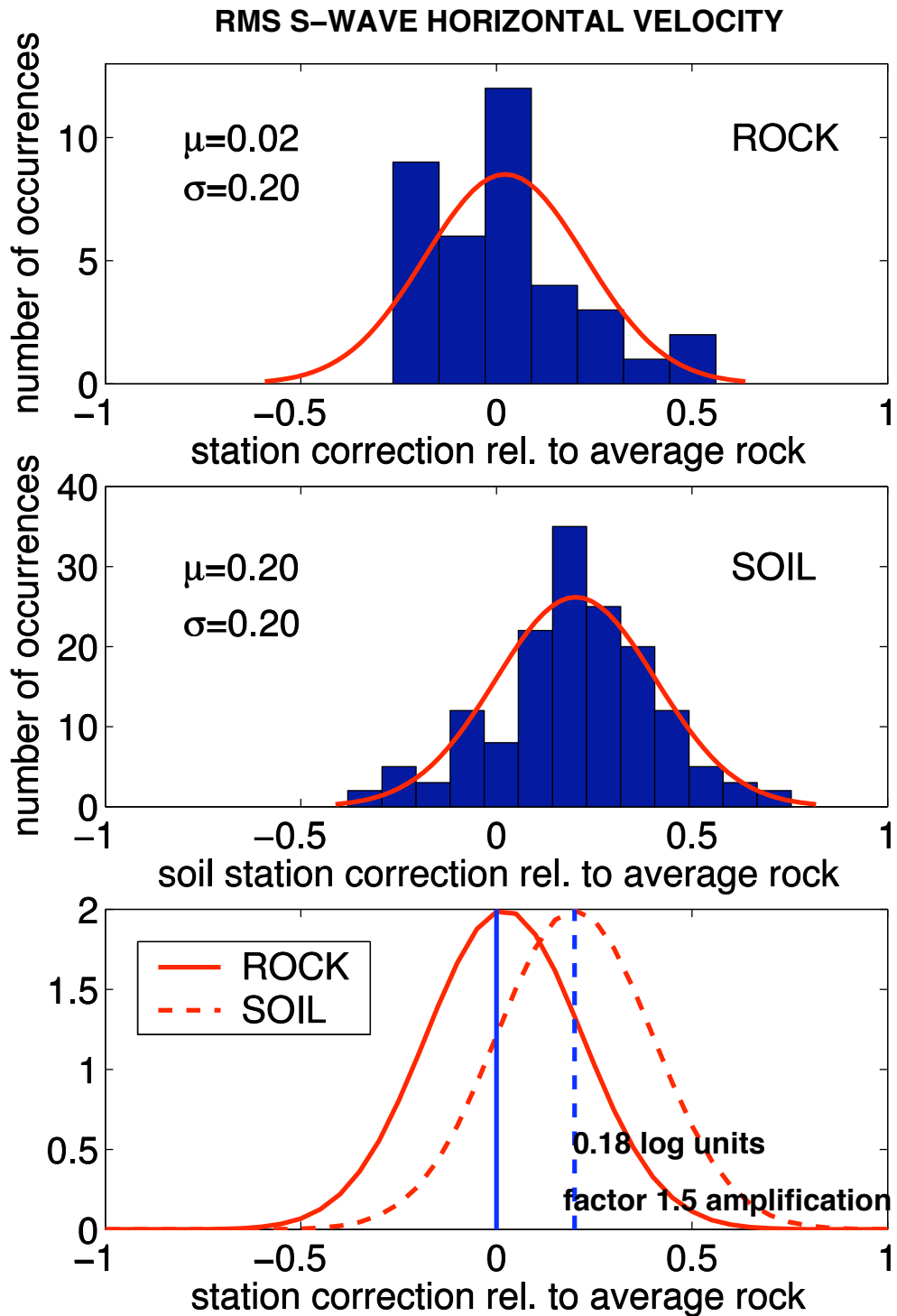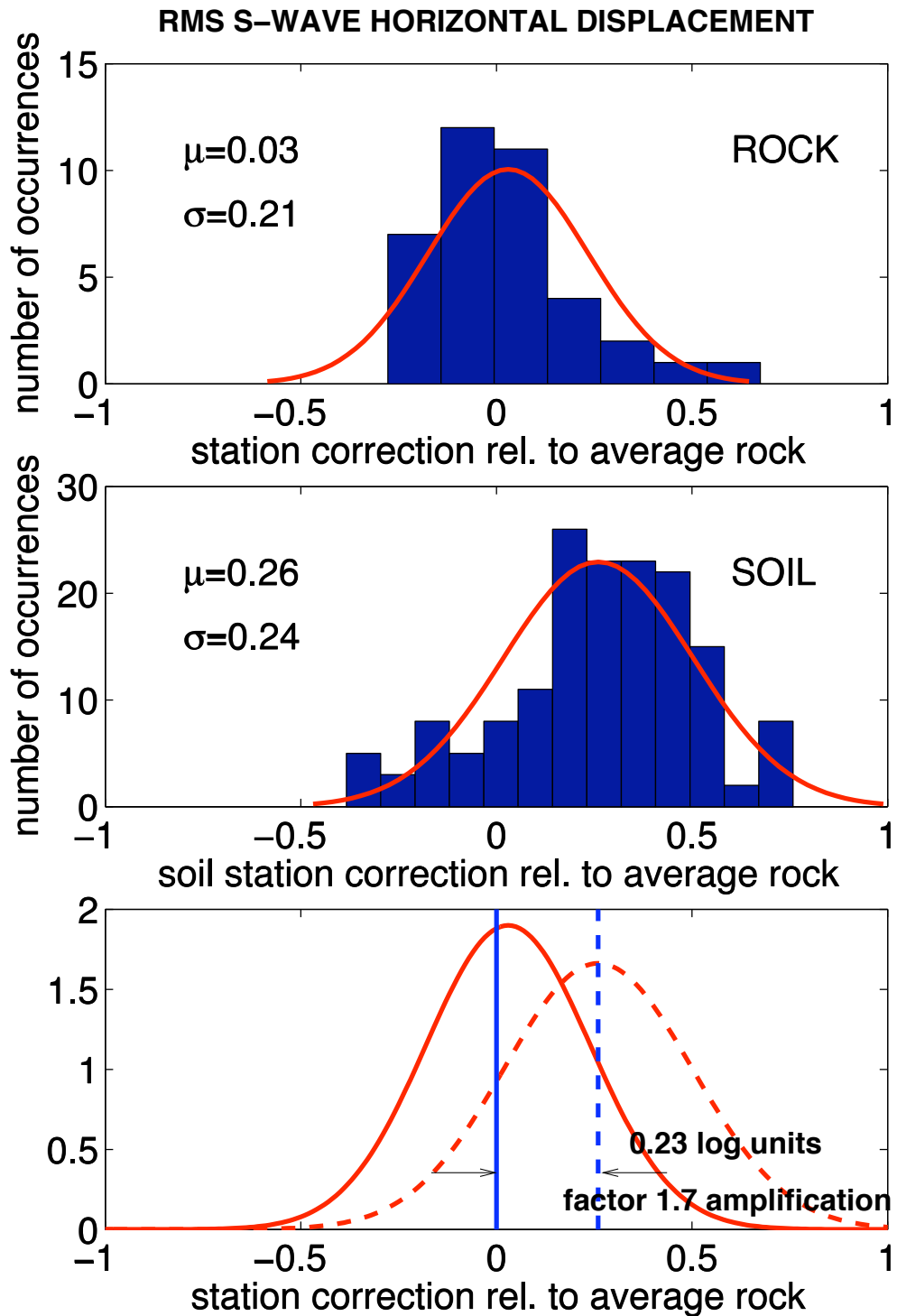
Figure 3.12: Histograms of rms velocity station corrections for rock and soil sites. Curves are normal densities that best fit the histograms. The mean amplification of soil sites relative to average rock velocity is a factor of 1.5.

Figure 3.13: Histograms of rms displacement station corrections for rock and soil sites. Curves are normal densities that best fit the histograms. The mean amplification of soil sites relative to average rock displacement is a factor of 1.7.
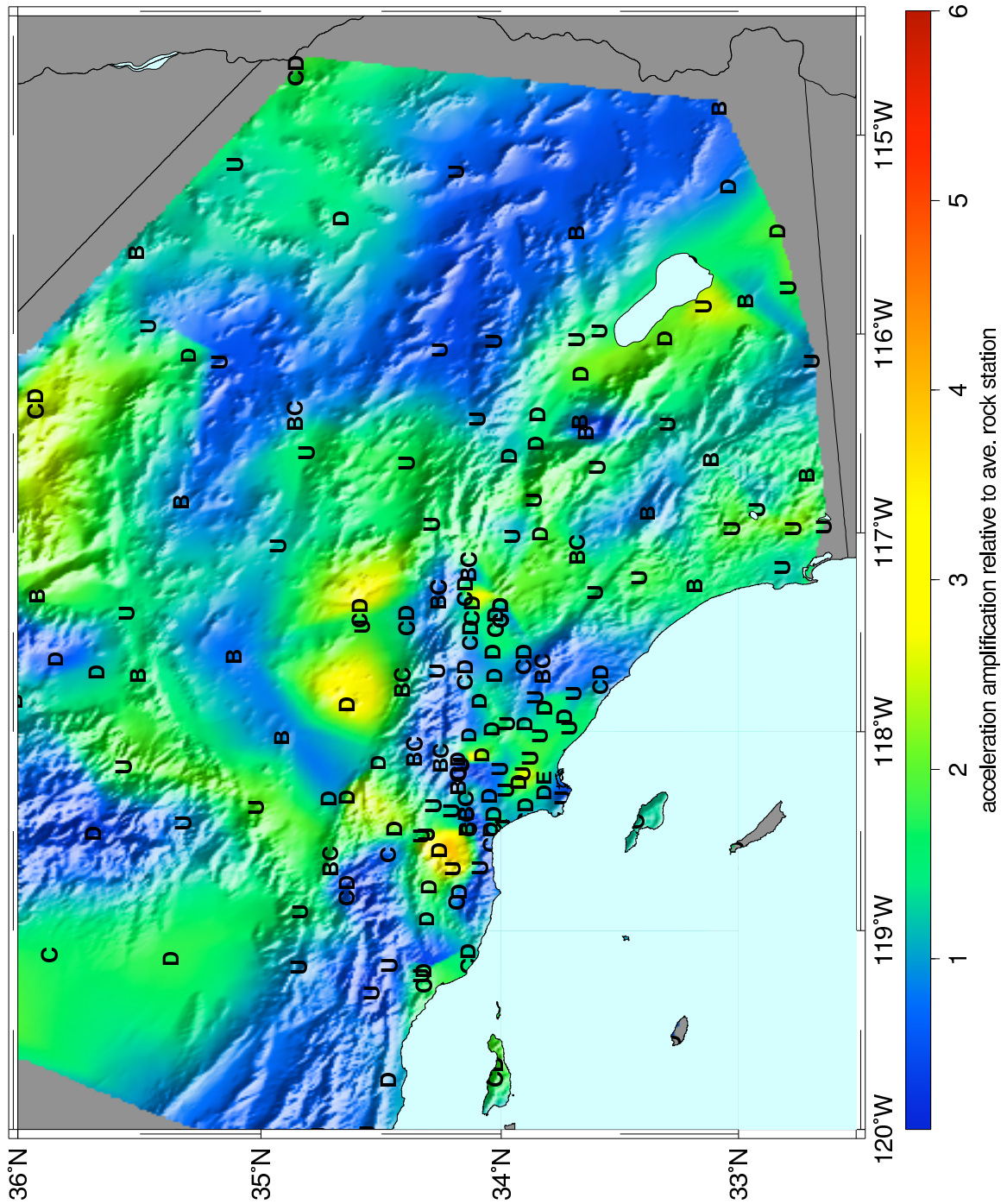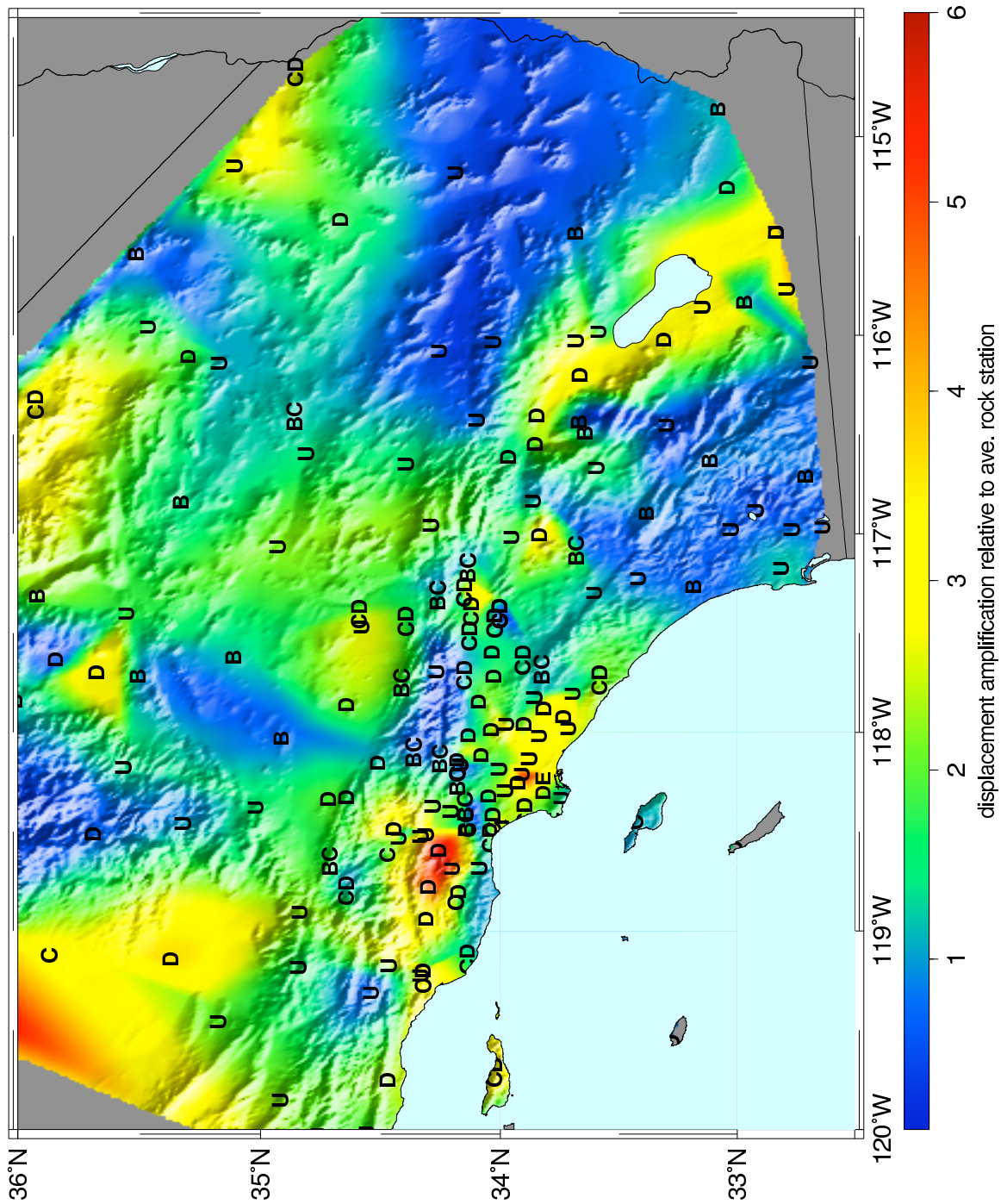
Figure 3.14: Amplification map for rms horizontal acceleration amplitudes. Amplification factors (linear scale) for acceleration range from 0.18 (deamplification) to ∼ 4. Station corrections relative to the average rock ground motions for 155 stations are calculated at the station locations (marked by NEHRP site classes, U=unknown), converted to amplification factors, and interpolated to obtain a smoothed amplification map.
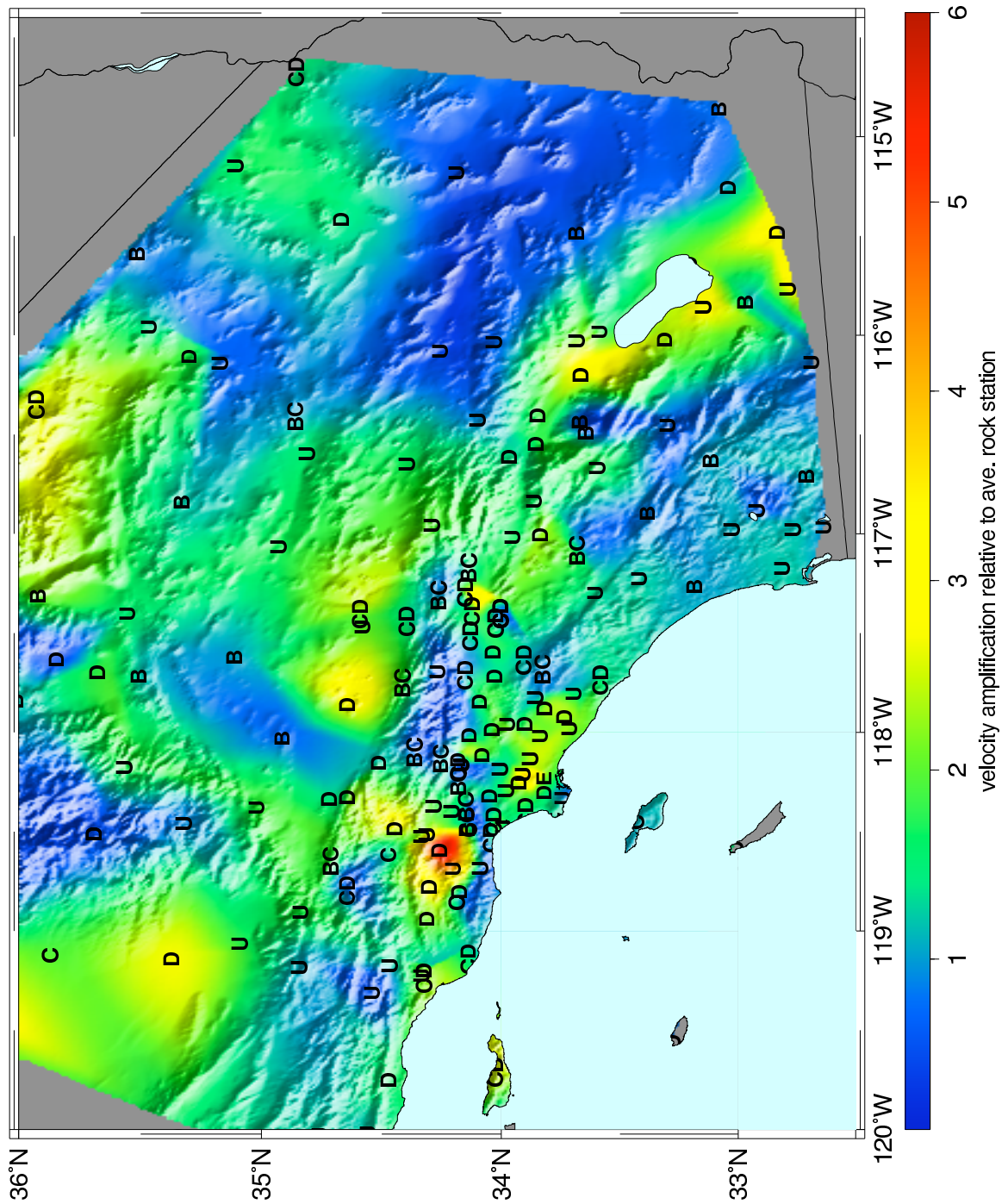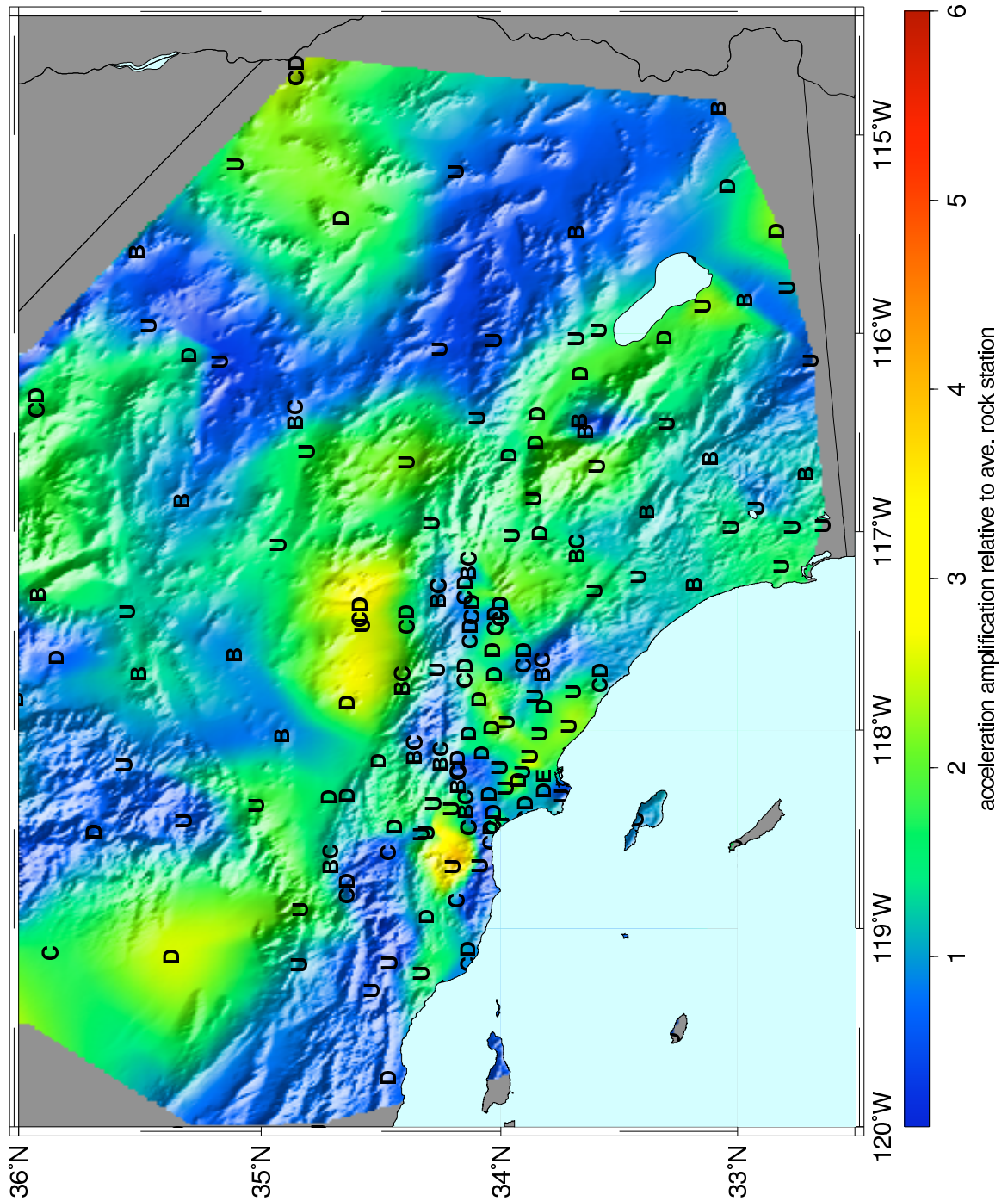
Figure 3.15: Amplification map for rms horizontal velocity amplitudes. Amplification factors (linear scale) for velocity range from 0.3 to 6. Station corrections relative to the average rock ground motions for 155 stations are calculated at the station locations (marked by NEHRP site classes, U=unknown), converted to amplification factors, and interpolated to obtain a smoothed amplification map.

Figure 3.16: Amplification map for rms horizontal displacement amplitudes. Amplification factors (linear scale) for displacement range from 0.4 to 6. Station corrections relative to the average rock ground motions for 155 stations are calculated at the station locations (marked by NEHRP site classes, U=unknown), converted to amplification factors, and interpolated to obtain a smoothed amplification map.

Figure 3.17: Amplification map for P-wave vertical acceleration amplitudes. Station corrections relative to the average rock ground motions for 155 stations are calculated at the station locations (marked by NEHRP site classes, U=unknown), converted to amplification factors, and interpolated to obtain a smoothed amplification map.
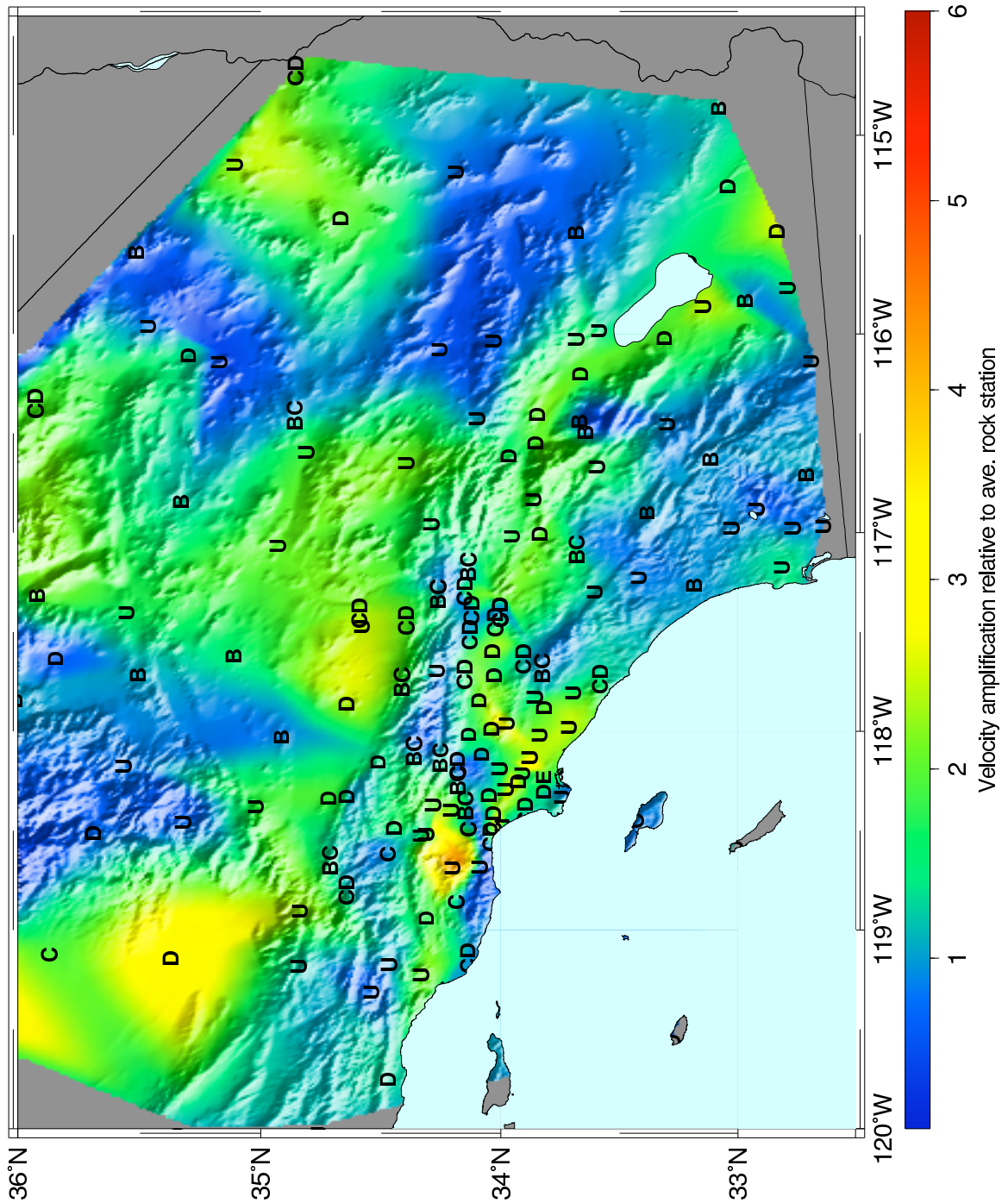
Figure 3.18: Amplification map for P-wave vertical velocity amplitudes. Station corrections relative to the average rock ground motions for 155 stations are calculated at the station locations (marked by NEHRP site classes, U=unknown), converted to amplification factors, and interpolated to obtain a smoothed amplification map.

# 3.3 Horizontal versus vertical ground motions

The S-wave envelope amplitude on horizontal channels usually corresponds to the peak ground motion of the record, facilitating comparisons with other attenuation relationships in the literature. On the vertical channels, this may not always the case (that the S-wave envelope amplitude corresponds to the peak ground motion of the record). In this Section, results for vertical S-wave attenuation relationships, for acceleration, velocity, and displacement on rock and soil sites are presented.

Table 3.3 shows the regression coefficients for the ground motion model represented by Eqn. 2.3 for acceleration, velocity, and displacement S-wave envelope amplitudes on rock and soil sites for both rms horizontal and vertical ground motion channels. Earlier in this chapter, the average characteristics of rms horizontal amplitudes were discussed. A similar approach is applied to the vertical channels.

Averaging the rock and soil coefficients for the vertical attenuation relationships (as we did for the horizontal attenuation relationships earlier in this chapter), the general magnitude and distance scaling for vertical ground motions (for small magnitudes, $M < 5$) is

$$
\begin{aligned}
\text{vertical acceleration, } \ddot{U} \quad &\sim \quad 10^{0.8M}10^{-2.6\times10^{-3}R}\frac{1}{R^{1.4}} \\
\text{vertical velocity, } \dot{U} \quad &\sim \quad 10^{0.9M}10^{-2.8\times10^{-4}R}\frac{1}{R^{1.5}} \\
\text{vertical displacement, } U \quad &\sim \quad 10^{1.0M}10^{-8.1\times10^{-6}R}\frac{1}{R^{1.4}}
\end{aligned}
\tag{3.8}
$$

From comparing Eqns. 3.1 and 3.8, vertical and horizontal have very similar magnitude and distance scaling for small magnitudes. Eqn. 3.1, which showed the general scaling characteristics of horizontal ground motions, and Eqn. 3.8 above are virtually identical.

From Table 3.3, which shows the coefficients for horizontal and vertical S-wave envelope amplitude attenuation relationships, the standard errors of regression (with and without station corrections) of vertical ground motions are very similar to those

rms horizontal S-wave acceleration attenuation coefficients

| Site type | a | b | d | $c_1$ | $c_2$ | e | $\sigma_{uncorr}$ | $\sigma_{corr}$ |
|---|---|---|---|---|---|---|---|---|
| rock | 0.779 | $2.555 \times 10^{-3}$ | 1.352 | 1.478 | 1.105 | -0.645 | 0.308 | 0.243 |
| soil | 0.836 | $2.324 \times 10^{-3}$ | 1.562 | 2.423 | 1.054 | -0.338 | 0.312 | 0.248 |

rms horizontal S-wave velocity attenuation coefficients

| Site type | a | b | d | $c_1$ | $c_2$ | e | $\sigma_{uncorr}$ | $\sigma_{corr}$ |
|---|---|---|---|---|---|---|---|---|
| rock | 0.894 | $4.286 \times 10^{-4}$ | 1.440 | 1.114 | 1.110 | -2.602 | 0.279 | 0.230 |
| soil | 0.960 | $8.328 \times 10^{-4}$ | 1.589 | 1.982 | 1.067 | -2.351 | 0.296 | 0.230 |

rms horizontal S-wave (filtered) displacement attenuation coefficients

| Site type | a | b | d | $c_1$ | $c_2$ | e | $\sigma_{uncorr}$ | $\sigma_{corr}$ |
|---|---|---|---|---|---|---|---|---|
| rock | 1.031 | $1.015 \times 10^{-7}$ | 1.438 | 1.098 | 1.133 | -4.342 | 0.277 | 0.233 |
| soil | 1.081 | $1.204 \times 10^{-6}$ | 1.556 | 1.946 | 1.091 | -4.101 | 0.326 | 0.236 |

vertical S-wave acceleration attenuation coefficients

| Site type | a | b | d | $c_1$ | $c_2$ | e | $\sigma_{uncorr}$ | $\sigma_{corr}$ |
|---|---|---|---|---|---|---|---|---|
| rock | 0.778 | $2.66 \times 10^{-3}$ | 1.385 | 1.763 | 1.112 | -0.751 | 0.300 | 0.238 |
| soil | 0.751 | $2.473 \times 10^{-3}$ | 1.474 | 1.593 | 1.106 | -0.355 | 0.300 | 0.235 |

vertical S-wave velocity attenuation coefficients

| Site type | a | b | d | $c_1$ | $c_2$ | e | $\sigma_{uncorr}$ | $\sigma_{corr}$ |
|---|---|---|---|---|---|---|---|---|
| rock | 0.900 | $1.027 \times 10^{-5}$ | 1.505 | 1.388 | 1.096 | -2.778 | 0.250 | 0.220 |
| soil | 0.882 | $5.41 \times 10^{-4}$ | 1.484 | 1.530 | 1.04 | -2.537 | 0.270 | 0.221 |

vertical S-wave displacement attenuation coefficients

| rock | 1.042 | $1.124 \times 10^{-5}$ | 1.367 | 1.379 | 1.178 | -4.738 | 0.253 | 0.232 |
|---|---|---|---|---|---|---|---|---|
| soil | 1.034 | $4.924 \times 10^{-6}$ | 1.363 | 1.549 | 1.082 | -4.569 | 0.286 | 0.230 |

Table 3.3: Regression coefficients for Eqn. 2.3 for S-wave envelope amplitude parameters for acceleration, velocity, and filtered displacement on rock and soil sites. This is an extended version of Table 3.1; the coefficients for vertical ground motions are included.

of horizontal channels. One possible interpretation is that the factors that cause variations or scatter in ground motions are isotropic, and have the about the same effect on horizontal and vertical directions (for small magnitudes, at least). This would not be expected for larger magnitudes, since surface waves and basin response are expected to be more significant on the horizontal components. It is also possible that all this means is that the horizontal and vertical regressions performed equally well - that is, all regressions converged to stable solutions. Figures 3.19, 3.20, and 3.21 show the observed vertical S-wave envelope amplitudes (acceleration, velocity, and displacement, on rock and soil sites) and the predicted amplitude levels as a function of distance at various prescribed magnitudes. Histograms of the residuals for the vertical ground motions exhibit the same characteristics as those for the horizontal channels, as shown in Figures 3.3, 3.5, and 3.7. They are not shown since they are virtually identical to the horizontal channel histograms; they show that the assumption of normally-distributed errors is satisfied, station corrections contribute about a 20% reduction in the standard deviation, and that the standard deviations of rock and soil are virtually identical after accounting for station corrections.

There are some slight differences between the vertical and horizontal regressions evident from Table 3.3:

- the anelastic attenuation terms are slightly different, though perhaps not to a statistically significant degree

- for horizontal channels, the magnitude dependence coefficient $a$ is always larger for soil than rock throughout the different frequency bands; the opposite is true for the vertical channels

- the saturation coefficients $c_1$ are very different between horizontal and vertical channels; the difference in $c_1$ between rock and soil is larger for the horizontals than the verticals

The ground motion model in Eqn. 2.3 allows saturation effects to come into play at close distances to events with magnitudes $M > 5$. Since it is difficult to see the

saturation effects from just examining the coefficients $(a, b, c_1, c_2, d, e)$, we find the effective magnitude scaling by examining the partial derivative of Eqn. 2.3 relative to magnitude (Eqn. 3.5), as discussed earlier for the horizontal channels. Table 3.4 is an extended version of Table 3.2. It shows the partial derivatives of Eqn. 2.3 evaluated at $M = 6, R = 0 km$ for horizontal and vertical acceleration, velocity, and displacement for rock and soil sites. An additional row showing approximate percentage change between rock and soil is appended. This $\%diff$ indicated how much larger the effective magnitude scaling is for rock than soil, or

$$\%diff = \frac{ES_{rock} - ES_{soil}}{ES_{rock}} \times 100 \tag{3.9}$$

where "ES" denotes "effective magnitude scaling". A positive $\%diff$ means that rock sites have larger "effective magnitude scaling" relative to soil sites; this means that soil sites exhibit stronger saturation effects.

$\frac{\partial \log_{10} A}{\partial M}$ evaluated at $M = 6, R = 0$
for rms horizontal S-wave envelope amplitudes

| site | acceleration | velocity | displacement |
|------|------|------|------|
| rock | 0.15 | 0.29 | 0.42 |
| soil | 0.064 | 0.22 | 0.36 |
| % diff | 57% | 24% | 14% |

$\frac{\partial \log_{10} A}{\partial M}$ evaluated at $M = 6, R = 0$
for vertical S-wave envelope amplitudes

| site | acceleration | velocity | displacement |
|------|------|------|------|
| rock | 0.094 | 0.25 | 0.40 |
| soil | 0.11 | 0.26 | 0.43 |
| % diff | -21% | -4 % | -8% |

Table 3.4: Effective magnitude scaling of horizontal and vertical acceleration, velocity, and displacement at close distances to large events. These values are the partial derivatives of $\log_{10}(A)$, where $A$ is rms acceleration, velocity, and displacement S-wave envelope amplitude for rock and soil sites, evaluated at $M = 6$ and $R = 0$. This is an expanded version of Table 3.2, with values for vertical S-wave envelope amplitudes included.

From the differences between rock and soil sites on horizontal and vertical chan-

nels, the effective magnitude scaling for horizontal ground motions is always larger for rock than soil ($\%diff$ values are all positive) on the horizontal channels regardless of frequency. If the differences are statistically significant, this means that soil sites consistently exhibit more saturation throughout the different frequency bands than rock sites for horizontal ground motions. This is consistent with what would be expected if a major contributor to saturation effects is non-linear soil response. It is a curious thing that $\%diff$ is consistently negative for the vertical channels. If these differences are statistically significant, this indicates that the rock sites exhibit slightly stronger saturation effects than soil sites for vertical ground motions. Saturation is not expected to be important for vertical ground motions, since non-linear soil response is typically associated with shear loading. One possibility is that the differences are *not* statistically significant, and there is no real difference in saturation between rock and soil on the vertical channels.

Figures 3.22, 3.23, and 3.24 show the amplitude curves predicted by the vertical S-wave attenuation relationships as functions of (a) distance and (b) magnitude for rock and soil sites. Figure 3.22 shows that the difference between rock and soil sites for acceleration has some slight magnitude and distance dependence; it appears that rock sites are saturating slightly stronger than the soil sites. (This over saturation of vertical ground motions on rock sites is also evident from the effective magnitude scaling being larger on rock than soil for vertical ground motions, as indicated by Table 3.4.) The difference between rock and soil becomes fairly constant for longer periods. In this case, the difference between the regression coefficients $e$ is a fair estimate of the average difference between vertical ground motions on rock and soil: for velocity, $\Delta e = e_{soil} - e_{rock} = 0.24$ log units, or a factor of 1.7, for displacement, $\Delta e = 0.17$ log units, or a factor of 1.5. That is soil sites amplify vertical S-wave envelope amplitudes by $\sim 70\%$ for velocity, and $\sim 50\%$ for displacement.

From Table 3.4, the effective magnitude scaling for S-wave velocity and displacement (averaging between rock and soil) is quite similar between the horizontal and vertical channels; they are quite different for acceleration, with the horizontal channel showing stronger saturation effects.

Since the differences between rock and soil on the vertical channels are smaller than differences on the horizontal, it is expected that vertical site amplification will be generally less than for horizontal ground motions. This can be verified by examining histograms of vertical S-wave station corrections relative to average rock ground motions predicted by our vertical attenuation relationships. Figures 3.25, 3.26, and 3.27 show such histograms. On average, vertical accelerations on soil sites are amplified by a factor of 1.2 relative to rock; the soil amplifications for vertical velocity and displacement relative to the average vertical rock ground motions are factors of 1.3 and 1.4, respectively. In general, soil amplification on the vertical channels relative to the average rock ground motions are smaller than those on the horizontal channels.

Figures 3.28, 3.29, and 3.30 compare horizontal and vertical S-wave envelope amplitudes on (a) rock and (b) soil sites for acceleration, velocity, and filtered displacement. At close distances to large magnitude events, there appears to be slightly stronger saturation effects on the vertical channels than the horizontals, as was also indicated by our tally of effective magnitude scaling with frequency band in this region the the parameter space (Table 3.4). It is difficult to determine whether such differences are statistically significant, since they involve a region in magnitude-distance space that is very sparse in terms of data.

## Average vertical to horizontal ratio

The average difference (over all magnitudes and distances considered in this study) between vertical and horizontal ground motions (or any two attenuation relationships we wish to compare) can be examined by subtracting the attenuation relationships, integrating over the appropriate area in magnitude-distance space, and dividing by this area. For the ratio of vertical to horizontal ground motion amplitudes,

$$\log(\overline{V/H}) = \frac{1}{(M_{max} - M_{min})} \frac{1}{(R_{max} - R_{min})} \int_M \int_R \log_{10}(A_V) - log_{10}(A_H) \, dM \, dR$$

(3.10)

where V denotes vertical, H horizontal, and $\log_{10}(A)$ are the attenuation relationships given by Eqn. 2.3 with the appropriate coefficients $(a, b, c_1, c_2, d, e)$ for the different channels. $\log(\overline{V/H})$ in Eqn. 3.10 is in log units. The scaling factor is thus $10^{\log(\overline{V/H})}$ on a linear scale.

Table 3.5 shows $\log(\overline{V/H})$ for acceleration, velocity, and displacement on rock and soil sites. The first number is $\log(\overline{V/H})$ in log units; the value in parenthesis is $\overline{V/H}$ on a linear scale. For rock sites, average $V/H$ is close to 0.6 independent of frequency. This is consistent with the standard engineering rule-of-thumb of assuming $V/H = 2/3$ when estimating vertical ground motion for design. However, for soil sites, it appears that $\overline{V/H}$ decreases with increasing period. In fact, $V/H$ has some dependence on magnitude and distance, as we can see from Figures 3.28, 3.29, and 3.30. This is consistent with findings of Bozorgnia and Campbell (2004) regarding $V/H$ ratios for response spectral quantities. They found $V/H$ to be a strong function of frequency, site conditions, and distance; and a weaker function of magnitude, faulting type, and sediment depth.

Average V/H ratio (S-wave)

| site | acceleration | velocity | displacement |
|------|--------------|----------|--------------|
| rock | -0.20 (0.63) | -0.24 (0.58) | -0.22 (0.60) |
| soil | -0.23 (0.59) | -0.29 (0.51) | -0.3 (0.5) |

Table 3.5: Average V/H ratio for rock and soil sites for acceleration, velocity, and filtered displacement.

## 3.4  P- versus S-waves

The parameterization of observed ground motion envelopes as a combination of P–wave, S-wave, and ambient noise envelopes as discussed in the previous chapter allows us to examine P-wave and S-wave envelope parameters independently. Attenuation relationships for P-wave envelope parameters can be obtained, as they were for the S-waves. P- and S-wave envelope amplitude attenuation relationships are compared
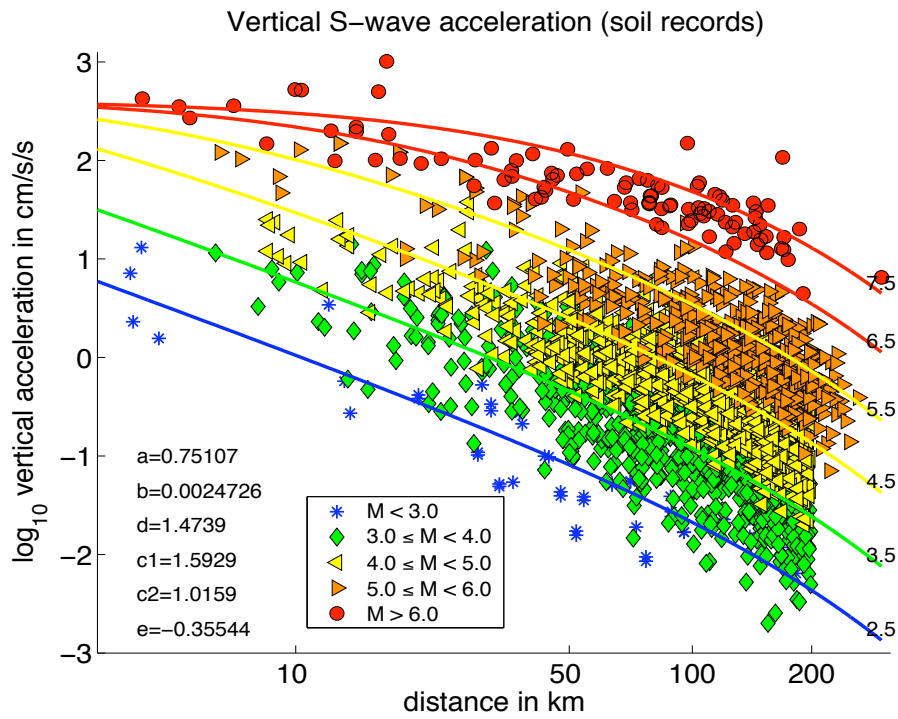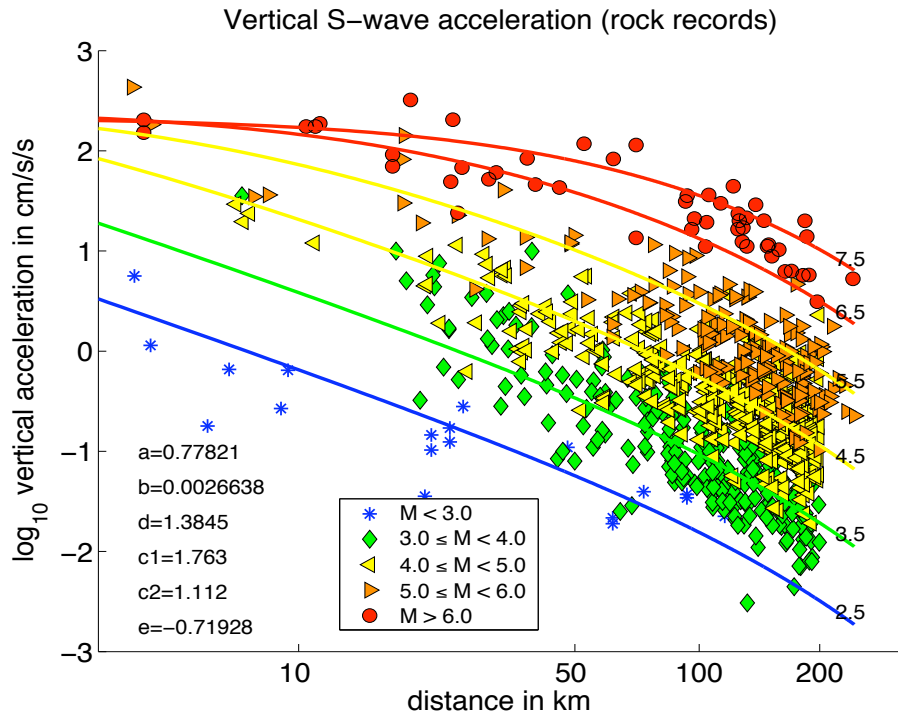
Figure 3.19: Observed S-wave envelope acceleration amplitudes (vertical, without station corrections) and curves of predicted amplitudes against distance at various prescribed magnitudes for (a) rock sites and (b) soil sites.
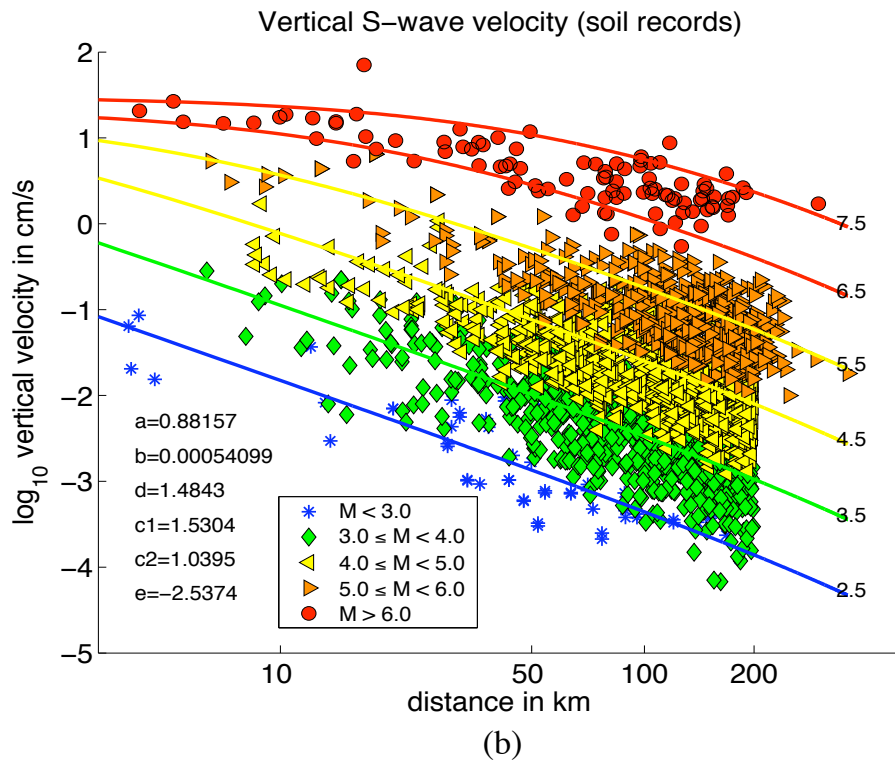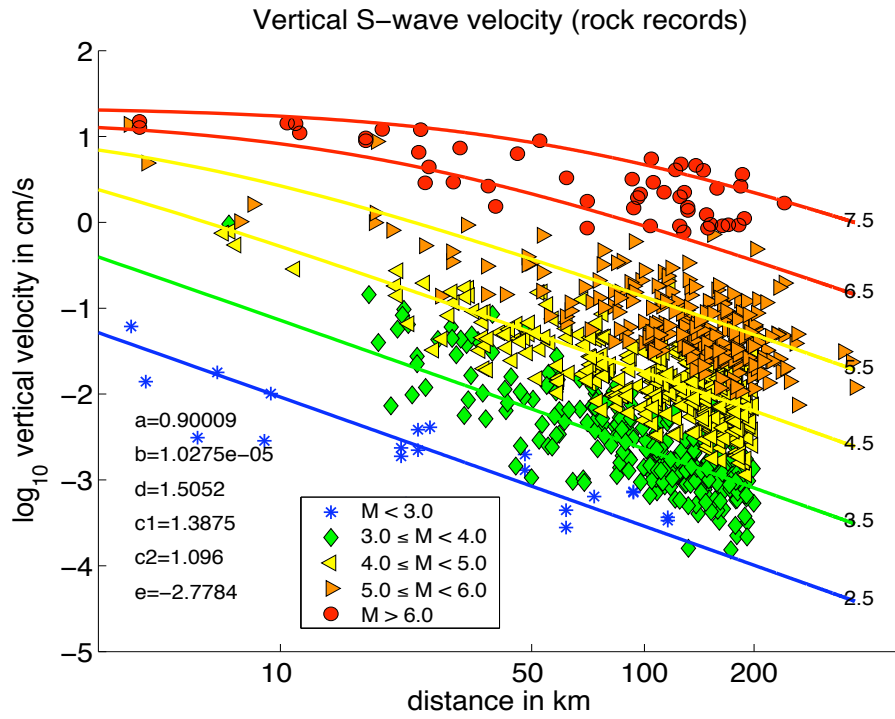
Figure 3.20: Observed S-wave envelope velocity amplitudes (vertical, without station corrections) and curves of predicted amplitudes against distance at various prescribed magnitudes for (a) rock sites and (b) soil sites.
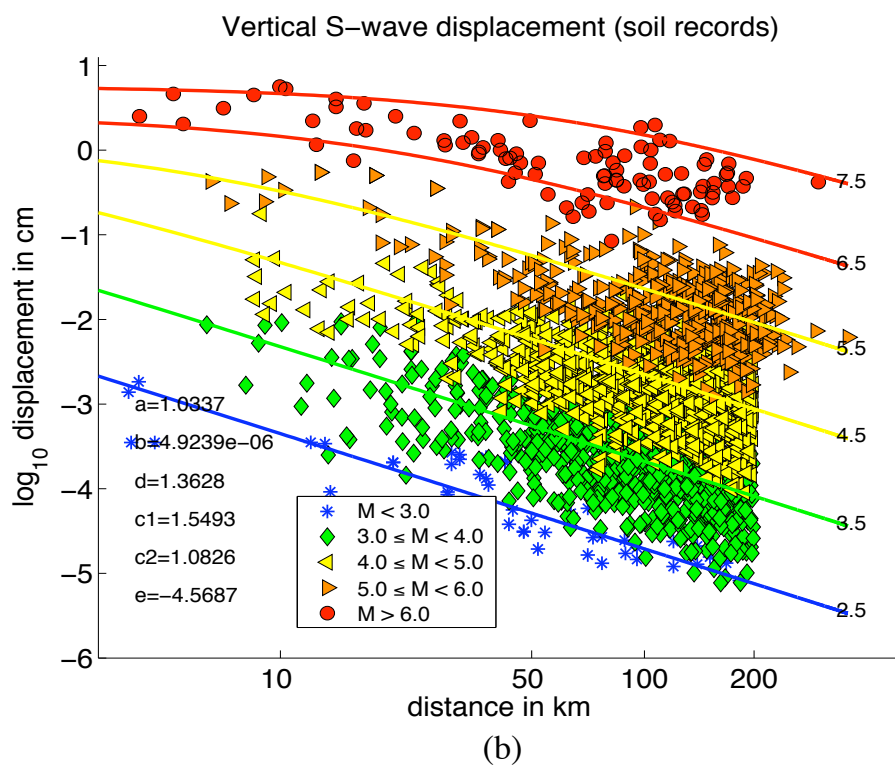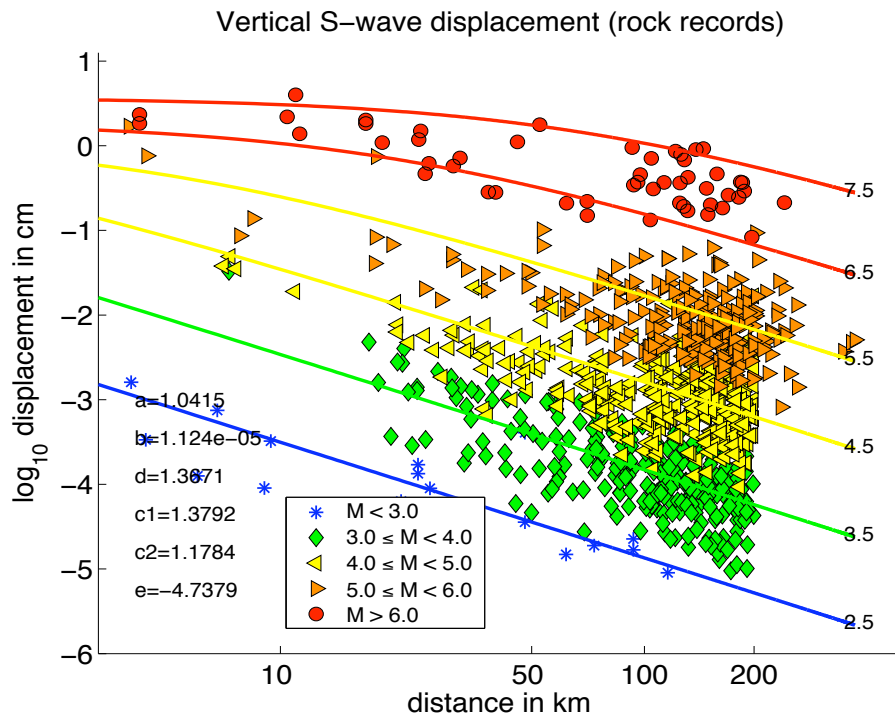
Figure 3.21: Observed S-wave envelope displacement amplitudes (vertical, without station corrections) and curves of predicted amplitudes against distance at various prescribed magnitudes for (a) rock sites and (b) soil sites.
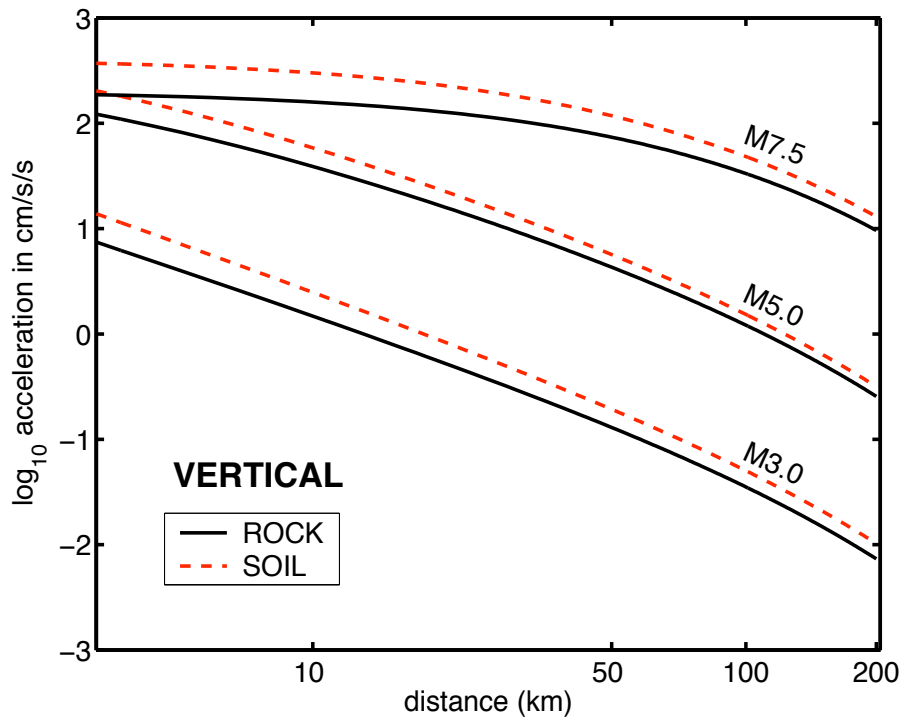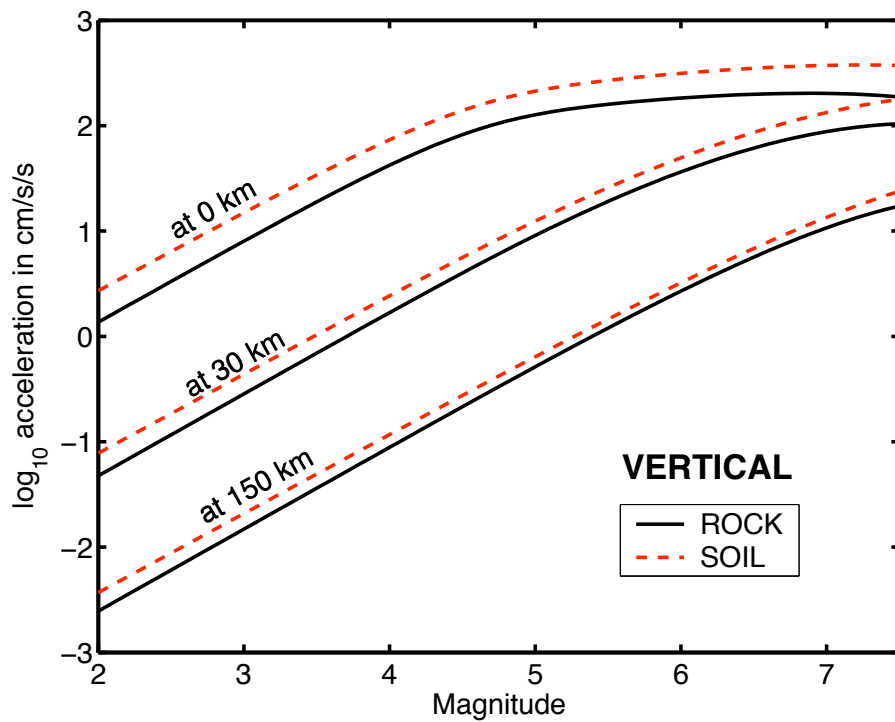
Figure 3.22: $\log_{10}$ vertical acceleration as a function of (a) distance and (b) magnitude. Vertical acceleration on rock sites appears to saturate slightly more than accelerations on soil sites.
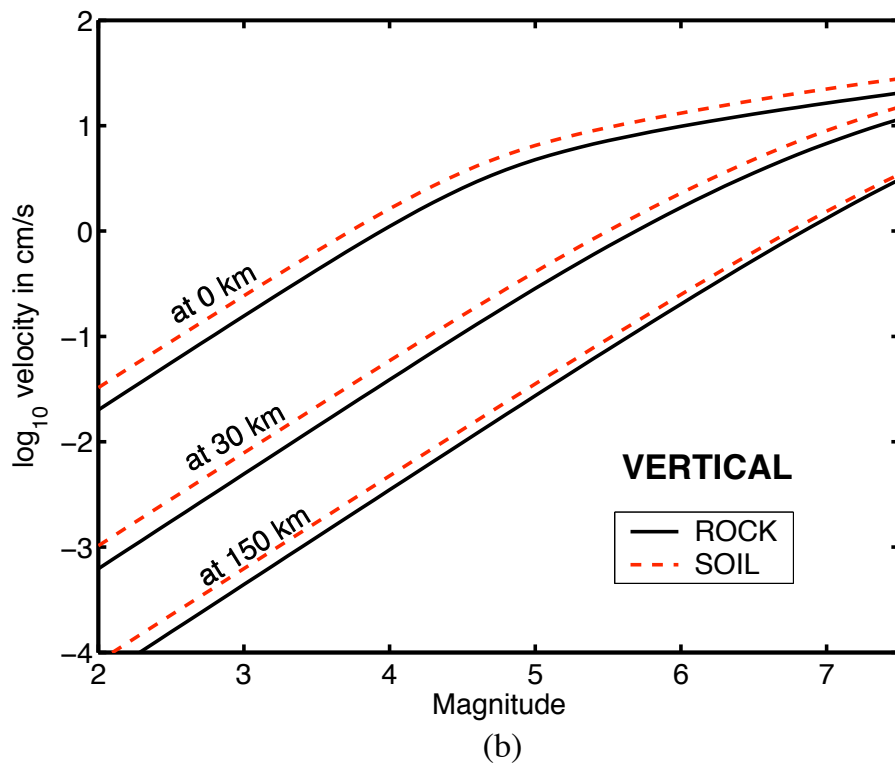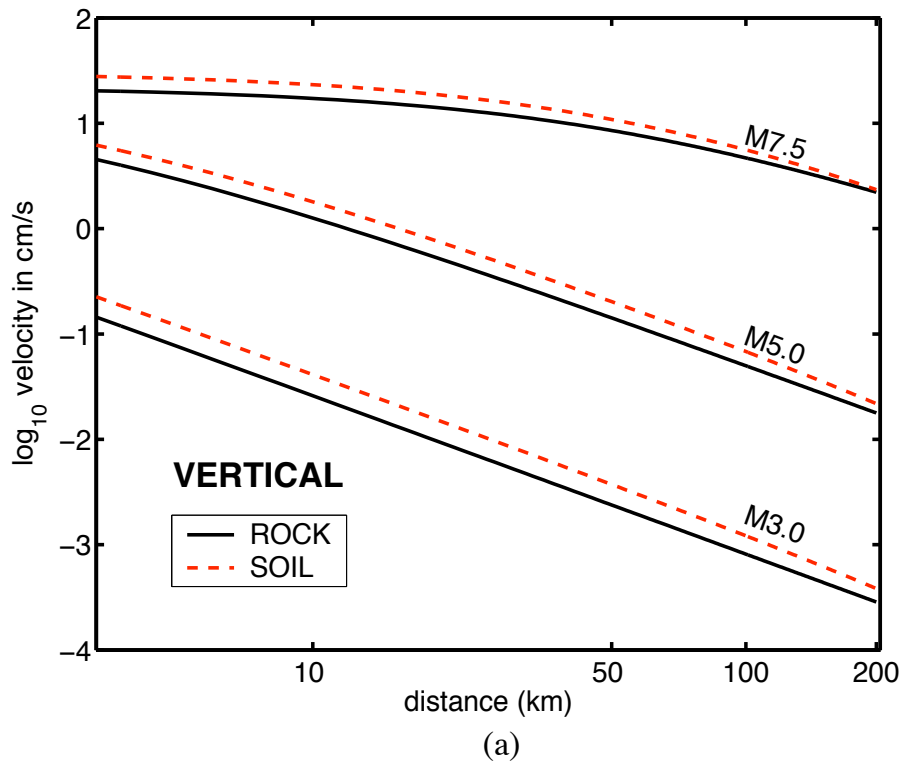
Figure 3.23: $\log_{10}$ vertical velocity as a function of (a) distance and (b) magnitude. The difference of vertical velocities on rock and soil is small and fairly independent of magnitude and distance.
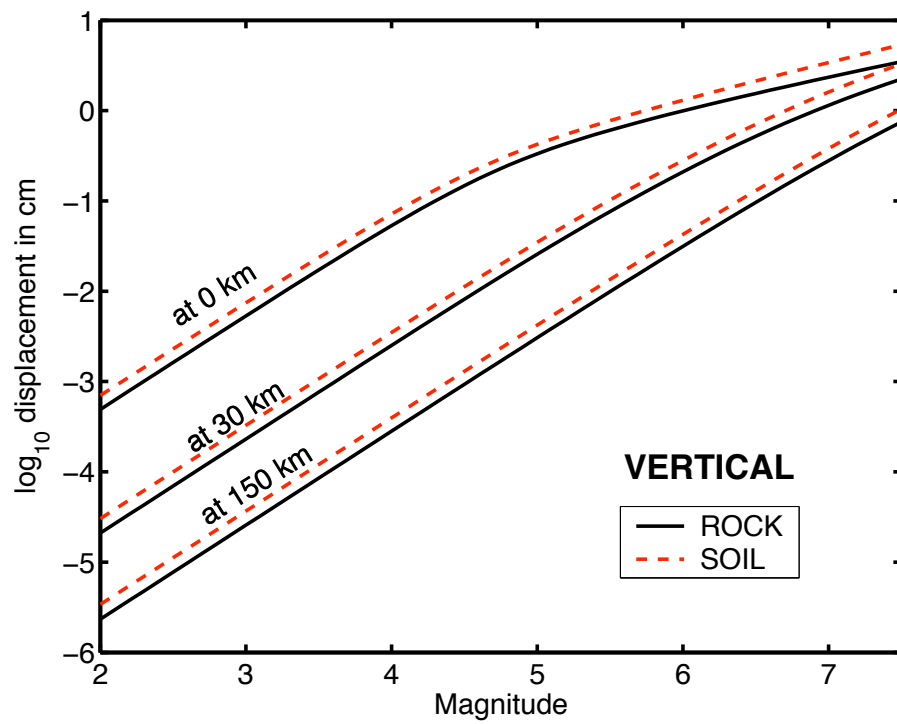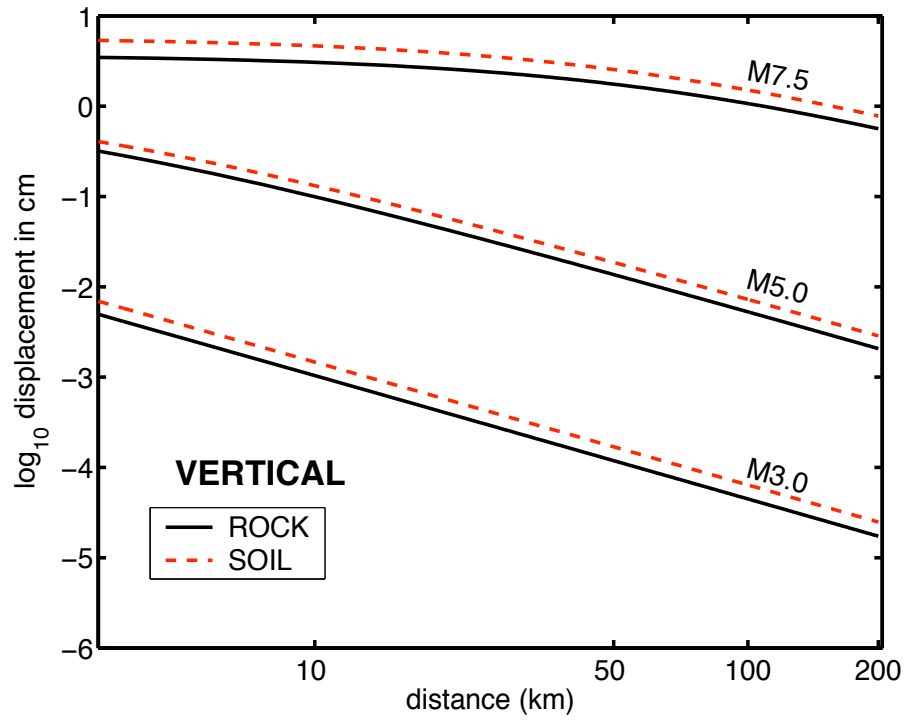
Figure 3.24: Predicted vertical S-wave displacement as a function of (a) distance and (b) magnitude. The difference in vertical filtered displacements on rock and soil sites is not very large.
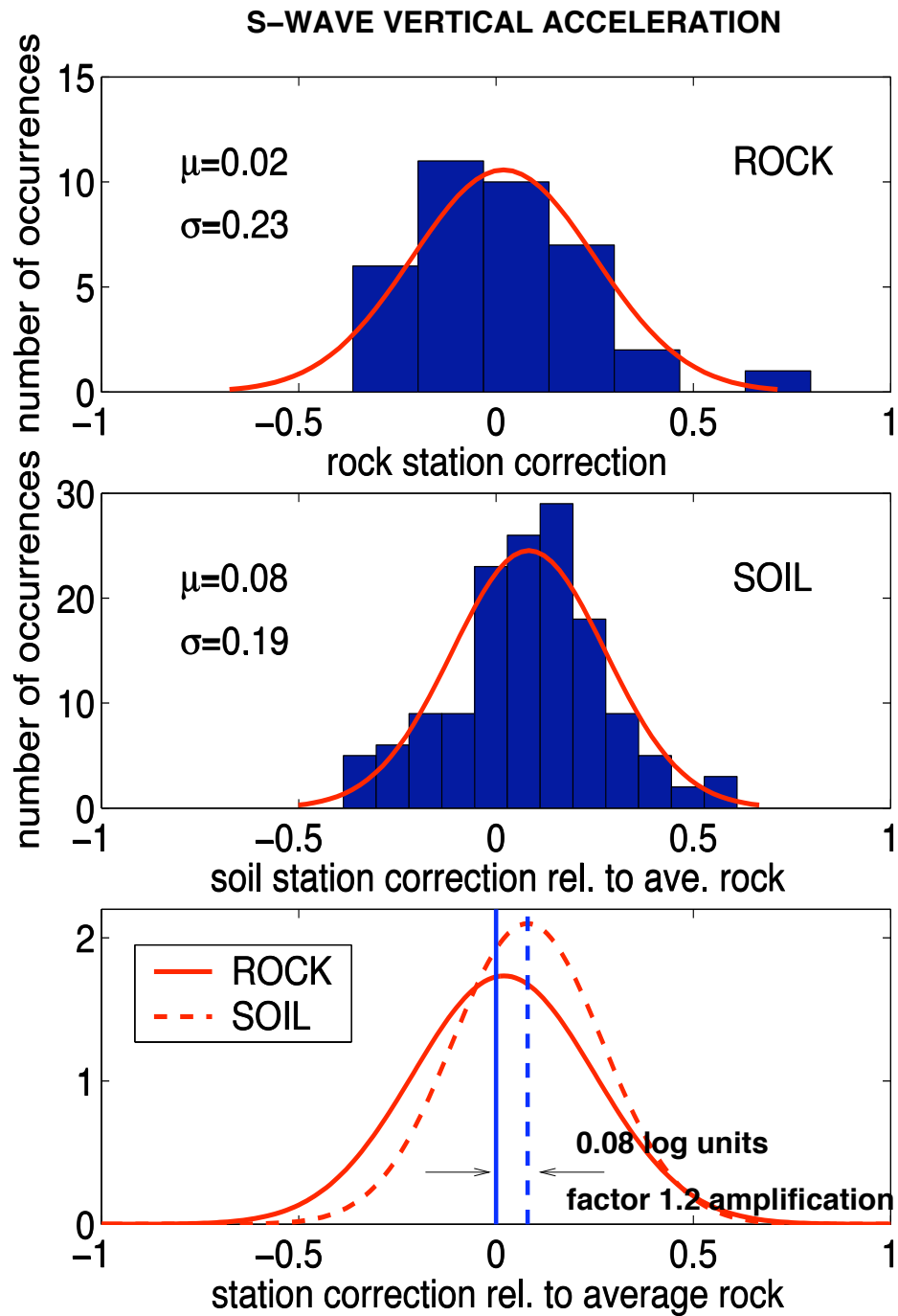
Figure 3.25: Histograms of vertical acceleration station corrections for rock and soil sites. Curves are normal densities that best fit the histograms. The mean amplification of vertical acceleration on soil sites relative to average rock acceleration amplitudes predicted by the attenuation relationships is a factor of 1.2.
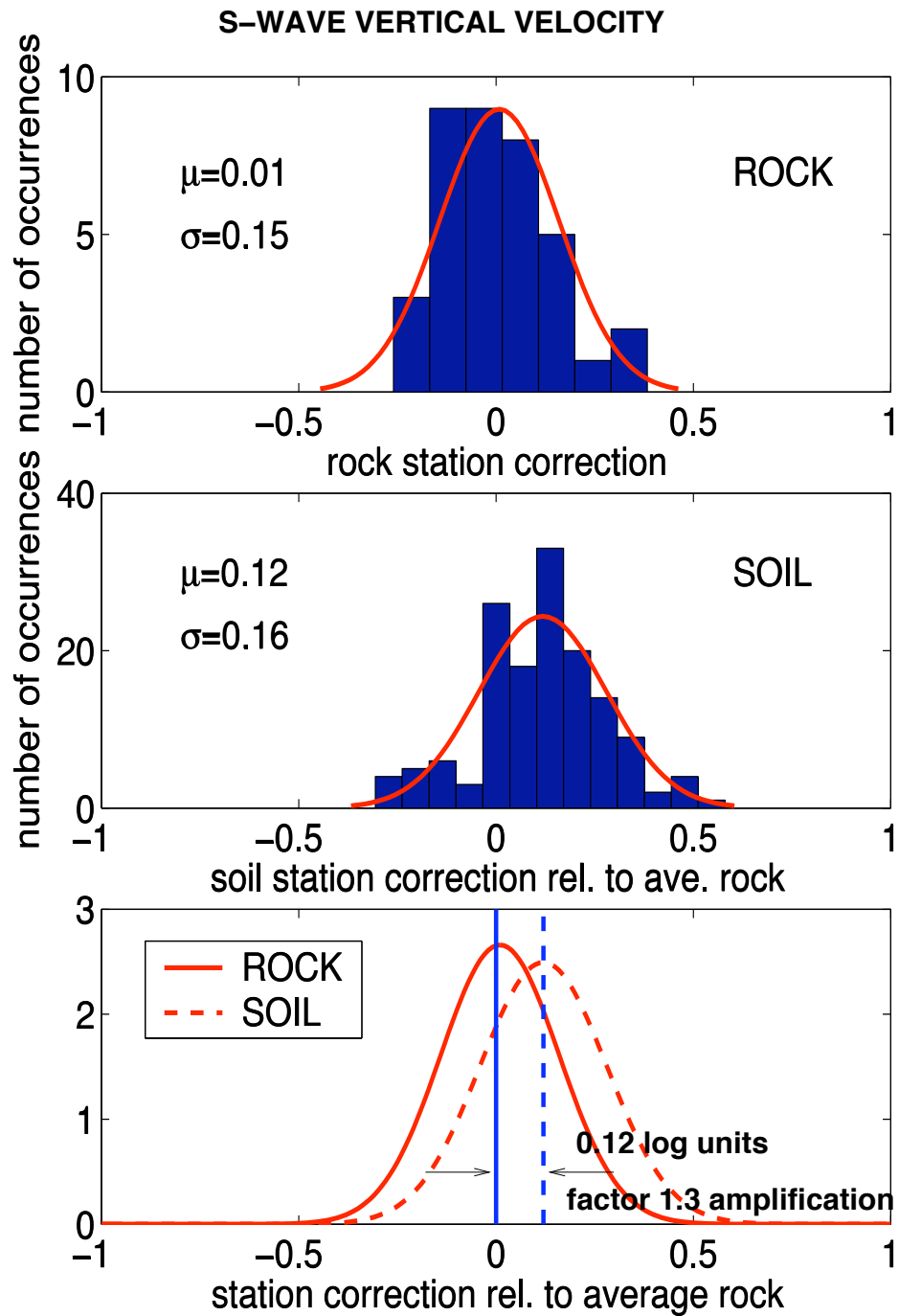
Figure 3.26: Histograms of vertical velocity station corrections for rock and soil sites. Curves are normal densities that best fit the histograms. The mean amplification of vertical velocity on soil sites relative to average rock velocities predicted by our attenuation relationships is a factor of 1.3.
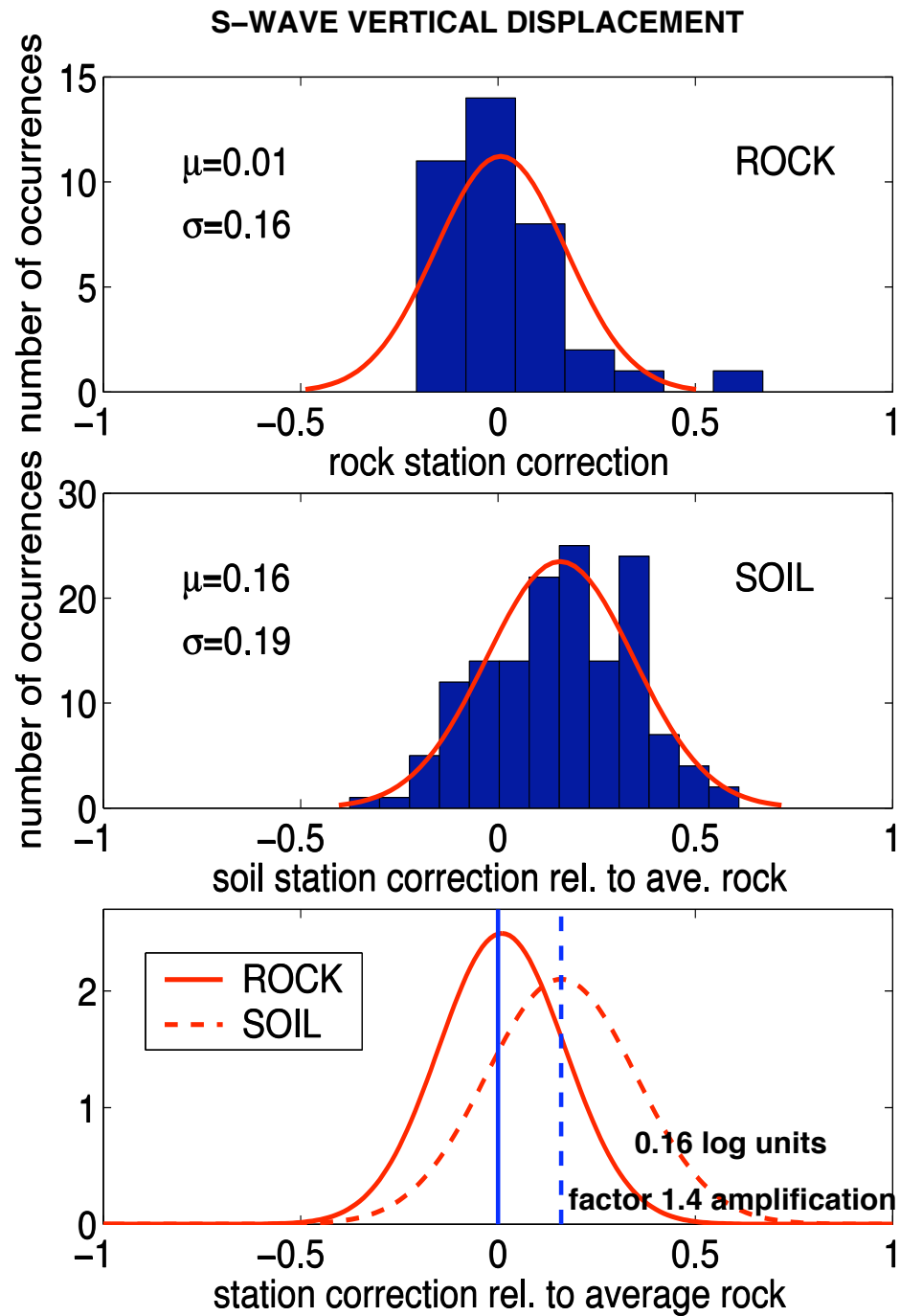
Figure 3.27: Histograms of vertical filtered displacement station corrections for rock and soil sites. Curves are normal densities that best fit the histograms. The mean amplification of vertical displacements on soil sites relative to average rock displacements predicted by our attenuation relationships is a factor of 1.4.
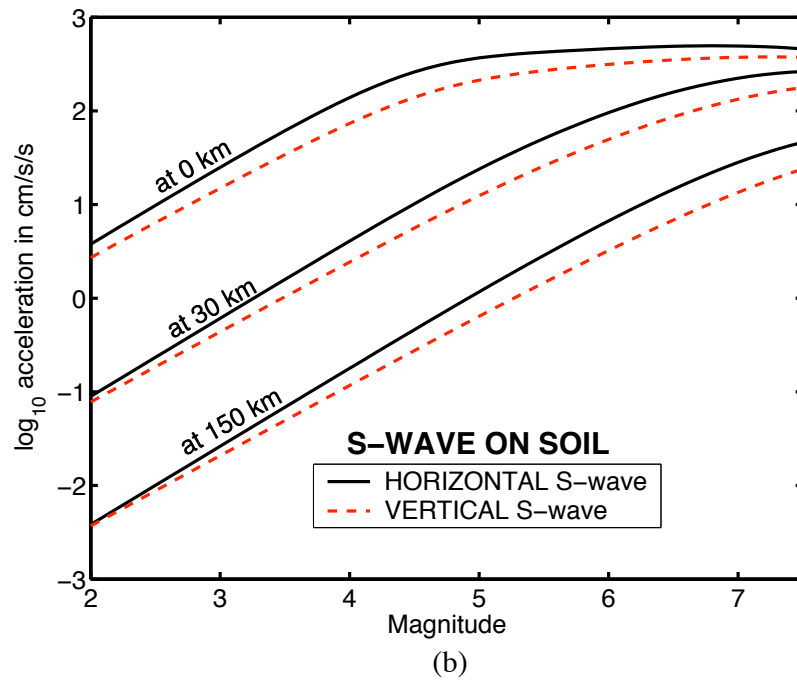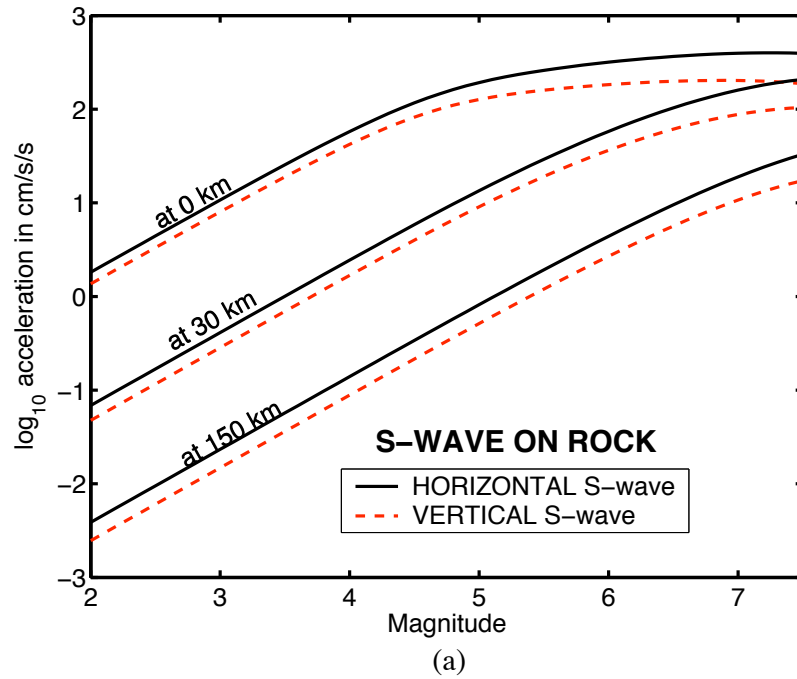
Figure 3.28: Comparison of horizontal to vertical S-wave accelerations on (a) rock and (b) soil sites. On rock sites, vertical S-wave accelerations appear to exhibit stronger saturation effects than horizontal S-waves. On soil sites, the difference between vertical and horizontal ground motions appears to be magnitude and distance dependent.
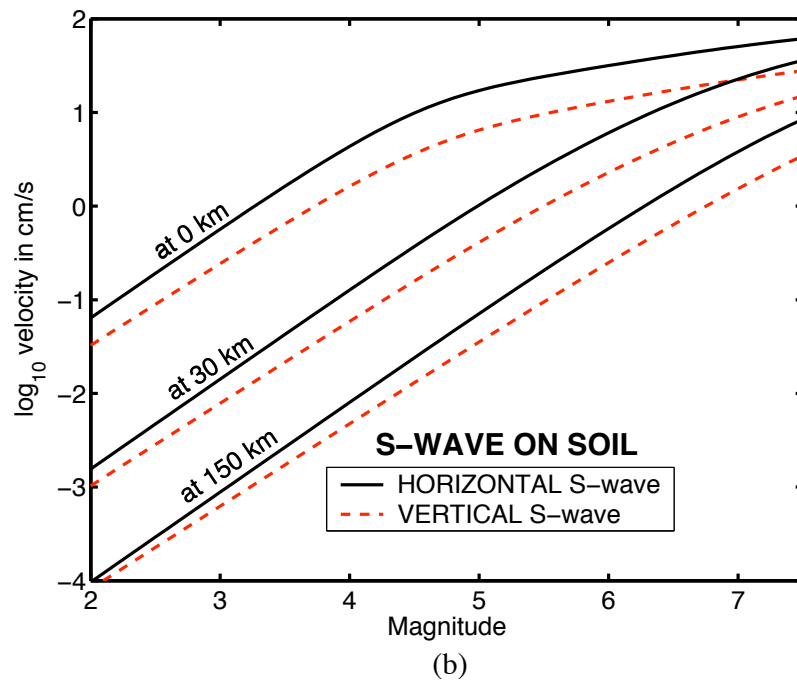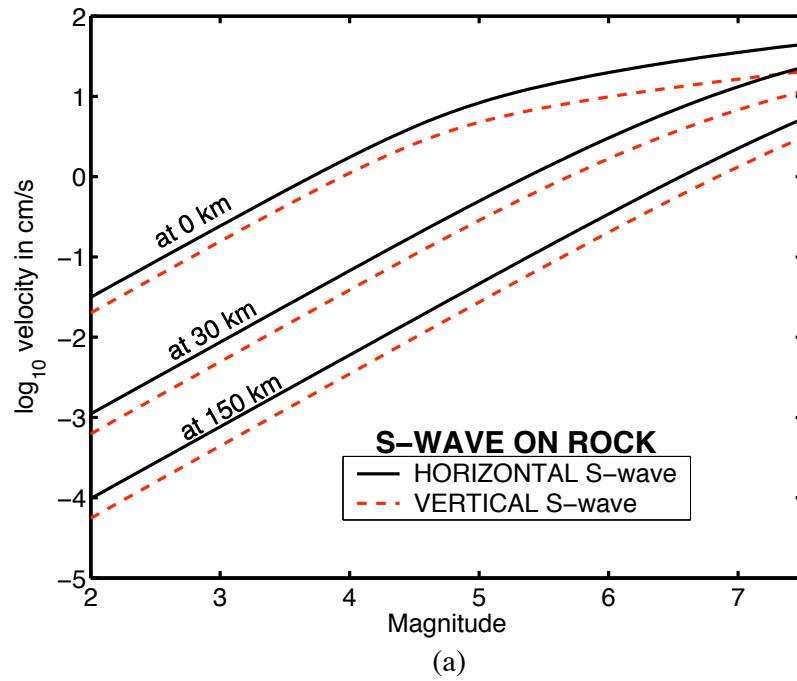
Figure 3.29: Comparison of horizontal to vertical velocities for S-waves on (a) rock and (b) soil sites. On rock sites, vertical velocities of S-waves appear to exhibit slightly stronger saturation effects than horizontal S-wave velocities. On soil sites, the difference between vertical and horizontal ground motions appears magnitude and distance dependent. These are similar to characteristics observed for vertical accelerations.
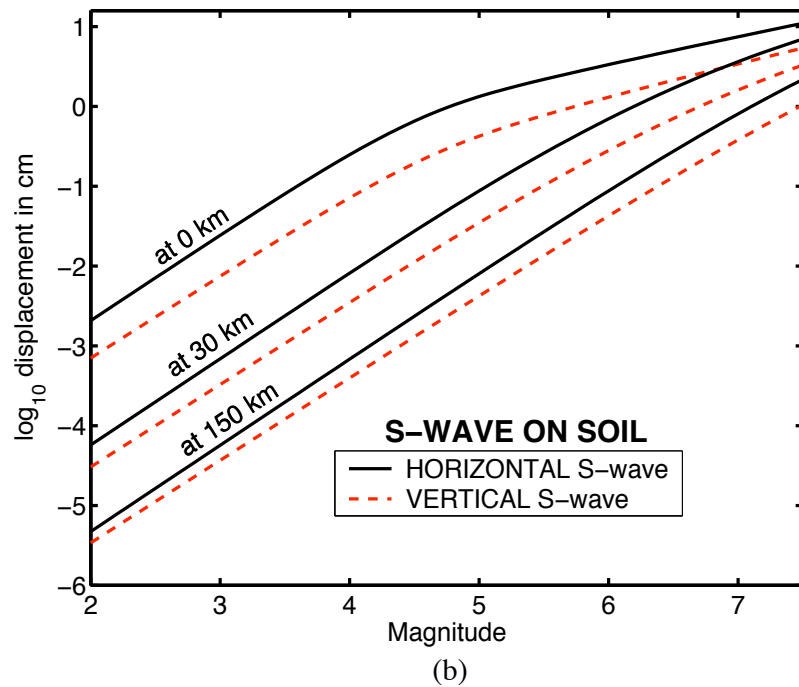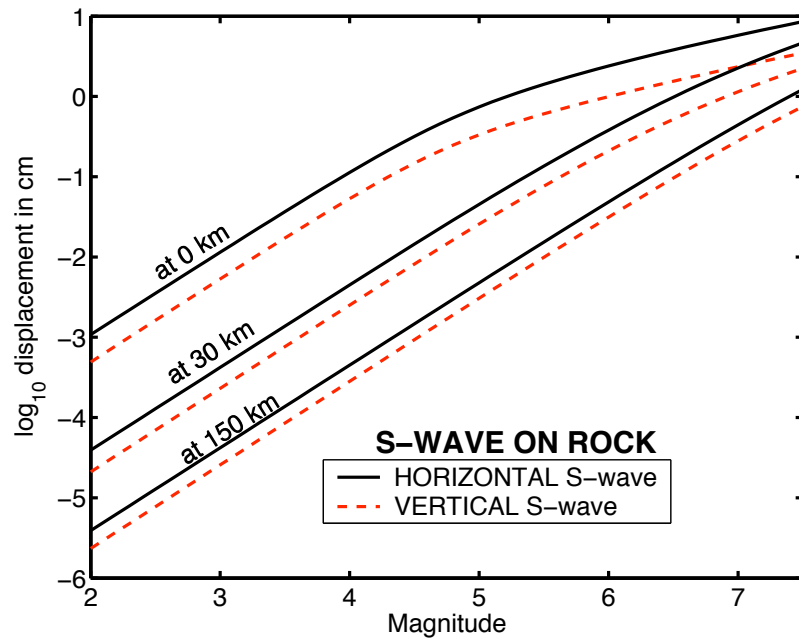
Figure 3.30: Comparison of horizontal to vertical filtered displacements for S-waves on (a) rock and (b) soil sites.

in this Section.

Eqn. 2.3 represents the dependence of P-wave envelope amplitude on magnitude, distance, and site; it is the same functional form used for the S-wave envelope amplitudes. As with the S-wave amplitudes, it allows saturation effects to come into play for larger events ($M > 5$). The degree of saturation is controlled by regression coefficient $c_1$; $c_1 \sim 0$ means no saturation. Table 3.6 lists the regression coefficients for P-wave envelope amplitudes for rms horizontal acceleration, velocity, and displacement on rock and soil sites.

For small magnitudes ($M < 5$), rms horizontal P-wave amplitudes scale as (averaging over rock and soil coefficients)

$$
\begin{aligned}
\text{horizontal acceleration, } \ddot{U}_{P,horiz} &\sim 10^{0.7M} 10^{-2.9 \times 10^{-3} R} \frac{1}{R^{1.2}} \\
\text{horizontala velocity, } \dot{U}_{P,horiz} &\sim 10^{0.8M} 10^{-6.9 \times 10^{-4} R} \frac{1}{R^{1.3}} \\
\text{horizontal displacement, } U_{P,horiz} &\sim 10^{0.9M} 10^{-1.1 \times 10^{-6} R} \frac{1}{R^{1.2}}
\end{aligned} \tag{3.11}
$$

Vertical P-wave amplitudes for small magnitudes ($M < 5$) scale as (averaging over rock and soil coefficients)

$$
\begin{aligned}
\text{vertical acceleration, } \ddot{U}_{P,vert} &\sim 10^{0.7M} 10^{-4.1 \times 10^{-3} R} \frac{1}{R^{1.2}} \\
\text{vertical velocity, } \dot{U}_{P,vert} &\sim 10^{0.8M} 10^{-4.3 \times 10^{-4} R} \frac{1}{R^{1.4}} \\
\text{vertical displacement, } U_{P,vert} &\sim 10^{0.9M} 10^{-1.0 \times 10^{-6} R} \frac{1}{R^{1.3}}
\end{aligned} \tag{3.12}
$$

Eqns. 3.11 and 3.12 are nearly identical. Although vertical P-waves are consistently larger amplitude than horizontal P-waves (regression coefficient $e$ is consistently less negative in the vertical direction), horizontal and vertical P-waves vary in a similar manner with magnitude and distance.

Comparing Eqns. 3.11 (horizontal P-waves) and 3.1 (horizontal S-waves), and Eqns. 3.12 (vertical P-waves) and 3.8 (vertical S-waves), it is observed (for horizontal and vertical directions) that

rms horizontal P-wave acceleration attenuation coefficients

| Site type | a | b | d | $c_1$ | $c_2$ | e | $\sigma_{uncorr}$ | $\sigma_{corr}$ |
|-----------|-----|------|------|-------|-------|--------|---------|---------|
| rock | 0.719 | $3.273 \times 10^{-3}$ | 1.195 | 1.600 | 1.045 | -1.065 | 0.307 | 0.233 |
| soil | 0.737 | $2.520 \times 10^{-3}$ | 1.26 | 2.410 | 0.955 | -1.051 | 0.286 | 0.229 |

rms horizontal P-wave velocity attenuation coefficients

| Site type | a | b | d | $c_1$ | $c_2$ | e | $\sigma_{uncorr}$ | $\sigma_{corr}$ |
|-----------|-----|------|------|-------|-------|--------|---------|---------|
| rock | 0.801 | $8.397 \times 10^{-4}$ | 1.249 | 0.761 | 1.340 | -3.103 | 0.268 | 0.211 |
| soil | 0.836 | $5.409 \times 10^{-4}$ | 1.284 | 1.214 | 0.978 | -3.135 | 0.263 | 0.219 |

rms horizontal P-wave (filtered) displacement attenuation coefficients

| Site type | a | b | d | $c_1$ | $c_2$ | e | $\sigma_{uncorr}$ | $\sigma_{corr}$ |
|-----------|-----|------|------|-------|-------|--------|---------|---------|
| rock | 0.950 | $1.685 \times 10^{-6}$ | 1.275 | 2.162 | 1.088 | -4.958 | 0.284 | 0.239 |
| soil | 0.943 | $5.171 \times 10^{-7}$ | 1.161 | 2.266 | 1.016 | -5.008 | 0.301 | 0.247 |

vertical P-wave acceleration attenuation coefficients

| Site type | a | b | d | $c_1$ | $c_2$ | e | $\sigma_{uncorr}$ | $\sigma_{corr}$ |
|-----------|-----|------|------|-------|-------|--------|---------|---------|
| rock | 0.745 | $4.010 \times 10^{-3}$ | 1.200 | 1.752 | 1.091 | -0.955 | 0.288 | 0.243 |
| soil | 0.739 | $4.134 \times 10^{-3}$ | 1.199 | 2.030 | 1.972 | -0.775 | 0.317 | 0.256 |

vertical P-wave velocity attenuation coefficients

| Site type | a | b | d | $c_1$ | $c_2$ | e | $\sigma_{uncorr}$ | $\sigma_{corr}$ |
|-----------|-----|------|------|-------|-------|--------|---------|---------|
| rock | 0.821 | $8.543 \times 10^{-4}$ | 1.362 | 1.148 | 1.100 | -2.901 | 0.263 | 0.231 |
| soil | 0.812 | $2.652 \times 10^{-6}$ | 1.483 | 1.402 | 0.995 | -2.551 | 0.298 | 0.239 |

vertical P-wave (filtered) displacement attenuation coefficients

| rock | 0.956 | $1.975 \times 10^{-6}$ | 1.345 | 1.656 | 1.164 | -4.799 | 0.283 | 0.254 |
|------|-------|------------------------|-------|-------|-------|--------|-------|-------|
| soil | 0.933 | $1.090 \times 10^{-7}$ | 1.234 | 1.515 | 1.041 | -4.749 | 0.312 | 0.248 |

Table 3.6: Regression coefficients for Eqn. 2.3 for P-wave envelope amplitude parameters for acceleration, velocity, and filtered displacement on rock and soil sites for rms horizontal and vertical ground motion channels.

- S-wave amplitudes increase faster with magnitude than do P-waves

- The anelastic (and scattering) coefficient decreases with period

- Geometric decay of P-waves ($\sim 1.2$) appears slower than that of S-waves ($\sim 1.5$)

Figures 3.4, 3.4, and 3.4 show observed P-wave envelope amplitudes (rock sites) for acceleration, velocity, and displacement, and amplitude curves predicted by Eqn. 2.3 as a function of distance for various prescribed magnitudes. From these plots, P-wave saturation effects are frequency dependent. Similar to S-waves, P-wave saturation is strongest in acceleration and decreases with period.

Figures 3.4 and 3.4 are useful in examining the differences between P- and S-wave attenuation as functions of magnitude and distance for the different frequency bands. In both Figures, the first column shows P-wave and S-wave attenuation for acceleration, velocity, and displacement as a function of magnitude; the second column shows P- and S-wave attenuation as a function of distance. Figures 3.4 and 3.4 are for rock sites; Figures 3.4 and 3.4 are for soil sites. In general, it appears that the difference between P- and S-waves increases with period. with P-waves exhibiting stronger saturation than S-waves at longer periods. P- and S-waves are more similar in acceleration than they are in displacements. Also, vertical P- and S-waves are more similar in amplitude than horizontal P- and S-waves.

It is a curious thing that P-waves appear to saturate more than S-waves. This is present in both horizontal and vertical channels, though it is much more pronounced in the horizontal channels. No explanation is proposed at the moment. P-waves have relatively higher frequency energy than S-waves, and in general, the mechanisms that generate high-frequency energy during earthquake ruptures are not as well-understood as those related to longer period ground motion. On the other hand, this P-wave over saturation may simply be a consequence of the parameterization of observed envelopes as combinations of P-wave, S-wave, and ambient noise envelopes; uniquely decomposing P- and S-waves at close distances is problematic, particularly in the horizontal direction.
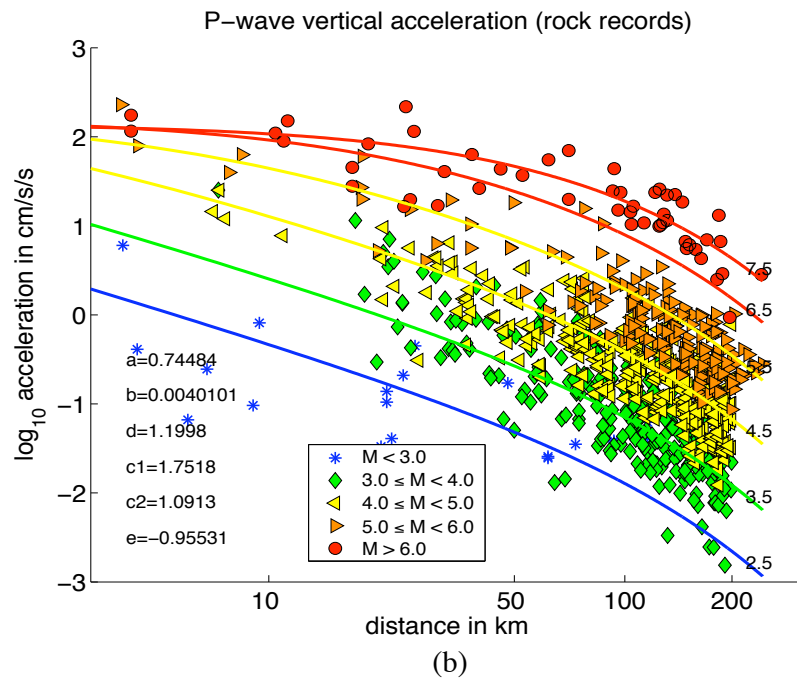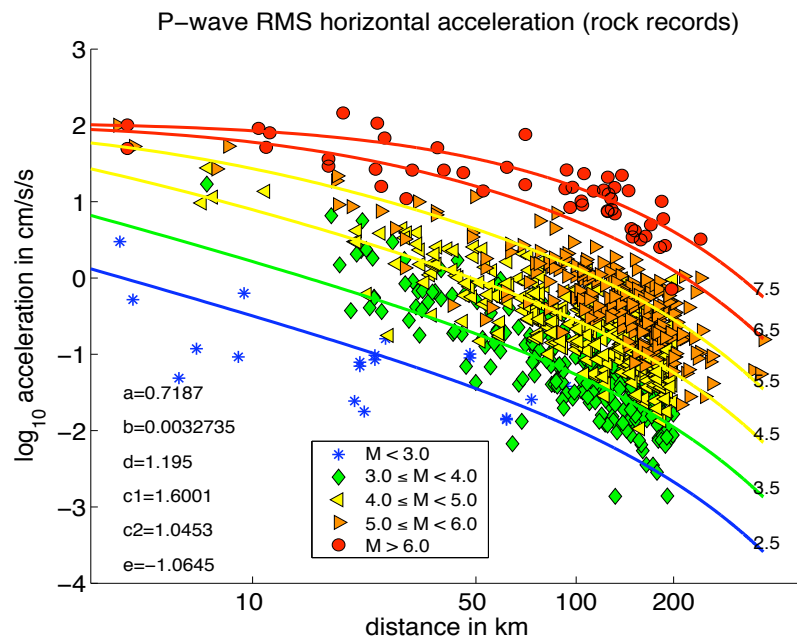
Figure 3.31: Observed P-wave envelope acceleration amplitudes on rock sites for (a) rms horizontal and (b) vertical channels of ground motion.
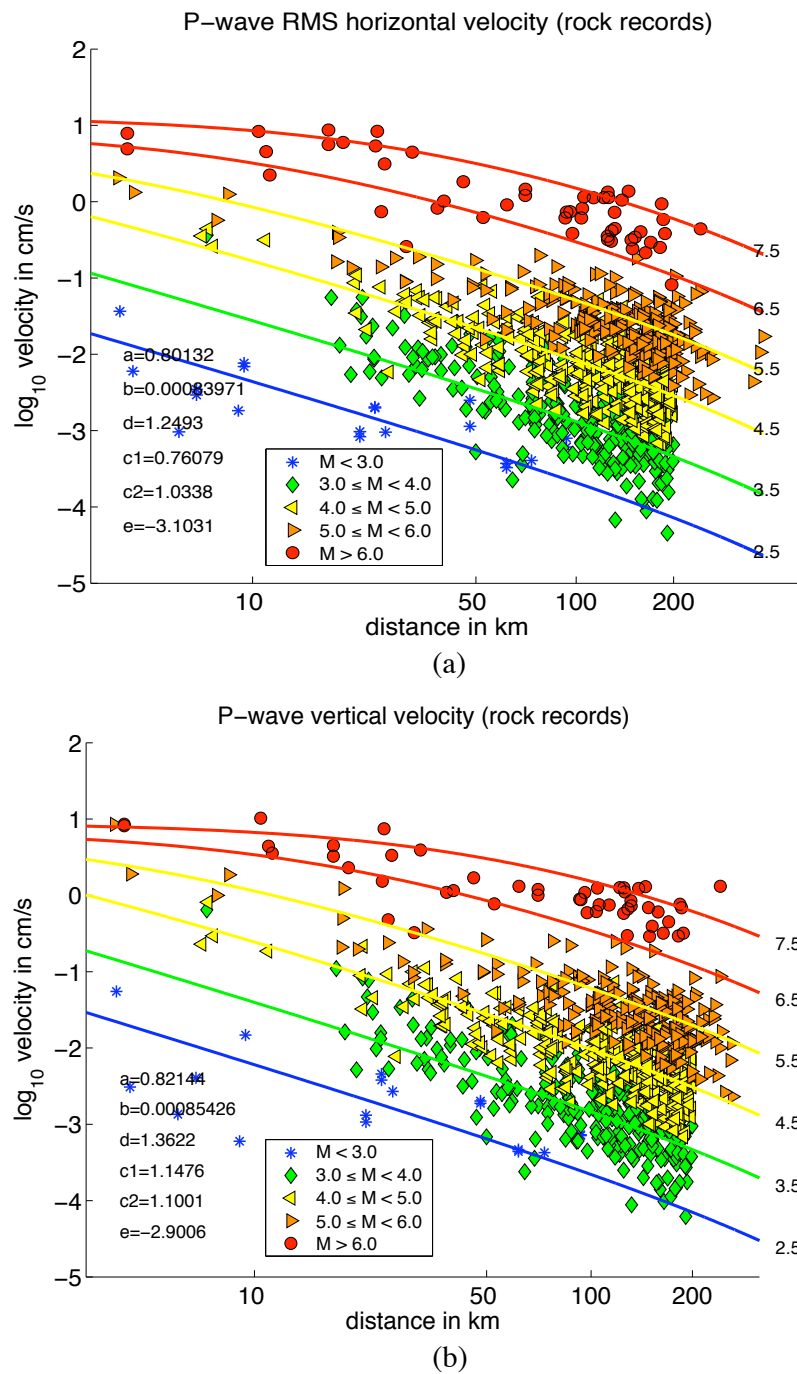
Figure 3.32: Observed P-wave envelope velocity amplitudes on rock sites for (a) rms horizontal and (b) vertical channels of ground motion.
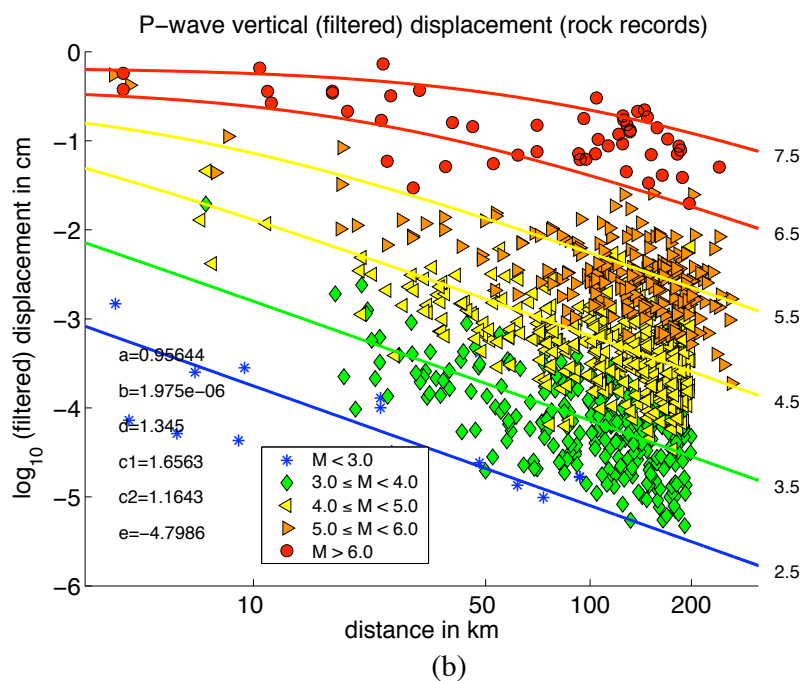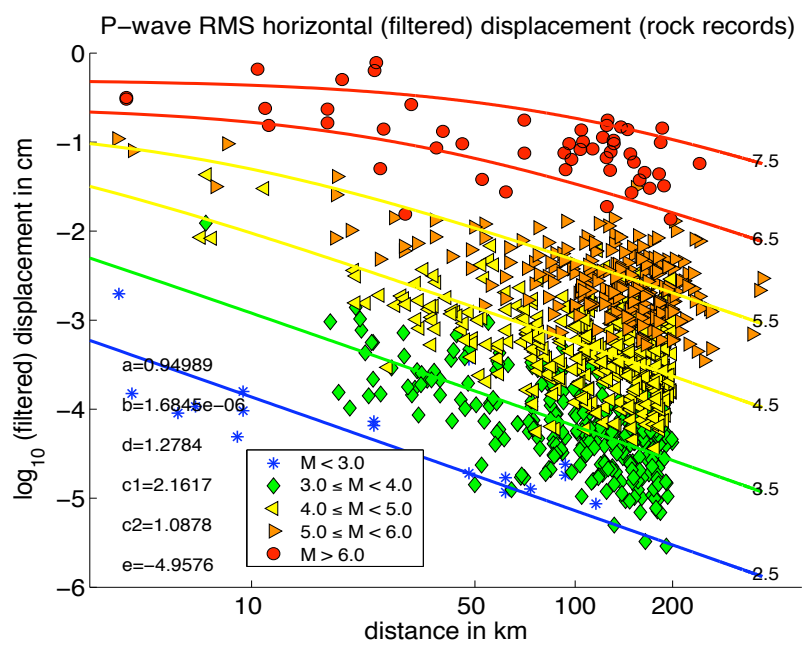
Figure 3.33: Observed P-wave envelope displacement amplitudes on rock sites for (a) rms horizontal and (b) vertical channels of ground motion.
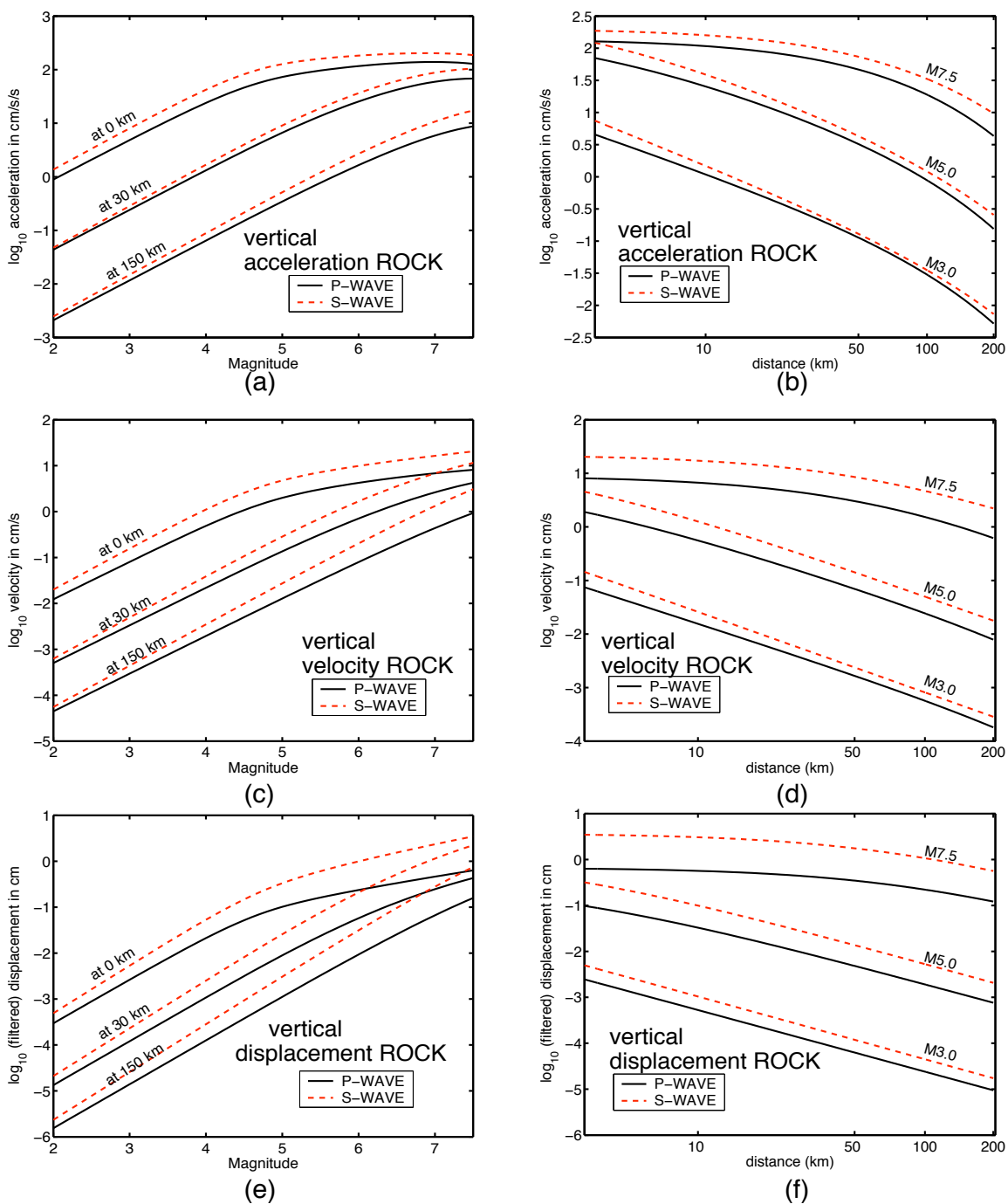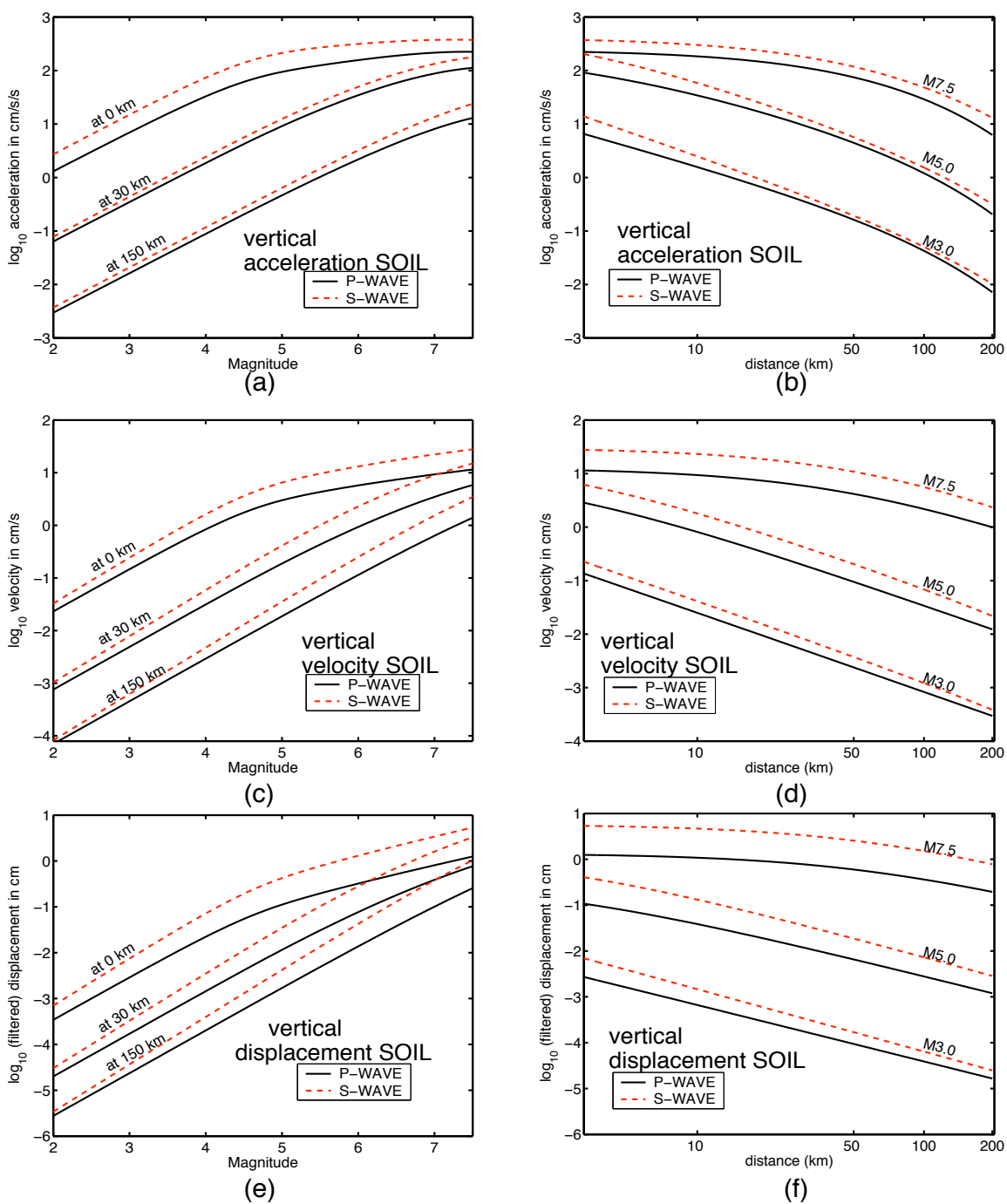
Figure 3.34: P- and S-wave attenuation for vertical acceleration, velocity, and displacement on rock sites. The first column compares predicted P- and S-wave amplitudes as a function of magnitude; the second column, as a function of distance. The difference between P- and S-waves seems to increase with period. P-waves tend to saturate more than S-waves at longer periods.
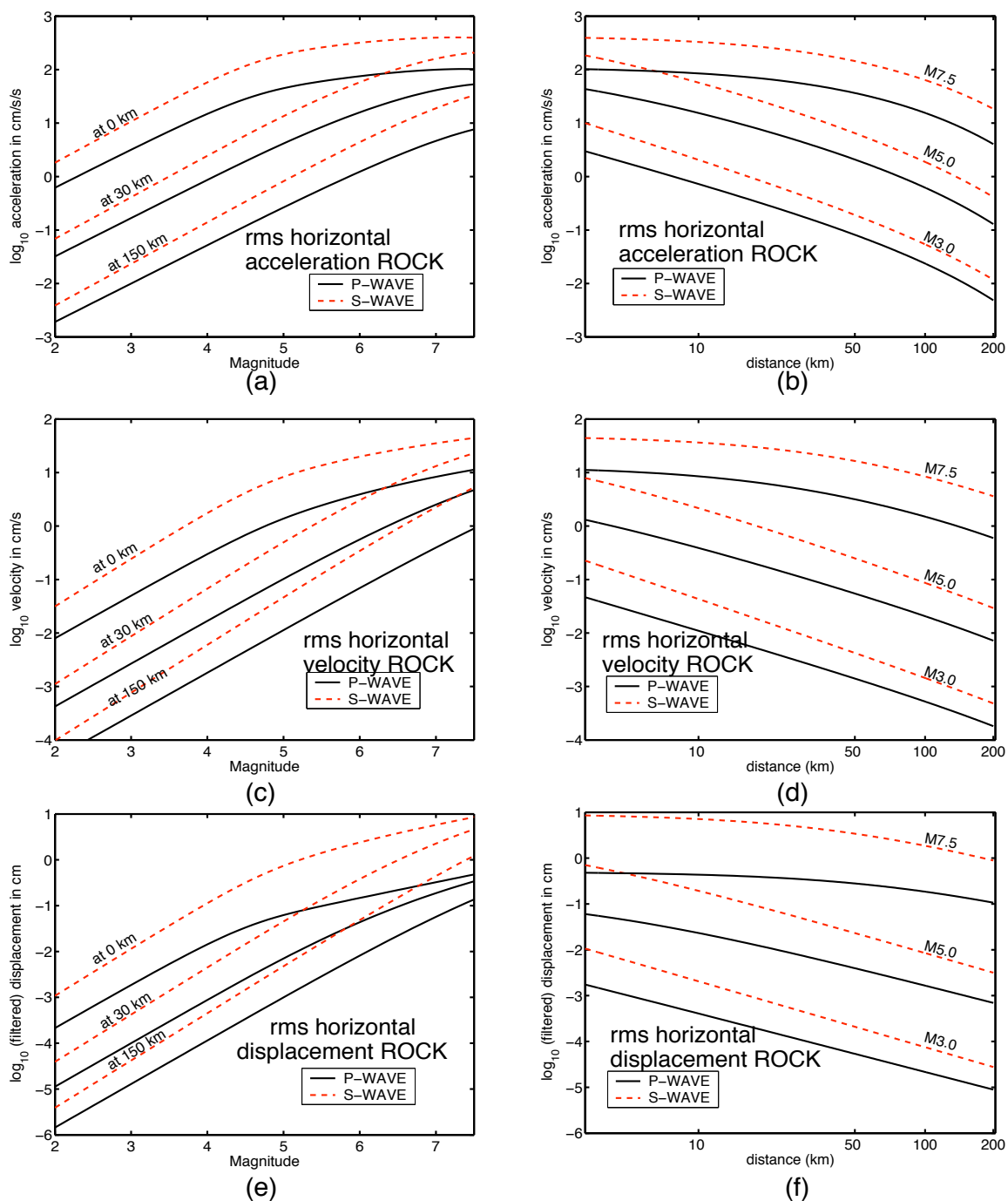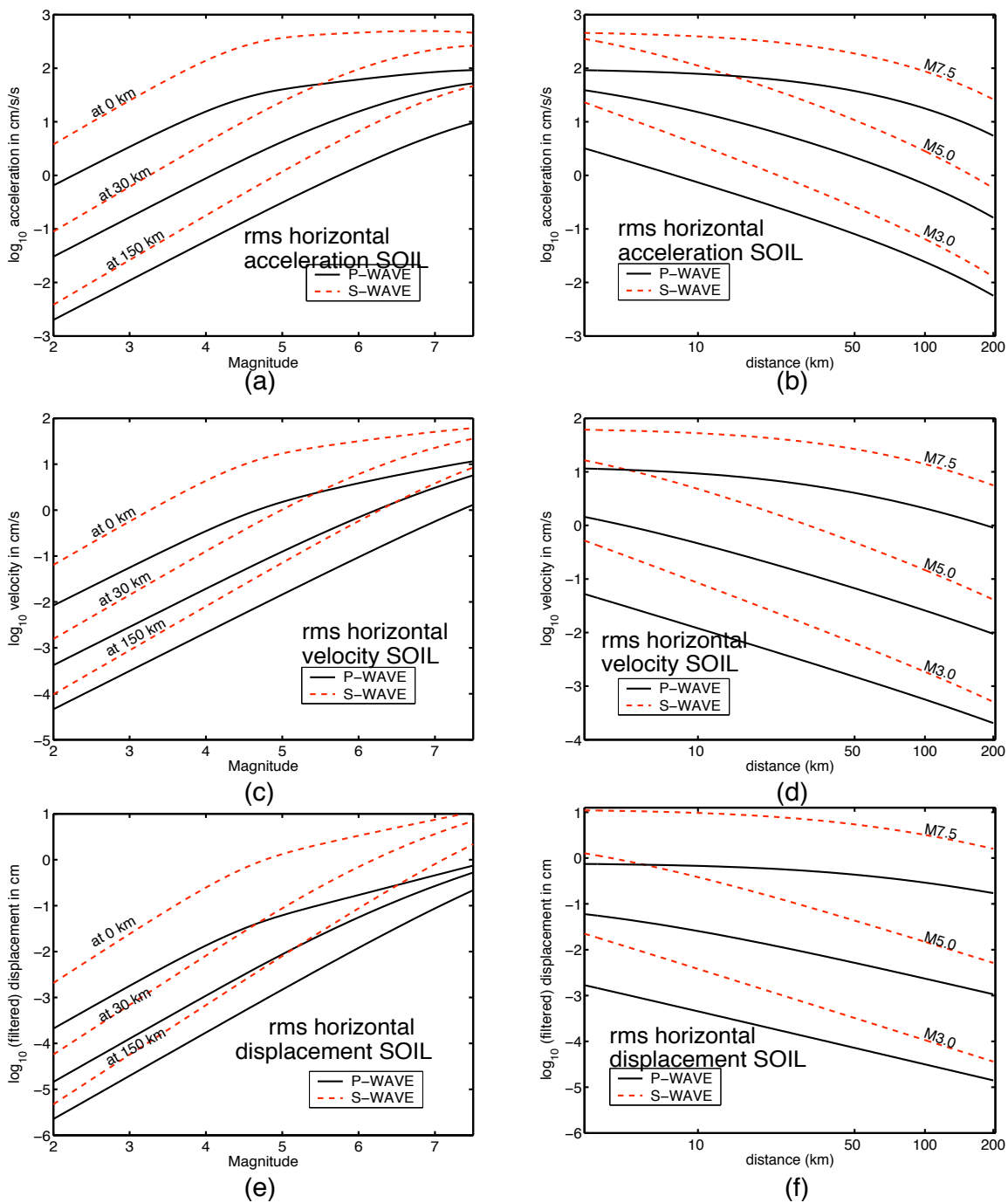
Figure 3.35: P- and S-wave attenuation for horizontal acceleration, velocity, and displacement on rock sites. The first column compares predicted P- and S-wave amplitudes on rock sites as a function of magnitude; the second column, as a function of distance. The difference between P- and S-waves is more pronounced on the horizontal channels than the verticals.

Figure 3.36: P- and S-wave attenuation for vertical acceleration, velocity, and displacement on soil sites. The first column compares predicted P- and S-wave amplitudes on soil sites as a function of magnitude; the second column, as a function of distance. The differences in P- and S-waves are a stronger function of direction (horizontal or vertical) than they are of site type (rock or soil).

Figure 3.37: P- and S-wave attenuation for horizontal acceleration, velocity, and displacement on soil sites. The first column compares predicted P- and S-wave amplitudes on soil sites as function s of magnitude; the second column, as a function of distance.

# 3.5 Predicting envelopes of various channels of ground motion

The main motivation for this study of envelopes of ground motion was to develop predictive relationships for application in seismic early warning. This and the previous chapter discussed the methods utilized for developing such predictive relationships. These envelope attenuation relationships are used to predict various channels of ground motion as functions of magnitude and distance on rock and soil sites in Figures 3.5 through 3.5. These Figures visually summarize the average characteristics of ground motion discussed in this chapter:

- Saturation effects are important at close distances to large earthquakes. Acceleration is most strongly affected, with velocity and displacement exhibiting some saturation, though to a lesser degree.

- For horizontal channels, soil sites exhibit stronger saturation than do rock sites. The difference between rock and soil amplitudes decreases with increasing ground motion amplitude.

- The difference between rock and soil sites is more pronounced on the horizontal channels than on the vertical channels. For horizontal channels, this difference is a function of magnitude and distance.

- The difference between rock and soil sites for vertical channels appears to be fairly constant; it is a weaker function of magnitude and distance than for the horizontal channels.

Having described the development of these predictive relationships, their applications to seismic early warning can now be discussed. Such applications are the subject of the subsequent chapters of this thesis.
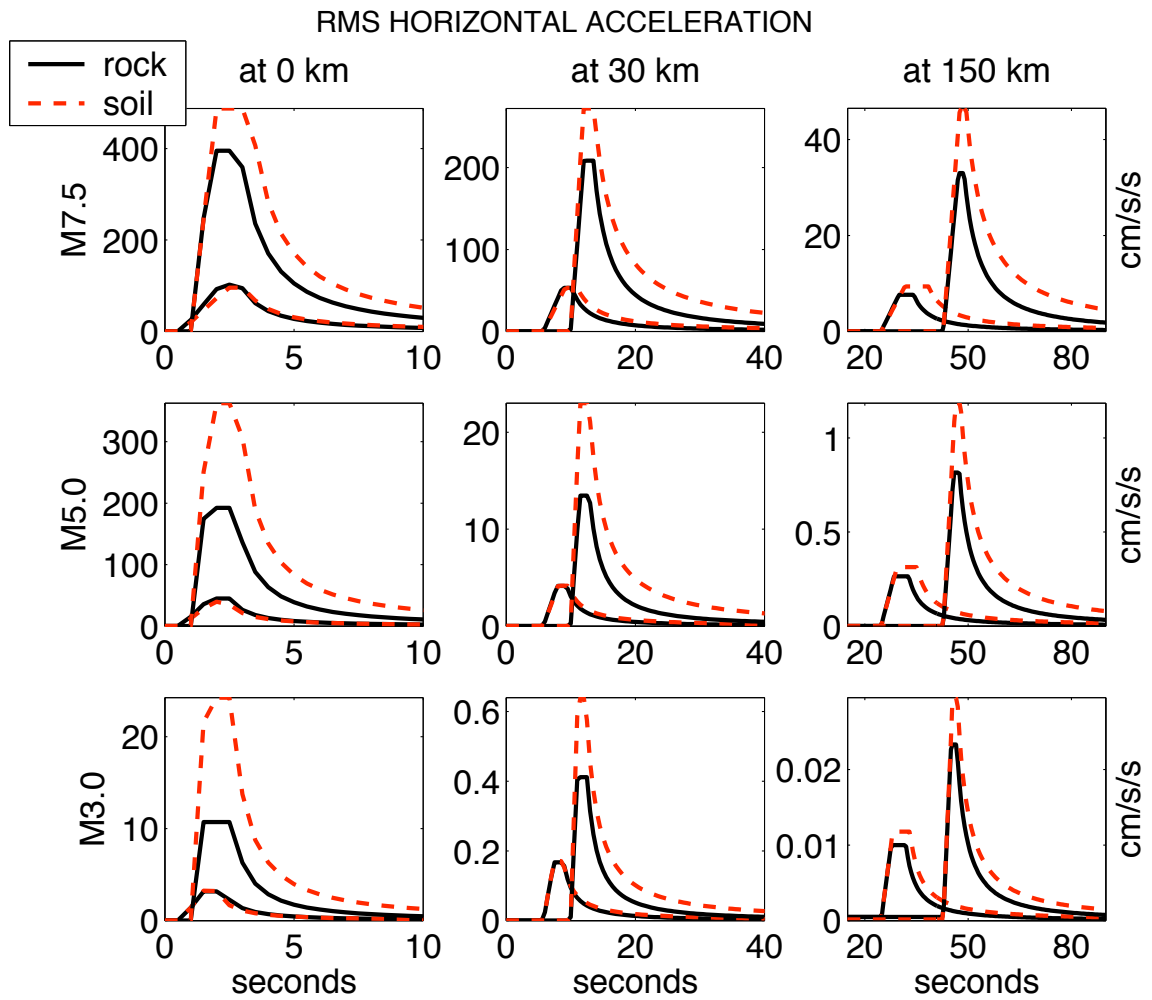
Figure 3.38: Predicted envelopes for rms horizontal acceleration at various magnitudes and distances.
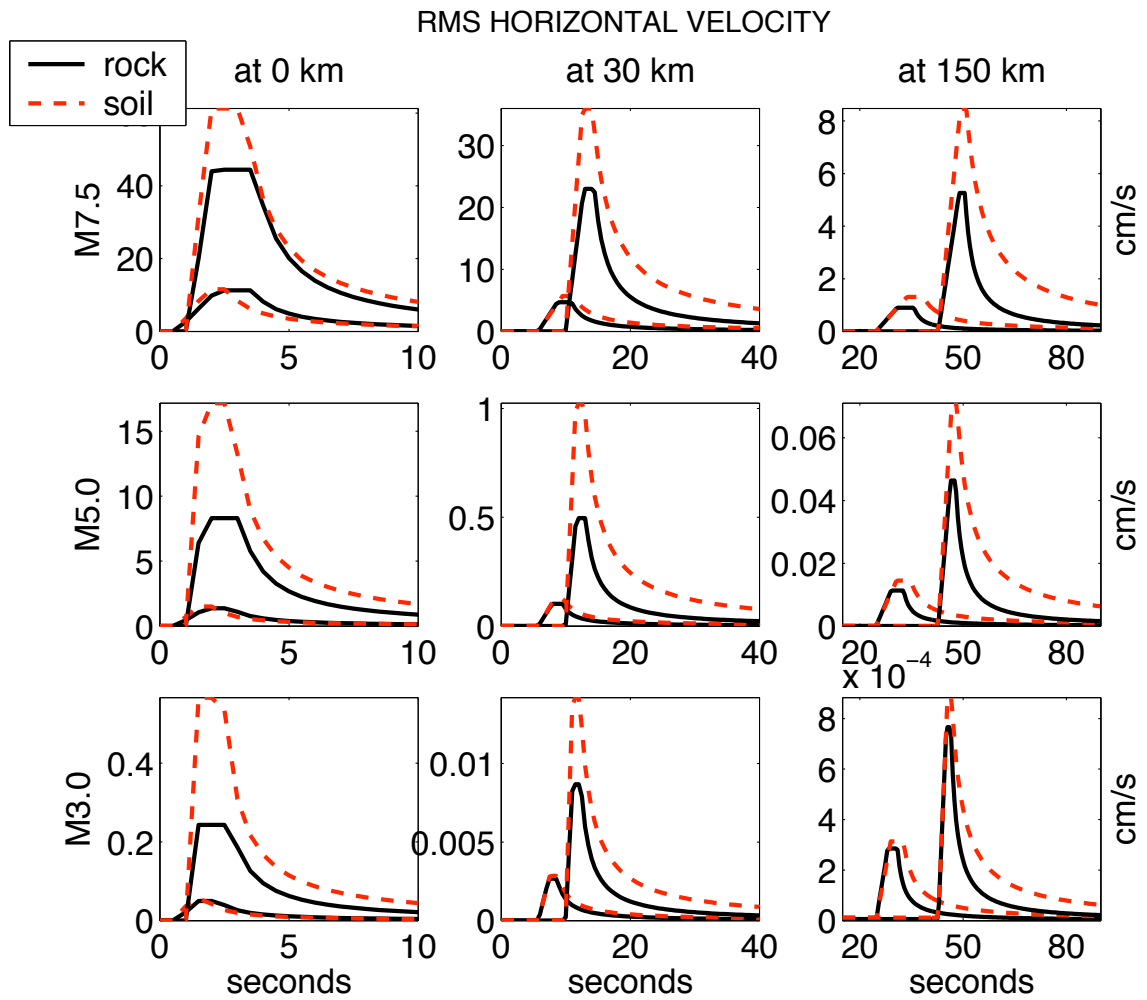
Figure 3.39: Predicted envelopes for rms horizontal velocity at various magnitudes and distances.
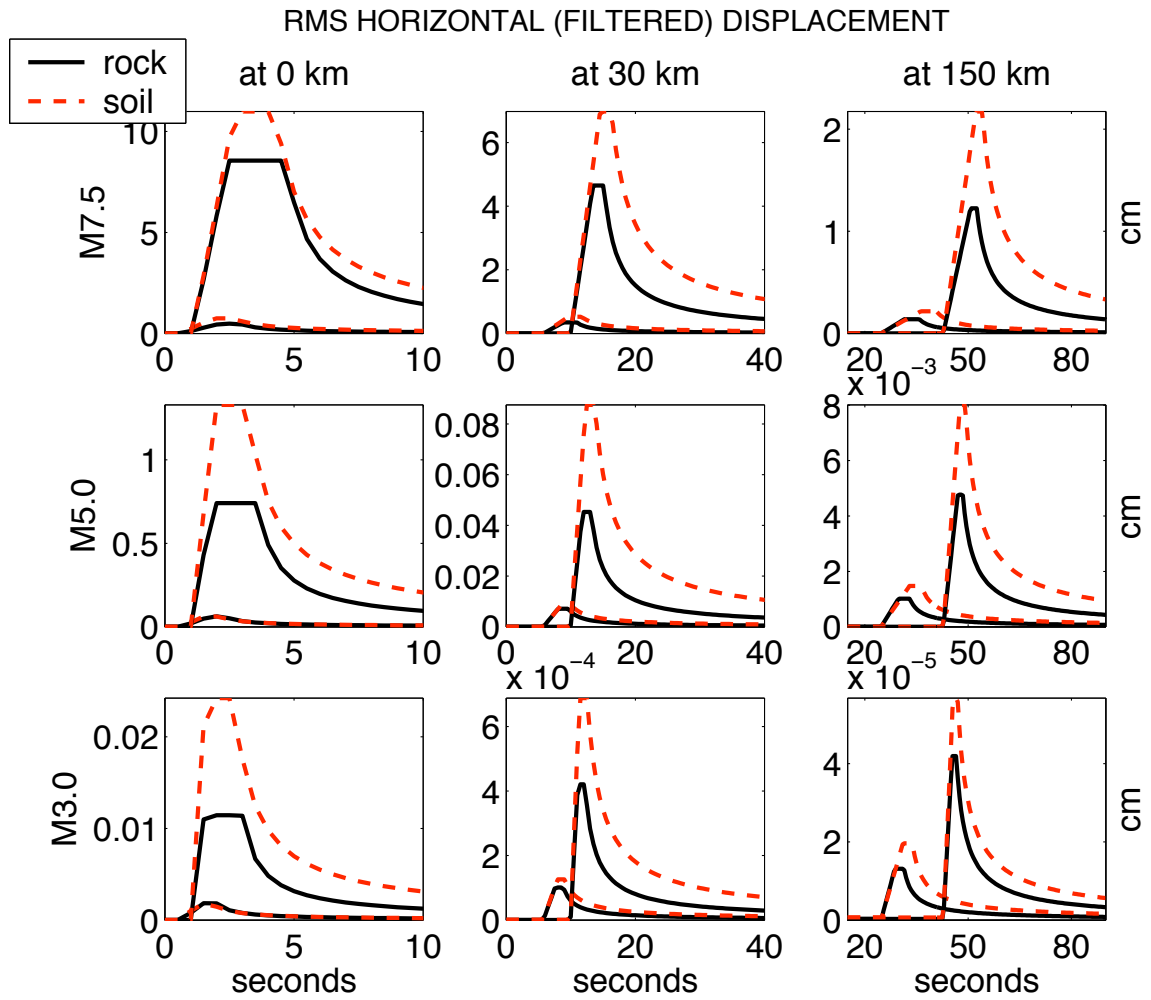
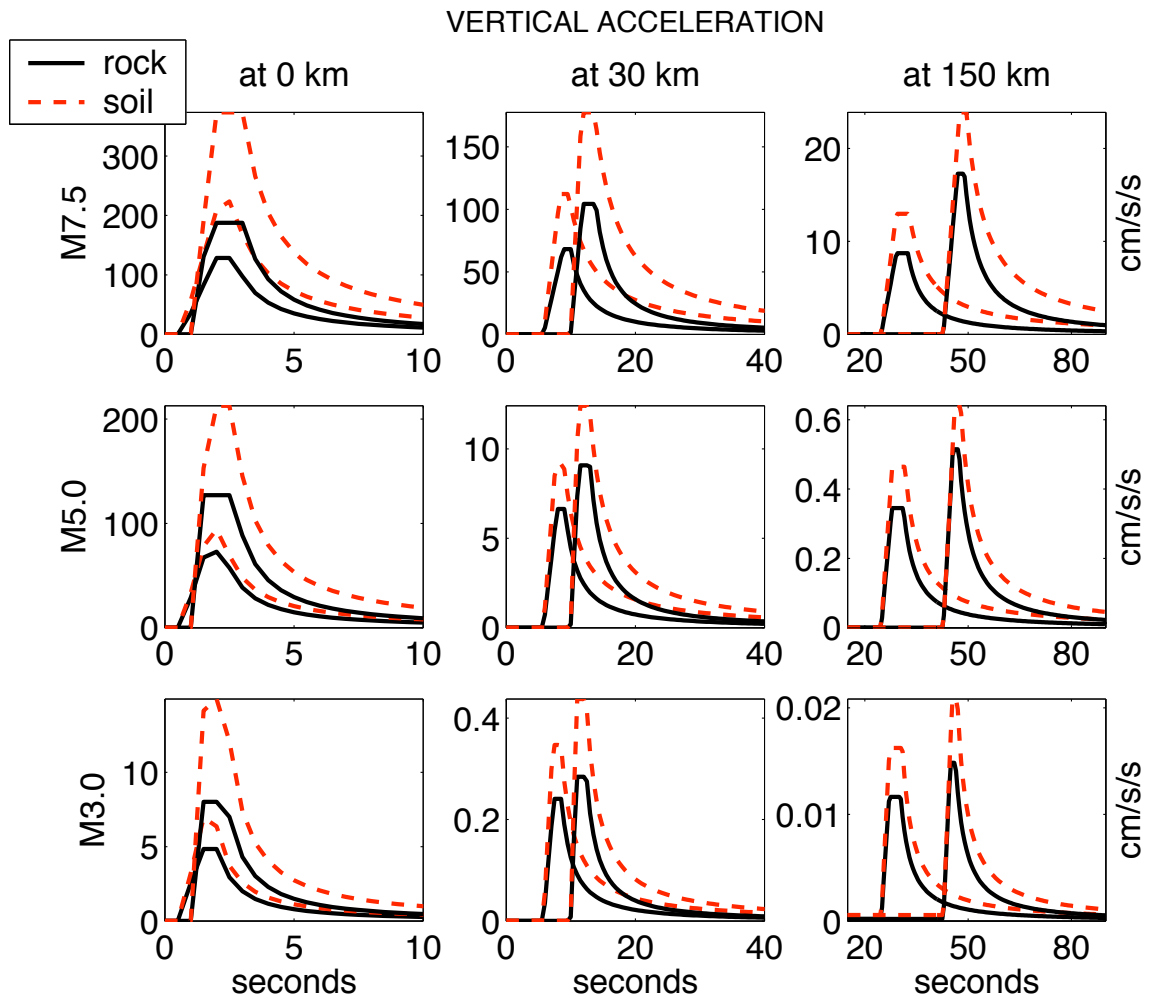Figure 3.40: Predicted envelopes for horizontal filtered displacements at various magnitudes and distances.

Figure 3.41: Predicted envelopes for vertical acceleration at various magnitudes and distances.
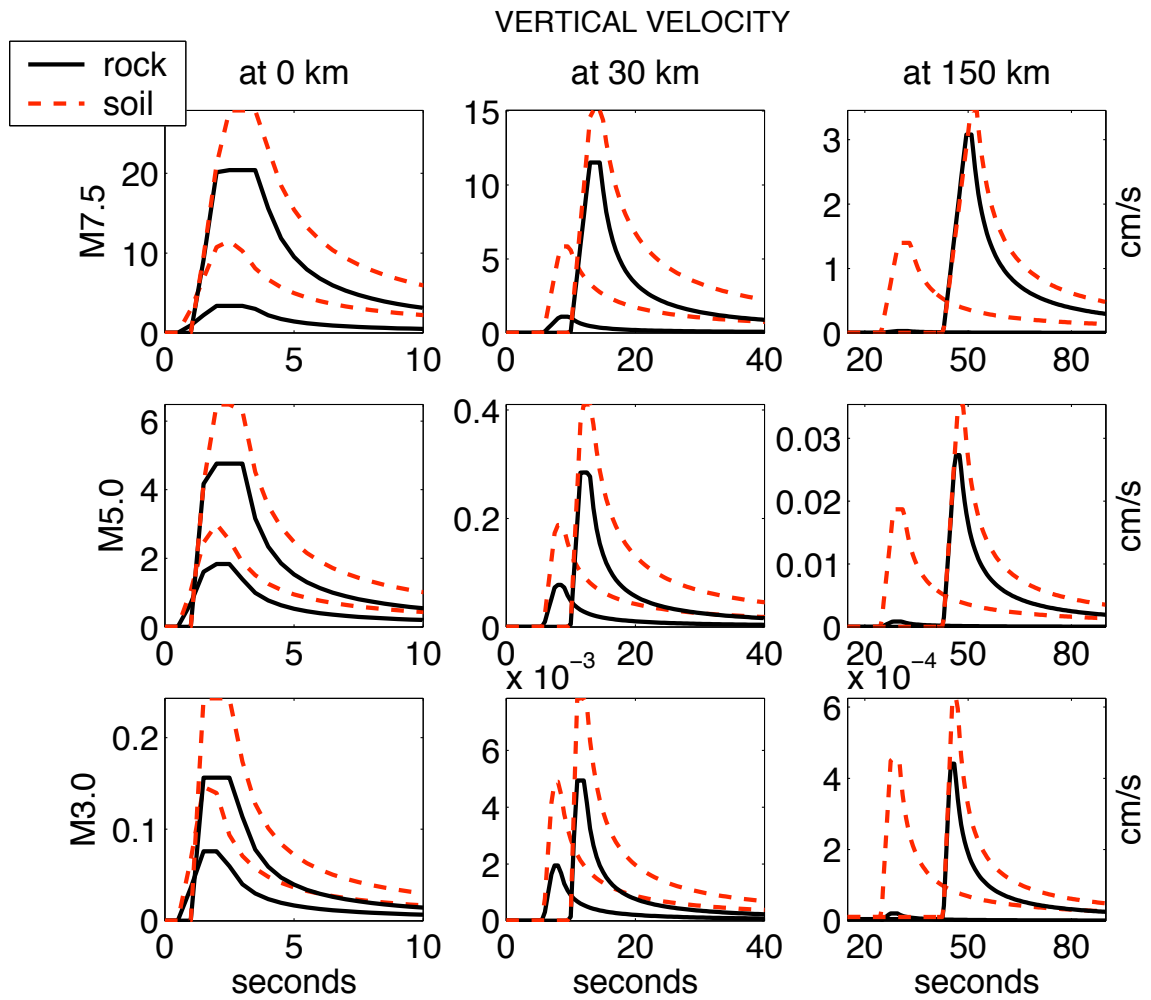
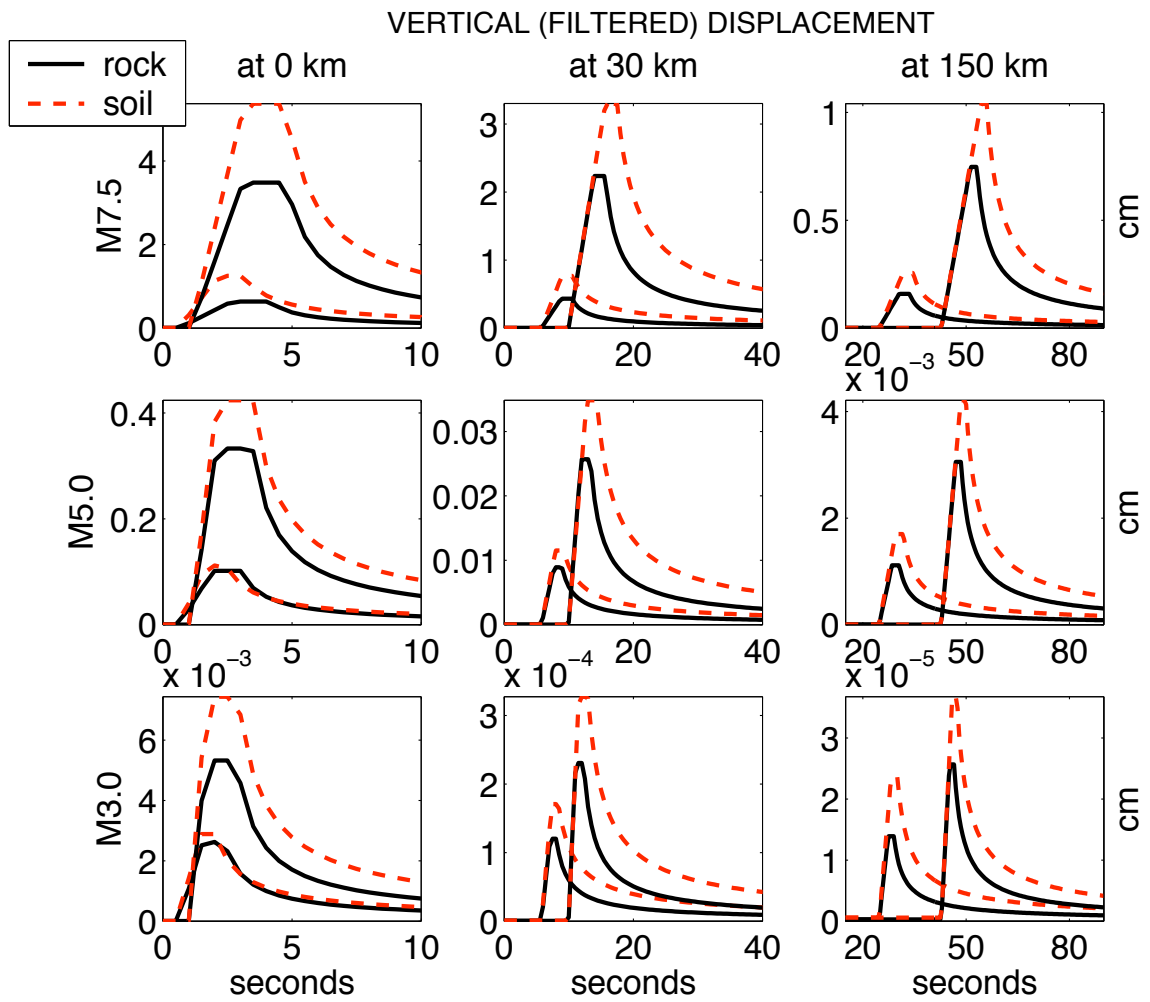Figure 3.42: Predicted envelopes for vertical velocity at various magnitudes and distances.

Figure 3.43: Predicted envelopes for vertical filtered displacements at various magnitudes and distances.